Fluctuation Analysis of Oxidation-Reduction Potential in Circumneutral pH Iron-Oxidizing Microbial Systems

by

Allison Marie Leigh Enright

A thesis submitted in conformity with the requirements
for the degree of Doctor of Philosophy

Department of Earth Sciences
University of Toronto

Fluctuation Analysis of Oxidation-Reduction Potential in Circumneutral pH Iron-Oxidizing Microbial Systems

Allison M.L. Enright
Doctor of Philosophy
Department of Earth Sciences
University of Toronto

2015

Abstract

The goal of this thesis was to assess the utility of using small-scale fluctuations in oxidation-reduction (redox) potential to distinguish microbial from chemical iron oxidation. Fluctuations in potential arise from the motion of particles in a fluid; measuring fluctuations is therefore a system-scale observable property of micro-scale chemical behaviour, as such particle motion constitutes diffusion. Fluctuations are described by the strength of their correlation, as measured by scaling exponents. A method for the calculation of scaling-exponents of long-range correlation in redox potential measurements was developed, including new instrumentation and the modification of an existing physiological processing algorithm for use with environmental microbiological data sets. Steady-state biological and chemical systems were compared, and scaling exponents calculated from each system were found to differ significantly. In a final study, a series of microcosms were used to determine the relationship between scaling exponent, measuring correlation strength, and oxidation rate. The biological systems are governed by the rate of reaction, while the chemical systems appear to be diffusion-controlled. Because in these systems, Fe(II) is a metabolite, redox potential can then be interpreted as a physically-constrained proxy for metabolic activity. This allows the characterization of biological activity *in situ*.

Table of Contents

List of Tables

List of Figures

has a scaling exponent of 0.7, the uncorrelated walk has a scaling exponent of 0.5, and the anti-correlated walk has a scaling exponent of 0.3.

Figure 2.1: Schematic diagram of the instrument designed to measure redox potential using a Pt working electrode and Ag/AgCl reference electrode. AI0+, AI0-, and GND describe specific pins on the NI-6009 USB Data Acquisition Device (DAQ).

Figure 2.2: Redox potential (ORP) raw time series and integrated profiles from each of the three processes; raw data, in mV, plotted against left axis, while integrated signal profiles are plotted against the right. Live system (BIOS) is in black, artificial groundwater medium (AGW) is in blue, and tap water (Tap) is in red.

Figure 2.3: Redox potential and random walk profiles recorded over a 10 s interval from each of the three time series. Raw data is plotted on the left as solid lines, and integrated profiles are plotted on the right as dashed lines. A. Live system (BIOS) is in black. B. Artificial groundwater medium (AGW) is in blue. C. Tap water (Tap) is in red.

Figure 2.4: Detrended fluctuation analysis results for three experimental systems. These results represent α calculated for a single realization of each process with $n = 2500$, downsampled from the raw data to 1 Hz. RMS is root-mean-square fluctuation as calculated using detrended fluctuation analysis (DFA). The live system (BIOS) is identified by filled black circles. The first chemical system, artificial groundwater medium (AGW) is shown with blue squares and a blue dashed line, and the second chemical system, tap water (Tap) is shown with red triangles and a red dashed line.

Figure 3.1: Temperature, pH, BIOS redox potential, inlet redox potential, and dissolved O_2 profiles over 30 minutes of data logging at one second intervals in the Äspö flow through cell, 297 m underground at experimental site 2200A.

Figure 3.2: The equilibrium redox potential calculated using PHREEQC for the Äspö flow cell inlet (solid line) and outlet (dashed line) as a function of pH. The observed pH and redox potentials are shown as solid symbols; open symbols represent measured redox potential values positioned at equilibrium pH.

Figure 3.3: The observed (bottom, left axis) and random walk (top, right axis) redox potential across an interval of 120 seconds for the inlet, BIOS, and randomly shuffled time series measurements in the Äspö flow through cell, 297 m underground at experimental site 2200A.

Figure 3.4: Log-log plot of root mean square fluctuations (mV) for inlet, BIOS, and randomly shuffled redox potential time series as a function of time interval window size *s* (seconds) in detrended fluctuation analysis.

Figure 4.1: Concentration of Fe(II), normalized to the initial concentration (t=0), as a function of time, in each of the four microcosms. ALL system (dark blue circles), LIVE system (light blue squares), AUTO system (white diamonds), and CREEK system (grey triangles).

Figure 4.2: Pseudo-first order oxidation rate constants as a function of the mass of dried precipitate in each microcosm.

Figure 4.3: Calculated scaling exponents (α) for time series n=1000, 1 Hz sampling frequency, and instantaneous oxidation rates r_{ox} as a function of the start time corresponding with n_0.

Figure 4.4: τ as a function of scaling exponent, α for each microcosm system. ALL is top left (dark blue circles), LIVE is top right (light blue circles), AUTO is bottom left (white diamonds), CREEK is bottom right (grey triangles).

List of Appendices

Chapter 1
Introduction

1.1 Rationale

The broad goal of this thesis was to develop a physically-constrained measurement which could act as a diagnostic signature of extant microbial activity. The specific physical signature which was evaluated was correlation structure of fluctuation time series of oxidation-reduction (redox) potential, and this structure could distinguish chemical and biological Fe(II)-oxidation *in situ*. Here, fluctuations in redox potential were characterized in two circumneutral aerobic iron-oxidizing microbial mats, and a series of mat-free, chemical and abiotic control solutions. Two steady state systems were examined, and the final study used a series of microcosms to examine how fluctuation behaviour was related to oxidation rate.

1.2 Iron as a Microbial Energy Source

The Fe(III)/Fe(II) redox couple has profound global significance, both in the context of early life evolution, where it was one of the first evolved metabolic pathways (Emerson, 2012), and by underpinning global cycling of iron (Weber *et al.*, 2006). In the context of microbiology, iron represents an enormous energy source (Emerson, 2012), and is a frontrunner in the search for life beyond Earth (Emerson & Weiss, 2004; Weber *et al.*, 2006; Druschel *et al.*, 2008). Growth on Fe is thought to be a very ancient metabolism on Earth (Konhauser *et al.*., 2005; Emerson, 2012), and Fe-based microbial ecosystems are hypothesized to be ancient, with both Fe(III)-reducing (FeRB) and Fe(II)-oxidizing (FeOB) microbes deeply rooted in the universal phylogenetic tree (Emerson *et al.*, 2010; Roden *et al.,* 2012).

Iron is 4th most abundant element in Earth's crust, making up about 5.1% by mass (Straub *et al.*, 2001); iron mainly occurs in one of two redox states in the environment: either oxidized as Fe(III) (ferric iron), which is poorly soluble at circumneutral pH; or reduced as Fe(II) (ferrous iron), which is easily soluble at circumneutral pH, and as such, tends to be more bioavailable (Melton *et*

al., 2014). The speciation of iron in the environment, and therefore, its bioavailability, are dynamically controlled by redox conditions (Melton *et al.*, 2014).

1.3 Environments Colonized by Fe(II)-Oxidizing Bacteria

Despite iron's global abundance, the rise of oxygen in Earth's atmosphere dramatically limited the spatial extent of Fe-metabolizing bacteria, but may have increased the diversity of niches available to them. Both iron-oxidizers and reducers continue to dominate biogeochemical cycling of iron (Kendall *et al.*, 2012). In 40% of the modern global ocean, iron is the limiting nutrient for algal growth (Emerson *et al.*, 2012). Despite this, in a number of niches of environmental interest and significance, especially oxic-anoxic interfacial environments, iron is so abundant that it acts as an electron source to sustain growth, supporting robust communities of Fe(II) oxidizing chemolithoautotrophic organisms (Emerson *et al.*, 2012). Sustained microbial iron redox cycling has been proposed in various redox interfacial environments, including:

- groundwater (Emerson & Moyer, 1997; Anderson & Pedersen, 2003; Anderson *et al.*, 2006)
- iron seeps and streams (Emerson *et al.*, 1999; James & Ferris, 2004; Rentz *et al.*, 2007; Druschel *et al.*, 2008; Blöthe & Roden, 2009; Langley *et al.*, 2009b; Gault *et al.*, 2011; Ferris *et al.*, in press),
- aquifers (Lovley, 1991; Bird *et al.*, 2011; Vollrath *et al.*, 2012),
- plant roots and the rhizosphere (Emerson *et al.*, 1999; Weiss *et al.*, 2003; Emerson & Weiss, 2004; Weber *et al.*, 2006; Emerson, 2012),
- wetlands (Puteanus *et al.*, 1991; Emerson *et al.*, 1999; Sobolev & Roden, 2001; Emerson & Weiss, 2004; Druschel *et al.*, 2008; Haaijer *et al.*, 2008; Bruun *et al.*, 2010; Emerson *et al.*, 2010; Vollrath *et al.*, 2012),
- the sediment-water interface in both circumneutral (Ghiorse & Ehrlich, 1993; Sobolev & Roden, 2002; Emerson & Weiss, 2004; Roden *et al.*, 2004) and acidic (Peine *et al.*, 2000) aquatic ecosystems,
- hot springs and hydrothermal vents (Pierson *et al.*, 1999; Kashefi *et al.*, 2003; Blöthe & Roden, 2009),
- caves (Kasama & Murakami 2001; Weber *et al.*, 2006),

- ocean ridges, volcanic seamounts, hydrothermal vents, and ridge flanks (Gold, 1999; Edwards *et al.*, 2003; Kennedy *et al.*, 2003; Edwards *et al.*, 2004; Little *et al.*, 2004; Weber *et al.*, 2006; Langley *et al.*, 2009a; Toner *et al.*, 2009),
- marine sediments (Emerson *et al.*, 2010; Kendall *et al.*, 2012),
- chalybeate springs (Ghiorse, 1984; Emerson & Revsbech, 1994).

FeOB also colonize a significant number of human-made environments, such as water distribution systems, water wells, pipes, drainage ditches and mines (Hanert, 1992; Emerson & Revsbech, 1994; Ralph & Stevenson, 1995; Tuhela *et al.*, 1997; Emerson, 2000; Ehrlich, 2002; Emerson & Weiss, 2004; James & Ferris, 2004; Weber *et al.*, 2006; Rentz *et al.*, 2007; Emerson, 2012; Emerson & de Vet, 2015). FeOB are also known to be capable of growth on steel, and contribute to biocorrosion through the alteration of pH and redox potential (Rozanova *et al.*, 2003; Zuo & Wood, 2004; Rentz *et al.*, 2007; McBeth *et al.*, 2011; Emerson & de Vet, 2015). In most of these settings, FeOB are nuisances.

1.4 Environmental and Geological Significance of Fe(II) -Oxidizing Bacteria

The geological and evolutionary significance of aerobic Fe(II)-oxidation at circumneutral pH was only recently taken seriously as a globally-significant process, due to the very rapid rate of abiotic Fe(II)-oxidation coupled to oxygen reduction (Davison & Seed, 1983; Weber *et al.*, 2006). FeOB are major players in a wide range of ancient and modern systems. These microbes play several key roles in sequestering contaminants in water systems (Straub *et al.*, 2001; Edwards *et al.*, 2004; Emerson & Weiss, 2004; Kappler & Newman, 2004; Roden *et al.*, 2004; Ferris, 2005; Anderson *et al.*, 2006; Weber *et al.*, 2006; Rentz *et al.*, 2007; Druschel *et al.*, 2008; Neubauer *et al.*, 2002; Langley *et al.*, 2009a; Emerson *et al.*, 2010; Gault *et al.*, 2011; Kennedy *et al.*, 2011; Emerson & Vet, 2015; Ferris *et al.*, in press), and the storage of nuclear waste (Warren & Ferris, 1998; Anderson & Pedersen, 2003; James & Ferris, 2004; Anderson *et al.*, 2006; Roden *et al.*, 2012). FeOB are also thought to contribute significantly to weathering processes (Edwards *et al.*, 2004; Weber *et al.*, 2006). Iron metabolism, both oxidation and reductive, is a strong contender for life outside of Earth (Emerson & Weiss, 2004; Druschel *et al.*, 2008), and played a major role in the evolution of Earth's atmosphere and oceans both before and after the great oxidation event (Konhauser *et al.*, 2005; Kendall *et al.*, 2012). Finally, FeOB are also used in microbial fuel cell applications (Rabaey *et al.*, 2007).

1.5 Energetics of Microbial Fe(II)-Oxidation

Both FeRB and FeOB have long been described in literature (Harder, 1919; Ghiorse, 1984); *Gallionella ferruginea* was the first FeOB described, in 1837 (Ehrenberg, 1837; Rentz *et al.*, 2007; Emerson *et al.*, 2010; McBeth *et al.*, 2011), while FeRB were first described in 1989 (Lovley et al., 1989). Aerobic oxidation of Fe(II) is the pathway studied here, however FeOB also can oxidize iron under anaerobic conditions by coupling oxidation to either anoxygenic photosynthesis (Widdel et al., 1993) or nitrate reduction (Straub et al., 1996; Emerson *et al.*, 2012; Melton *et al.*, 2014; Ferris *et al.*, in press). FeOB are also known to be capable of acquiring iron from insoluble Fe(II)-bearing minerals (Emerson *et al.*, 2012).

Two of the most ubiquitous microaerophilic FeOB genera, and the two species which dominate the systems studied here, are *Gallionella spp.* and *Leptothrix spp.;* specifically, *Gallionella ferruginea and Leptothrix ochracea* are two of the most ubiquitous FeOB (Emerson & Revsbech, 1994). These two are especially well-known because of their distinctive morphologies; *Gallionella spp.* form stalks, while *Leptothrix spp.* form sheaths (Druschel *et al.*, 2008). Phylogenetically, these bacteria belong to the phylum Proteobacteria, which includes the freshwater genera *Leptothrix* (Fleming *et al.*, 2011; Melton *et al.*, 2014), *Gallionella* (Kucera & Wolfe, 1957; Melton *et al.*, 2014), and *Sideroxydans* (Weiss *et al.*, 2007; Melton *et al.*, 2014), and the marine genus *Mariprofundus* (Singer *et al.*, 2011; Melton *et al.*, 2014). *Leptothrix* is known to be a common inhabitant of iron seeps (Emerson & Revsbech, 1994), and *Leptothrix ochracea* is abundant in waters that contain large amounts of organic C, as well as Fe and Mn, which have gentle redoxclines (Fleming *et al.*, 2013; Melton *et al.*, 2014). In contrast, *Gallionella spp.* inhabit waters with low organic C content and steep redoxclines (Melton *et al.*, 2014).

1.6 Geochemical Conditions Supporting Circumneutral, Microaerophilic Fe(II) - Oxidizing Bacteria

The pH range of circumneutral microaerophilic FeOB is typically from 5.5 to 7.2 (Emerson *et al.*, 2010). The two most important requirements for survival are a constant source of Fe(II), and low pO_2 (Emerson & Revsbech, 1994; Neubauer *et al.*, 2002; Emerson & Weiss, 2004; James & Ferris, 2004; Roden *et al.*, 2004; Ferris, 2005; Weber *et al.*, 2006; Druschel *et al.*, 2008; Emerson,

2012; Kendall *et al.*, 2012; Vollrath *et al.*, 2013; Melton *et al.*, 2014; Emerson & de Vet, 2015), this is because the kinetics of Fe(II) are critically dependent upon pH and oxygen concentration (Stumm & Morgan, 1996; Emerson & Weiss, 2004).

Fairly strict chemical realities confine the niches of circumneutral FeOB (Emerson *et al.*, 2010; Vollrath *et al.*, 2012). These limits are due to the rapid abiotic oxidation of Fe(II) at circumneutral pH (Neubauer *et al.*, 2002; Edwards *et al.*, 2004; James & Ferris, 2004; Ferris, 2005; Druschel *et al.*, 2008; Emerson *et al.*, 2010; Emerson, 2012). At pH 7, the half-life for Fe(II) in fully aerated freshwater is <15 min (Stumm & Morgan, 1996; Emerson & Weiss, 2004; Emerson, 2012; Emerson & de Vet, 2015); this half-life increases to about 2 hours at 12°C (Emerson and Weiss, 2004; Emerson & de Vet, 2015).

Low levels of dissolved O_2 slow abiotic oxidation, making it possible for bacteria to compete with abiotic oxidation of Fe(II) (Stumm & Morgan, 1996; Emerson & Moyer, 1997; Sobolev & Roden, 2001; James & Ferris, 2004; Roden *et al.*, 2004; Ferris, 2005; Weber *et al.*, 2006; Rentz *et al.*, 2007; Druschel *et al.*, 2008; Emerson *et al.*, 2010; McBeth *et al.*, 2011; Vollrath *et al.*, 2012; Vollrath *et al.*, 2013; Melton *et al.*, 2014). Within these narrowly-constrained zones, however, these organisms thrive (Emerson & Moyer, 1997; Sobolev & Roden, 2001; Neubauer *et al.*, 2002; Emerson & Weiss, 2004; James & Ferris, 2004; Roden *et al.*, 2004; Ferris, 2005; Weber *et al.*, 2006; Druschel *et al.*, 2008; Emerson, 2012; Vollrath *et al.*, 2013; Melton *et al.*, 2014; Emerson & de Vet, 2015). Generally, these conditions arise at redox boundaries between an anoxic Fe(II) source, and an oxygenated body of water (James & Ferris 2004; Emerson *et al.*, 2010; Gault *et al.*, 2011; McBeth *et al.*, 2011; Melton *et al.*, 2014).

The oxidation of Fe(II) by O_2 at circumneutral pH was initially assumed to be a completely abiotic process, but is now known to be microbially mediated (Weber *et al.*, 2006; Melton *et al.*, 2014). The rapid abiotic oxidation of Fe(II) in fully aerated systems at circumneutral pH makes the kinetics of iron oxidation at circumneutral pH extremely challenging for FeOB (Neubauer *et al.*, 2002; Emerson *et al.*, 2010; Gault *et al.*, 2011). Metabolic reactions must be both thermodynamically and kinetically favourable (Bird *et al.*, 2011), and the energy available from Fe(II) oxidation is low (Figure 1.1; Ehrlich *et al.*, 1991; Neubauer *et al.*, 2002). When O_2 levels are approximately 10% of air saturation, microbial oxidation can effectively compete with abiotic oxidation (Roden *et al.*, 2004; Roden *et al.*, 2012).

1.7 Kinetics of Fe(II) Oxidation

FeOB survive by harnessing energy liberated when they catalyze the transfer of electrons from a reduced species (in this case, Fe(II)) to an oxidized species (in this case, O_2) (Figure 1.1; Bethke *et al.*, 2011; Bird *et al.*, 2011). FeOB then use the energy to carry out cellular functions such as maintenance, as well as to create biomass (Bethke *et al.*, 2011). FeOB obtain both energy and reducing power from Fe(II)-oxidation to fix CO^2 (Emerson & Moyer, 1997; Weber *et al.*, 2006; Bird *et al.*, 2011).

Both bacterial and abiotic oxidation of Fe(II) in the presence of oxygen depend on the Fe(III)/Fe(II) and O_2/H_2O redox couples, which have half-cell reactions:

$$Fe^{3+} + e^- \leftrightarrow Fe^{2+} \qquad (1.1)$$

$$0.25\ O_2 + H^+ + e^- \leftrightarrow 0.5H_2O \qquad (1.2)$$

with the corresponding overall reaction

$$Fe^{2+} + 0.25O_2 + H^+ \leftrightarrow Fe^{3+} + 0.5H_2O \qquad (1.3).$$

For the above reaction, $\Delta G° = -48.4$ kJ/mol at standard conditions (Stumm & Morgan, 1996; James & Ferris, 2004).

Oxidation of Fe(II)at circumneutral pH always comes with the concomitant precipitation and hydrolysis of Fe(III) (King *et al.*, 1995; Schwertmann *et al.*, 1995; Ferris, 2005; Emerson *et al.*, 2010), according to

$$Fe^{2+} + 3H_2O \leftrightarrow Fe(OH)_3 + 3H^+ \qquad (1.4).$$

In this case, $\Delta G° = -44.2$ kJ/mol at standard conditions (Stumm & Morgan, 1996); and the precipitation of hydrous ferric oxides (HFO) increases the energy FeOB can harness from Fe(II) oxidation (James & Ferris, 2004), but values of approximately $\Delta G = -90$ kJ/mol for environmental conditions have been reported (James & Ferris, 2004; Roden *et al.*, 2004; Emerson *et al.*, 2010).

Geochemical conditions can control microbial ecology in a number of ways; one of the most significant when assessing microbial and chemical contributions is the rate at which Fe(II) oxidation occurs (Druschel *et al.*, 2008). The rate law for the abiotic oxidation of iron by oxygen can be written as

$$\frac{-\mathrm{d}[Fe^{2+}]}{\mathrm{dt}} = \frac{\mathrm{k}[O_2][Fe^{2+}]}{[H^+]^2} \qquad (1.5)$$

with the overall fourth-order rate constant $\mathrm{k} = 3 \times 10^{-12}$ mol L^{-1} min^{-1} at 25 °C (Stumm & Morgan, 1996).

A very useful simplification of this rate law can be introduced when pH and dissolved O_2 are constant; the rate expression becomes pseudo-first order with respect to Fe(II)

$$-\frac{\mathrm{d}[Fe^{2+}]}{\mathrm{dt}} = \mathrm{k}'[Fe^{2+}] \qquad (1.6)$$

with rate constant, k'

$$\mathrm{k}' = \frac{\mathrm{k}[O_2]}{[H^+]^2} \qquad (1.7).$$

This rate law describes the rate for homogenous, abiotic Fe(II) oxidation, where both Fe(II) and oxygen are dissolved (Melton *et al.,* 2014). The abiotic oxidation rate is proportional to O_2 concentration and pH (Singer & Stumm, 1970; Rentz *et al.*, 2007).

Two additional processes are known to contribute to the total oxidation rate of Fe(II) at circumneutral pH: microbially-mediated Fe(II) oxidation, and autocatalytic, or heterogeneous Fe(II) oxidation (Sung & Morgan, 1980; Wehrli *et al.*, 1989; Rentz *et al.*, 2007; Emerson, 2012; Vollrath *et al.*, 2012; Melton *et al.*, 2014). Autocatalytic Fe(II) oxidation occurs when precipitated Fe(III) oxyhydroxides act as an adsorbent for dissolved Fe(II), which is then heterogeneously oxidized by oxygen; the reductant and oxidant are in two different physical phases (Melton *et al.*, 2014).

The reaction rates of autocatalytic and microbial Fe(II)oxidation are significantly (as much as six-fold) higher than that of homogeneous Fe(II) oxidation (Neubauer *et al.*, 2002; James &

Ferris, 2004; Rentz *et al.*, 2007; Druschel *et al.*, 2008; Melton *et al.*, 2014). As a consequence, the biogenic mineral product is a substrate competitor for microbial Fe(II)-oxidation (Warren & Ferris, 1998; Neubauer *et al.*, 2002; James & Ferris, 2004; Rentz *et al.*, 2007; Melton *et al.*, 2014). This presents another hurdle for FeOB to overcome; not only must they compete with their own product, unless Fe(III) precipitates are prevented from accumulating cells may become entombed in them, cutting off their energy source (Emerson *et al.*, 2010; Vollrath *et al.*, 2012).

1.8 Hydrous Ferric Oxides

Hydrous ferric oxides (HFO) are the nanoparticulate, poorly crystalline Fe(III) minerals produced by the hydrolysis of Fe(III) which follows Fe(II)-oxidation (Bird *et al.*, 2001; Kasama & Murakami, 2001; Emerson & Weiss, 2004; Druschel *et al.*, 2008; Blöthe & Roden, 2009; Duckworth *et al.*, 2009; Emerson, 2012; Kato *et al.*, 2012; Melton *et al.*, 2014; Ferris *et al.*, in press) most commonly two-line ferrihydrite, but they can also crystallize as goethite, lepidocrocite, akaganeite, hematite, and magnetite (Fortin & Langley, 2005; Melton *et al.*, 2014; Ferris *et al.*, in press).

Bacteriogenic iron oxides (BIOS) refer to HFO that precipitate in close association with bacterial cells, ether as a result of direct microbial enzymatic oxidation or through autocatalysis (Warren & Ferris, 1998; Banfield *et al.*, 2000; Châtelier *et al.*, 2001; Rentz *et al.*, 2007; Emerson *et al.*, 2010; Emerson, 2012; Vollrath *et al.*, 2013; Ferris *et al.*, in press); typically intermixed with cellular debris and associated organic matter (Gault *et al.*, 2011). The most common mineral associated with *Gallionella* and *Leptothrix* is 2-line ferrihydrite (Kasama & Murakami, 2001; Kennedy *et al.*, 2003; James & Ferris, 2004; Vollrath *et al.,* 2013); this is the most common mineral produced in circumneutral systems (Kasama & Murakami, 2001; Kennedy *et al.*, 2003; Ferris, 2005; Emerson *et al.*, 2010).

Changes in physicochemical conditions, such as temperature, iron and oxygen concentration, and the presence of organic matter or other chemical species, can modify the characteristics of the mineral precipitates, such as the size and crystal properties of iron oxides (Sung & Morgan, 1980; Schwertmann *et al.*, 1985; Schwertmann & Cornell, 1991; Cornell & Schwertmann, 1996; Berquo *et al.*, 2009; Vollrath *et al.*, 2013). It is thought that low oxidation rates should favor the growth of crystalline oxides, while XRD-amorphous and poorly crystalline precipitates, such as ferrihydrite, are expected at higher oxidation rates (Vollrath *et al.*, 2013). Increasing oxidation rates lead to higher intermediate concentrations of dissolved Fe(III), which

promotes nucleation of more soluble and less stable iron oxides (Steefel & Van Cappellen, 1990; Vollrath *et al.*, 2013).

1.9 Redox Potential

When they transfer electrons, microbes oxidize the electron donor species and reduce the electron acceptor, directly regulating the redox state and chemical properties of their environment (Bethke *et al.*, 2011). This is not the only way FeOB can manipulate the geochemistry of their environment. Microaerophilic FeOB contribute to iron cycling in oxic environments where they couple metabolism to growth (Ghiorse, 1984; Emerson & Moyer, 1997; Sobolev & Roden, 2001; Edwards *et al.*, 2003; Weber *et al.*, 2006). FeOB may significantly impact the geochemistry of their environment as they control the movement of chemical species within their niche (Druschel *et al.*, 2008). Additionally, the presence of organic ligands may cause changes in the coordination chemistry of iron and hence its redox kinetics (Stone, 1997; King, 1998; Emerson & Weiss, 2004).

Redox potential is related to ΔG by

$$E = -\frac{\Delta G}{nF} \qquad (1.8).$$

In this way, redox potential represents the chemical energy available in a system (DeLaune & Reddy, 2004).The redox state of an environment is inherently linked to redox potential, which is described by the Nernst equation:

$$E = E^0 + \frac{RT}{nF} \ln \frac{[\text{oxidized species}]}{[\text{reduced species}]} \qquad (1.9)$$

where E is the redox potential of the cell (mV), E° is the electrochemical potential of the cell at standard conditions, R is the universal gas constant, T is absolute temperature, n is the number of electrons participating per ion, F is Faraday's constant, and Q is the reaction quotient, $\frac{[\text{oxidized species}]}{[\text{reduced species}]}$. Environmental factors including temperature, pH, and the presence of multiple redox couples can influence the redox potential of a microbial system, in addition to microbe-specific factors including nutrient levels, solution chemistry, growth substrate factors, and oxygen

availability (Newman & Banfield, 2002). Redox potential is sensitive even to subtle changes in chemical speciation. This encompasses the distribution of all species of H, C, N, O, S, Mn, Fe, Co, and Cu in aqueous systems (Bohn, 1971). It is important to note that redox potential is determined by the ratio of oxidized and reduced chemical species in the system, and not their absolute concentration (Whitfield, 1969). Considering its sensitivity to so many elements, it is no surprise that redox potential is intricately linked to biological activity (Swerhone *et al.*, 1999; Ferris, 2005).

Redox potentials are measured in soil, biological, limnological, geochemical, and marine systems because all microbial bioenergetic metabolic reactions are redox reactions (Bohn, 1971). In this way, all metabolically active microorganisms directly influence the relative abundance of redox active substances in their environment (van Bochove *et al.*, 2002). Microbes interact with their environment by driving redox reactions that have the potential to cause significant changes in pH and redox potential (Druschel *et al.*, 2008). Continuous measurement of redox potential over time in soils and wetlands using Pt electrodes has been used as an indicator of transitions from aerobic to anaerobic conditions with a concomitant change in microbial community composition (van Bochove *et al.*, 2002).

In the context of circumneutral iron-oxidizing microbial communities, it is possible to simplify the Nernst equation if certain conditions are met. If the concentrations of all other redox active species remain constant, as in the case of pseudo-first order kinetics (Wiuf & Feliu, 2013), the Nernst equation can be rewritten to attribute all changes in redox potential to redox transformations of iron species (Nemati & Webb, 1997):

$$E = E^0 + \frac{RT}{nF} \ln \frac{[Fe^{3+}]}{[Fe^{2+}]} \qquad (1.10).$$

In this special case of steady-state conditions, with no other relevant redox couples changes in the redox state of the system are directly attributed to changes in the oxidation states of iron.

1.10 Linking Redox Potential to Fe(II)-Oxidizing Microbial Activity

As has been established, biological activity exerts a direct influence on redox potential in circumneutral Fe(II)-oxidizing systems (Druschel *et al.*, 2008; Bethke *et al.*, 2011). As redox potential represents a physically-constrained measurement of a biological system, it provides an opportunity

to examine how biological activity influences physicochemical system behaviour, in a way that can be compared and distinguished from abiotic systems. In light of the fact that FeOB are known to contribute to biocorrosion (McBeth *et al.*, 2011), and, knowing that redox and phase transformations of Fe are particularly sensitive to bacterial manipulation (Ferris, 2005), electrochemical noise analysis becomes a technique worth exploring in the context of studying FeOB. Electrochemical noise analysis was first identified in 1968 (Iverson, 1968), and has evolved as a suite of techniques to study corrosion mechanisms based on fluctuations in current and potential (Cottis, 2001 and references therein). This link is what initially prompted the exploration of time series and signal processing techniques.

Electrochemical noise analysis uses time series techniques to characterize fluctuations of current and potential (Gabrielli *et al.*, 1993a; Gabrielli *et al.*, 1993b; Bertocci *et al.*, 1998; Cottis, 2001, and references therein). Generally, this includes both frequency and time domain signal processing techniques. The oft-employed Fourier transform does not recommend itself well to the analysis of biologically-influenced systems. This is because Fourier analysis requires that the time series being processed be stationary, linear, and uncorrelated. However, physiological time series are inherently far-from-equilibrium, non-linear, and non-stationary, and exhibit long-range temporal correlation (Eke *et al.*, 2002).

1.11 Fluctuation Analysis and Brownian Motion

Generally, fluctuations in potential are sub-mV in size (Gabrielli *et al.*, 1993a), and are thought to arise from random particle collisions (Gabrielli *et al.*, 1993a). The patterns in fluctuations which allow them to be distinguished are the result of interactions between disturbances from control mechanisms, either internal or external to the system of study (Eke *et al.*, 2000). This basis in particle collisions has very important implications for how these systems can be modelled. By examining fluctuations in redox potential as they arise from the random passive movement, or diffusion, of dissolved chemical species and the interactions of these species with the electrode surface, we can adopt the Brownian motion, or random walk, model to characterize them. We will return to this point momentarily.

A process is said to be strictly stationary if all moments (e.g., mean; variance; kurtosis) do not change with time t and, in particular, do not depend on the length of the considered time series over multiple time series realizations (Witt & Malamud, 2013). A weakly stationary process has

mean and variance for different sections of the time series which have approximately similar autocorrelation functions (taken over many realizations) (Witt & Malamud, 2013). Stationary processes are described by measures of central tendency, such as mean, mode, and median (Hardstone *et al.*, 2012), and have a characteristic scale or size, represented by the mean of the distribution (Hardstone *et al.*, 2012). Gaussian white noise is a classic example of a stationary process (Witt & Malamud, 2013). In white noise, the values are uncorrelated; each measurement has an equal likelihood of being followed by a larger or smaller value (Witt & Malamud, 2013).

The classic example of a non-stationary process would be Brownian motion (Metzler & Klafter, 2000; Witt & Malamud, 2013). Brownian motion is a stochastic process characterized by increments which are stationary, independent, and Gauss-distributed (Wiener, 1923; Eliazar & Shlesinger, 2013). The properties of a random walk are illustrated in Figure 1.2. Note here the distinction between uncorrelated values and uncorrelated increments. The Gaussian distribution of the Brownian increments implies that Brownian motion does not fluctuate wildly (Mandelbrot, 1997; Mandelbrot *et al.*, 2010; Eliazar & Shlesinger, 2013). Brownian motion has independent increments; implying no correlation in between values (Eliazar and Shlesinger, 2013). Correlated processes with stationary, Gauss-distributed increments are called fractional Brownian motions (Eliazar & Shlesinger, 2013).

1.11.1 Correlation Behaviour

Correlation is a property of a time series or process that describes the statistical dependence of directly and distantly neighboured values (Witt & Malamud, 2013). These statistical dependencies can be assessed in many different ways, including joint probability distributions, autocorrelation functions (Shannon & Weaver 1949) or correlation coefficients (Witt & Malamud, 2013). Long-range correlations are where all or almost all values are correlated with one another, that is, values are correlated with one another at very long lags in time (Taqqu & Samorodnitsky, 1992; Beran 1994; Witt & Malamud, 2013); what is 'very long' is dependent on the process being observed. An example of uncorrelated, positively correlated, and anti-correlated walks is illustrated in Figure 1.3.

Persistence is where large values tend to follow large ones, and small values tend to follow small ones, on average, more of the time than if the time series were uncorrelated (Witt & Malamud, 2013). This contrasts anti-persistence, where large values tend to follow small ones and small values large ones, again, on average, more of the time than if the time series were uncorrelated

(Witt & Malamud, 2013). The strength of both persistence and anti-persistence can vary from weak to very strong; as defined by the magnitude of the correlation coefficient (Witt & Malamud, 2013).

Long-range persistence has been quantified and explored for many geophysical time series and processes, as well as time series data in many other disciplines, both biological and physical. These include: the 1/f behaviour of voltage and current amplitude fluctuations in electronic systems modelled as a superposition of thermal noises (Schottky 1918; Johnson 1925; van der Ziel 1950), trajectories of tracer particles in hydrodynamic flows (Solomon *et al.*, 1993) and in granular material (Weeks *et al.*, 2000), neurosciences (Linkenkaer-Hansen *et al.*, 2001; Bedard *et al.*, 2006), biological receptor systems (Bahar *et al.*, 2001), human gait (Hausdorff *et al.*, 1996; Dingwell & Cusumano, 2010), human sensory motor control system (Cabrera & Milton, 2002; Patzelt *et al.*, 2007), heart beat intervals (Kobayashi & Musha, 1982; Peng *et al.*, 1993a; Goldberger *et al.*, 2002), and swimming behaviour of parasites (Uppaluri *et al.*, 2011; Witt & Malamud, 2013). Long-range persistence is also typical for musical pitch, rhythms, and loudness fluctuations (Voss & Clarke 1975; Jennings *et al.*, 2004; Hennig *et al.*, 2011; Levitin *et al.*, 2012; Witt & Malamud, 2013) and for dynamics on networks such as internet traffic (Leland *et al.*, 1994; Willinger *et al.*, 1997; Witt & Malamud, 2013).

1.12 Detrended Fluctuation Analysis

One frequently used method of assessing the strength of correlation or persistence in a time series, is detrended fluctuation analysis (DFA) (Peng *et al.*, 1994). DFA calculates a relationship between root-mean-square (RMS) fluctuation and time window length in time series fluctuation data. It is widely used in a number of disciplines, such as DNA sequences (Peng *et al.*, 1993b; Peng *et al.*, 1994), solar radio astronomy (Kurths *et al.*, 1995), heart rate variability (Peng *et al.*, 1993a; Peng *et al.*, 1995; Penzel *et al.*, 2003), river run-off series (Koscielny-Bunde *et al.*, 2006), long-term weather records and simulations (Fraedrich & Blender 2003), liver cell function in rats (Ramanujan *et al.*, 2006), atmospheric pollutant chemistry (Varotsos *et al.*, 2005), and gait analysis (Dingwell & Cusumano, 2010).

The first step in DFA is to generate a random walk profile of the realization by subtracting the mean and integrating the time series. The profile (length n) is divided into j windows of length s and local linear least squares fits are calculated for each window. Fluctuations are measured by subtracting the linear trend calculated for each window from the integrated random walk profile and summing the differences from the local trend. The root-mean-square (RMS) deviations are

subsequently averaged across the corresponding number of windows j and plotted against window size s in log-log space. A linear relationship between window size and average RMS deviation indicates scale-invariant power law behavior

$$\mathrm{RMS} \cong \mathrm{C}s^{\alpha} \qquad (1.11)$$

where C represents a constant fluctuation coefficient and the scaling exponent α is a quantitative measure of long-range persistence, or time-domain self-similarity, in the time series (Witt & Malamud, 2013). The scaling exponent is estimated by fitting experimental data to the relationship

$$\log \mathrm{RMS} = \alpha \log s + \log \mathrm{C} \qquad (1.12).$$

1.13 Anomalous Diffusion

Brownian motion describes the motion of a single particle diffusing according to Fick's laws (Metzler & Klafter, 2000). The path of the particle is called a random walk; and this random walk can be experimentally observed, creating a link between the microscopic dynamics of small atoms bombarding a larger particle in suspension, and macroscopic observables like diffusion coefficient (Metzler & Klafter, 2000), and, perhaps, correlation or scaling coefficients. In a plot of the mean-squared-displacement (MSD) through time, a Brownian motion will give a linear result (Metzler & Klafter, 2000; Witt & Malamud, 2013; Jeon *et al.*, 2014; Kim, 2014). When the MSD is described by non-linear growth through time, diffusion is described as "anomalous" (Metzler & Klafter, 2000; Witt & Malamud, 2013; Jeon *et al.*, 2014; Kim, 2014). Anomalous diffusion was first described in 1926 (Richardson, 1926; Metzler & Klafter, 2000). Both anomalous diffusion and fractional Brownian motion have been described in a wide variety of physical systems (Metzler & Klafter, 2000; Witt & Malamud, 2013, and references therein).

Diffusion processes are known to be self-affine, with self-similar spatial trajectories (Levy, 1965; Feller, 1971; Mandelbrot, 1983; Fedder, 1988; Falconer, 1990; Takayasu, 1990; Gouyet, 1992; Hughes, 1995; Metzler & Klafter, 2000). A non-stationary stochastic process is said to be self-affine if a rescaled version of a small part of its time series has the same properties as a larger part (Hardstone *et al.*, 2012). Physiological time series often exhibit statistical self-affine properties (Eke *et al.*, 2000, Eke *et al.*, 2002; Hardstone *et al.*, 2012). Self-affine processes have at least one

measurement, temporal, or statistical distribution which follows a power-law function, which is the only mathematical function without a characteristic scale (Hardstone *et al.*, 2012). Self-affine phenomena are therefore called "scale-free" (Hardstone *et al.*, 2012). By contrast to stationary processes which can be described by measures of central tendency, a scale-free process has no typical scale or size (Hardstone *et al.*, 2012). Scale-free phenomena are better described by the exponent of a power-law function, because it captures the relationship between objects or fluctuations on different scales (Hardstone *et al.*, 2012).

In the context of DFA, and conforming with random walk theory, Brownian motion should give rise to a scaling exponent, $\alpha = 1$ (Metzler & Klafter, 2000; Ramanujan *et al.*, 2006), and $1 < \alpha < 2$ relating to processes exhibiting fractional Brownian motion (Metzler & Klafter, 2000; Eliazar & Shlesinger, 2013). Additionally, in random uncorrelated time series $\alpha = 0.5$, whereas $\alpha < 0.5$ indicates negative persistence and $\alpha > 0.5$ indicates positive persistence (Peng *et al.*, 1994; Peng *et al.*, 1995; Metzler & Klafter, 2000; Hardstone *et al.*, 2012; Witt & Malamud, 2013). This further implies that exponents deviating from 1 represent systems governed by anomalous diffusion processes.

1.14 Relating Diffusion to Electrode Response

The relationship between diffusion coefficients and electrochemical potential was first described by Oldham (1966):

$$E_{cell} = E^0 + \frac{RT}{2nF}\ln\left[\frac{D'}{D}\right] + \frac{RT}{nF}\ln\left[\frac{\sqrt{\tau} - \sqrt{t}}{\sqrt{t}}\right] \qquad (1.13)$$

E_{cell} is the electrochemical potential of the cell, E° is the electrochemical potential of the cell at standard conditions, R is the universal gas constant, T is absolute temperature (K), n is the number of participating electrons, F is Faraday's constant, D' is the diffusion coefficient of the oxidized species, D is the diffusion coefficient of the reduced species, t is the time from the onset of the reaction, and τ is the reaction transition time. The relationship between diffusivity and potential was also described elsewhere (Frateur *et al.*, 1999; Mampallil *et al.*, 2013). This equation provides a link between the system-scale observed electrode response, and microscopic behaviour of dissolved ions in solution.

1.15 Electrode Selection

Here, redox potential was measured using a standard laboratory Pt electrode. Pt electrodes have been used extensively in environmental electrochemical studies (Flühler *et al.*, 1976; Faulkner *et al.*, 1989; Vershinin & Rozanov, 1993; Sampedro *et al.*, 1999; Swerhone *et al.*, 1999; van Bochove *et al.*, 2002; Kasem & Jones, 2008; Ojumu *et al.*, 2008), often for measuring redox potential and dissolved O_2 (Whitfield, 1969; Swerhone *et al.*, 1999). These electrodes have been deployed in studies lasting months and years, with either no or minimal changes in performance over the time scale of the study (Smith *et al.*, 1978; Austin & Huddleston, 1999; Swerhone *et al.*, 1999; van Bochove *et al.*, 2002), and are known to be reliable under a variety of environmental conditions (Kasem & Jones, 2008).

Some of the benefits of using Pt electrodes include that they can generally be approximated to be inert under most environmental conditions (Bohn, 1971), that they act as a reference without any associated solvated ions (Kasem & Jones, 2008), and that they are especially responsive to iron species when concentrations exceed 10^{-5} M (Vershinin & Rozanov, 1993; Stumm & Morgan, 1996).

When describing electrode response in diffusion-limited systems, both theoretical and laboratory studies have indicated that current is influenced by the redox state of the species in bulk solution, and not by the electrode making the measurements (Mampallil *et al.*, 2013); this is important as it confirms that redox potential and fluctuations being measured arise from the dynamics of the system as a whole, and not from the microenvironment immediately surrounding the electrode tip.

1.16 Organization

The chapters are organized as follows: this introduction was designed outline why time series measurements of redox potential fluctuations are worth measuring, and develop a framework for the physicochemical significance of these results. The second chapter describes an instrument optimized to collect suitable time series for this type of analysis. This was necessary as the novelty of this type of analysis meant that few existing instruments could collect appropriate data sets and those few were limited by both time series length and maximum measurement frequency. The third chapter describes a study at the Äspö Hard Rock Laboratory in Oskarshamm, Sweden, where fluctuation analysis was implemented in a bioreactor fed by anaerobic, Fe(II)-rich groundwater. By

comparing the FeOB-active reactor to its BIOS-free inflow pipe, it could be determined that the activity of FeOB influenced the fluctuation behaviour in a consistent, statistically significant way. The fourth chapter describes a study using a series of microcosms to compare fluctuation behaviour with a variety of different rates and settings, such as the presence and absence of a reactive substrate, as well as biological and chemical systems. The final chapter places these results in context of where future research might go.

1.17 References

Anderson CR, Pedersen K (2003) In situ growth of Gallionella biofilms and partitioning of lanthanides and actinides between biological material and ferric oxyhydrides. *Geobiology*, **1**, 169-178.

Anderson CR, James RE, Fru EC, Kennedy CB, Pedersen K (2006) In situ ecological development of a bacteriogenic iron oxide-producing microbial community from a subsurface granitic rock environment. *Geobiology*, **4**, 29-42.

Austin WE, Huddleston JH (1999) Visibility of permanently installed platinum redox electrodes. *Soil Science Society of America Journal*, **63**, 1757-1762.

Banfield JF, Welch SA, Zhang H, Ebert TT, Penn RL (2000) Aggregation-based growth and microstructure development in natural iron oxyhydroxide biomineralization products. *Science*, **289**, 751-754.

Bedard C, Kroeger H, Destexhe A (2006) Does the 1/f frequency scaling of brain signals reflect self-organized critical states? *Physical Review Letters*, **97**, 118102.

Beran J (1994) *Statistics for long-memory processes*. Chapman & Hall/CRC, New York.

Berquo TS, Erbs JJ, Lindquist A, Penn RL, Banerjee SK (2009) Effects of magnetic interactions in antiferromagnetic ferrihydrite particles. *Journal of Physics: Condensed Matter*, **21**, 176005.

Bertocci U, Frydman J, Gabrielli C, Huet F, Keddam, MJ (1998) Analysis of Electrochemical Noise by Power Spectral Density Applied to Corrosion Studies. *Journal of the Electrochemical Society*, **145**, 2780-2786.

Bethke CM, Sanford RA, Kirk MF, Jin Q, Flynn TM (2011) The Thermodynamic Ladder in Geomicrobiology. *American Journal of Science*, **311**, 183-210.

Bird LJ, Bonnefoy V, Newman DK (2011) Bioenergetic challenges of microbial iron metabolisms. *Trends in Microbiology*, **19**, 330-340.

Blöthe M, Roden EE (2009) Microbial Iron Redox Cycling in a Circumneutral-pH Groundwater Seep. *Applied and Environmental Microbiology*, **75**, 468-473.

Bohn HI (1971) Redox Potentials. *Soil Science*, **112**, 39-45.

Bruun A-M, Finster K, Gunnlaugsson H, Nornberg P, Friedrich MW (2010) A comprehensive investigation on iron cycling in a freshwater seep including microscopy, cultivation and molecular community analysis. *Geomicrobiology Journal*, **27**, 15–34.

Cabrera JL, Milton JM (2002) On–off intermittency in a human balancing task. *Physical Review Letters*, **89**, 158702.

Châtellier X, Fortin D, West M, Leppard GG, Ferris FG (2001) Effect of the presence of bacterial surfaces during the synthesis of Fe-oxides by oxidation of ferrous ions. *European Journal of Mineralogy*, **13**, 705-714.

Cornell RM, Schwertmann U (1996) *The Iron Oxides: Structure, Properties, Reactions, Occurrences and Uses.* Wiley VCH, Weinheim, New York.

Cottis RA (2000) Interpretation of Electrochemical Noise Data. *Corrosion*, **57**, 265-285.

Davison W, Seed G (1983) The kinetics of the oxidation of ferrous iron in synthetic and natural waters. *Geochimica et Cosmochimica Acta* **47**, 67–79.

Dingwell JB, Cusumano JP (2010) Re-Interpreting Detrended Fluctuation Analyses of Stride-To-Stride Variability in Human Walking. *Gait Posture*, **32**, 348-353.

Druschel GK, Emerson D, Sutka R, Suchecki P, Luther GW (2008) Low-oxygen and chemical kinetic constraints on the geochemical niche of neutrophilic iron(II) oxidizing organisms. *Geochimica et Cosmochimica Acta*, **72**, 3358-3370.

Duckworth OW, Holmström SJM, Peña J, Sposito G (2009) Biogeochemistry of iron oxidation in a circumneutral freshwater habitat. *Chemical Geology*, **260**, 149-158.

Edwards KJ, Bach W, Rogers DR (2003) Geomicrobiology of the ocean crust: a role for chemoautotrophic Fe-bacteria. *Biology Bulletin*, **204**, 180–185.

Edwards KJ, Bach W, McCollom TM, Rogers DR (2004) Neutrophilic iron-oxidizing bacteria in the ocean: their habitats, diversity, and roles in mineral deposition, rock alteration, and biomass production in the deep-sea. *Geomicrobiology Journal*, **21**, 393–404.

Ehrenberg CG (1837) Remarks on the real occurrence of fossil infusoria, and their extensive diffusion. *Taylor's Scientific Memoirs* 1:400–13, plate V.

Ehrlich HL (2002) *Geomicrobiology* (4th ed.). Marcel Dekker, New York, pp. 768–800.

Eke A, Herman P, Bassingthwaite JB, Raymond GM, Percival DB, Cannon M, Balla I, Ikrenyi C (2000) Physiological time series: distinguishing fractal noises from motions. *European Journal of Physiology*, **439**, 403-415.

Eke A, Herman P, Kocsis L, Kozak LR (2002) Fractal characterization of complexity in temporal physiological signals. *Physiologic Measurement,* **23**, R1-R38.

Eliazar II, Shlesinger MF (2013) Fractional motions. *Physics Reports*, **527**, 101-129.

Emerson D, Revsbech NP (1994) Investigation of an Iron-Oxidizing Microbial Mat Community Located near Aarhus, Denmark: Field Studies. *Applied and Environmental Microbiology*, **60**, 4022-4031.

Emerson D, Moyer CL (1997) Isolation and characterization of novel iron-oxidizing bacteria that grow at circumneutral pH. *Applied and Environmental Microbiology*, **63**, 4784–92.

Emerson D, Weiss JV, Megonigal JP (1999) Iron-oxidizing bacteria are associated with ferric hydroxide precipitates (Fe-plaque) on the roots of wetland plants. *Applied and Environmental Microbiology*, **65**, 2758–2761.

Emerson D (2000) Microbial oxidation of Fe(II) and Mn(II) at circumneutral pH. In: Lovely DR (ed.), *Environmental Microbe-Metal Interactions*. ASM Press, Washington, DC, pp. 31–52.

Emerson D, Weiss JV (2004) Bacterial iron oxidation in circumneutral freshwater habitats: findings from the field and the laboratory. *Geomicrobiology Journal*, **21**, 405–414.

Emerson D, Fleming EJ, McBeth JM (2010) Iron-oxidizing bacteria: an environmental and genomic perspective. *Annual Reviews of Microbiology*, **64**, 561–583.

Emerson D (2012) Biogeochemistry and microbiology of microaerobic Fe(II) oxidation. *Transactions of the Biochemical Society*, **40**, 1211-1216.

Emerson D, Roden E, Twining BS (2012) The microbial ferrous wheel: iron cycling in terrestrial, freshwater, and marine environments. *Frontiers in Microbiology*, **3**, 383.

Emerson D, de Vet W (2015) The Role of FeOB in Engineered Water Ecosystems: A Review. *Journal AWWA*, **107**, E47-E57.

Ehrlich HL, Ingledew WJ, Salerno JC (1991) Iron- and manganese oxidizing bacteria. In JM Shively and LL Barton (ed.), *Variations in autotrophic life*. Academic Press, San Diego, Calif. p 147-170.

Falconer K (1990) *Fractal Geometry: Mathematical Foundations and Applications*, Wiley, Chichester, UK.

Faulkner SP, Patrick WH, Gambrell RP (1989) Field techniques for measuring wetland soil parameters. *Soil Science Society of America Journal*, **59**, 1044-1051.

Feder J (1988) *Fractals*, Plenum, New York.

Feller W (1971) *An Introduction to Probability Theory and its Applications*, Vol. 2, Wiley, New York.

Ferris FG (2005) Biogeochemical properties of bacteriogenic iron oxides. *Geomicrobiology Journal*, **22**, 79–85.

Ferris FG, Enright AML, Fortin D, Clark ID. In press. Rates of Fe(II)-oxidation and Solubility of Bacteriogenic Iron Oxides. *Geomicrobiology Journal*.

Fleming EJ, Langdon AE, Martinez-Garcia M, Stepanauskas R, Poulton NJ, Masland EDP, Emerson D (2011) What's new is old: resolving the identity of Leptothrix ochracea using single cell genomics, pyrosequencing and FISH. *PLoS ONE*, **6**, 1–10.

Fleming EJ, Davis, RE, McAllister SM, Chan CS, Moyer CL, Tebo BM, Emerson D (2013) Hidden in plain sight: discovery of sheath-forming, iron-oxidizing Zetaproteobacteria at Loihi Seamount, Hawaii, USA. *FEMS Microbiology Ecology*, **85**, 116–127.

Flühler H, Ardakani MS, Stolzy LH (1976) Field measured nitrous oxide concentrations, redox potentials, oxygen diffusion rates, and oxygen partial pressures in relation to denitrification. *Soil Science*, **122**, 107-114.

Fortin D, Langley S (2005) Formation and occurrence of biogenic iron-rich minerals. *Earth Sciences Reviews*, **72**, 1-19.

Fraedrich K, Blender R (2003) Scaling of atmosphere and ocean temperature correlations in observations and climate models. *Physical Review Letters*, **90**, 108501.

Frateur I, Bayet E, Keddam M, Tribollet B (1999) Local redox potential measurement. *Electrochemistry Communications*, **1**, 336-340.

Gabrielli C, Huet F, Keddam H (1993a) Fluctuations in electrochemical systems. I. General theory on diffusion limited electrochemical reactions. *Journal of Chemical Physics*, **99**, 7232-7239.

Gabrielli C, Huet F, Keddam M (1993b) Fluctuations in electrochemical systems. II. Application to a diffusion limited redox process. *Journal of Chemical Physics*, **99**, 7232-7239.

Gault AG, Ibrahim A, Langley S, Renaud R., Takahashi Y, Boothman C, Lloyd JR, Clark ID, Ferris FG, Fortin D (2011) Microbial and geochemical features suggest iron redox cycling within bacteriogenic iron oxide-rich sediments. *Chemical Geology*, **281**, 41-51.

Ghiorse WC, Ehrlich HL (1993) Microbial biomineralization of iron and manganese. In: Fitzpatrick RW, Skinner HCW (ed.) *Iron and manganese biomineralization processes in modern and ancient environments*. Cremlingen-Destedt, Germany: Catena. p 75–107.

Ghiorse WC (1984) Biology of iron-and manganese-depositing bacteria. *Annual Reviews of Microbiology*, **38**, 515–50.

Gold T (1992) The deep, hot biosphere. *Proceedings of the National Academy of Sciences*, **89**, 6045–6049.

Goldberger AL, Amaral LAN, Hausdorff JM, Ivanov PCh, Peng C-K, Stanley HE (2002) Fractal dynamics in physiology: alterations with disease and aging. *Proceedings of the National Academy of Sciences*, **99**, 2466–2472.

Gouyet J-F (1992) *Physique et Structures Fractales*, Masson, Paris.

Haaijer SCM, Harhangi HR, Meijerink BB, Strous M, Pol A, Smolders AJP, Verwegen K, Jetten MSM, den Camp HJMO (2008) Bacteria associated with iron seeps in a sulfur-rich, neutral pH, freshwater ecosystem. *The ISME Journal*, **2**, 1231–42.

Hanert HH (1992) The genus Gallionella. In *The Prokaryotes*, Balows A, Truper HG, Dworkin M, Harder W, Scleifer KH (eds.), Springer-Verlag: New York, pp 4082-4088.

Harder EC (1919) *Iron-Depositing Bacteria and Their Geological Relations*. Washington, DC: US Geological Survey.

Hardstone R, Poil S-S, Schiavone G, Jansen R, Nikulin VV, Mansvelder HD, Linkenkaer-Hansen K (2012) Detrended fluctuation analysis: a scale-free view on neuronal fluctuations. *Frontiers in Physiology*, **3**, 450.

Hausdorff JM, Purdon PL, Peng CK, Ladin Z, Wei JY, Goldberger AL (1996) Fractal dynamics of human gait: stability of long-range correlations in stride interval fluctuation. *Journal of Applied Physiology*, **80**, 1448–1457.

Hennig H, Fleischmann R, Fredebohm A, Hagmayer Y, Nagler J, Witt A, Theis FJ, Geisel T (2011) The nature and perception of fluctuations in human musical rhythms. *PLoS One,* **7**, e26457.

Hughes BD (1995) *Random Walks and Random Environments*, Vol. 1: Random Walks, Oxford University Press, Oxford.

Ivarson KC, Sojak M (1978) Microorganisms and ochre deposition in field drains of Ontario. *Canadian Journal of Soil Science*, **58**, 1–17.

James RE, Ferris FG (2004) Evidence for microbial-mediated iron oxidation at a neutrophilic groundwater spring. *Chemical Geology*, **212**, 301-311.

Jennings H, Ivanov P, Martins A, Dasilva A, Viswanathan G (2004) Variance fluctuations in nonstationary time series: a comparative study of music genres. *Physica A*, **336**, 585–594.

Jeon J-H, Chechkin AV, Metzler R (2014) Scaled Brownian motion: a paradoxical process with a time dependent diffusivity for the description of anomalous diffusion. *Physical Chemistry Chemical Physics*, **16**, 15811.

Johnson JB (1925) The Schottky effect in low frequency circuits. *Physics Reviews*, **26**, 71–85.

Kappler A, Newman DK (2004) Formation of Fe(III)- minerals by Fe(II)-oxidizing photoautotrophic bacteria. *Geochimica et Cosmochimica Acta*, **68**, 1217–1226.

Kasama T, Marakami T (2001) The effect of microorganisms on Fe precipitation rates at neutral pH. *Chemical Geology*, **180**, 117 - 128.

Kasem KK, Jones S (2008) Platinum as a Reference Electrode in Electrochemical Measurements. *Platinum Metals Review*, **52**, 100-106.

Kashefi K, Holmes DE, Baross JA, Lovley DR (2003) Thermophily in the Geobacteraceae: Geothermobacter ehrlichii gen. nov., sp. nov., a novel thermophilic member of the Geobacteraceae from the "Bag City" hydrothermal vent. *Applied and Environmental Microbiology*, **69**, 2985–2993.

Kato S, Kikuchi S, Kashiwarbara T, Takahashi Y, Suzuki K, Itoh T, Ohkuma M, Yamagishi A (2012) Prokaryotic abundance and community composition in a freshwater iron-rich microbial mat at circumneutral pH. *Geomicrobiology Journal*, **29**, 896-905.

Kendall B, Anbar AD, Kappler A, Konhauser, KO (2012) The Global Iron Cycle. In *Fundamentals of Geobiology*. Knoll AH, Canfield DE, and Konhauser KO (eds.) Blackwell.

Kennedy CB, Scott SD, Ferris FG (2003) Characterization of bacteriogenic iron oxide deposits from axial volcano, Juan de Fuca Ridge, Northeast Pacific Ocean. *Geomicrobiology Journal*, **20**, 199-214.

Kennedy CB, Gault AG, Fortin D, Clark ID, Ferris FG (2011) Retention of iodide by bacteriogenic iron oxides. *Geomicrobiology Journal*, **28**, 387-395.

Kim H-J (2014) Anomalous diffusion induced by enhancement of memory. *Physical Reviews E*, **90**, 012103.

King DW (1998) Role of carbonate speciation on the oxidation rate of Fe(II) in aquatic systems. *Environmental Science & Technology*, **32**, 2997–3003.

King DW, Lounsbury HA, Millero FJ (1995) Rates and mechanism of Fe(II) oxidation at nanomolar total iron concentrations. *Environmental Science & Technology*, **29**, 818–24.

Kobayashi M, Musha T (1982) 1/f fluctuation of heartbeat period. *Transactions on Biomedical Engineering*, **29**, 456–457.

Konhauser KO, Newman DK, Kappler A (2005) The potential significance of microbial Fe(III) reduction during deposition of Precambrian banded iron formations. *Geobiology*, **3**, 167–177.

Kucera S, Wolfe RS (1957) A selective enrichment method for *Gallionella ferruginea*. *Journal of Bacteriology*, **74**, 344–349.

Kurths J, Schwarz U, Witt A (1995) Non-linear data analysis and statistical techniques in solar radio astronomy. *Lecture Notes in Physics*, **444**, 159–171, Springer, Berlin. doi: 10.1007/3-540-59109-5_48.

Langley S, Gault AG, Ibrahim A, Takahashi Y, Renaud R, Fortin D, Clark ID, Ferris FG (2009a) Sorption of strontium onto bacteriogenic iron oxides. *Environmental Science & Technology*, **43**, 1008-1014.

Langley S, Gault AG, Ibrahim A, Takahashi Y, Renaud R, Fortin D, Clark ID, Ferris FG (2009b) A comparison of the rates of Fe(III) reduction in synthetic and bacteriogenic iron oxides by Shewanella putrefaciens CN32. *Geomicrobiology Journal*, **26**, 57-70.

Leland WE, Taqqu MS, Willinger W, Wilson DV (1994) On the self-similar nature of ethernet traffic (Extended Version). *IEEE ACM Transactions on Networks*, **2**, 1–15.

Levitin DJ, Chordia P, Menon V (2012) Musical rhythm spectra from Bach to Joplin obey a 1/f power law. *Proceedings of the National Academy of Sciences*, **109**, 3716–3720.

Levy P (1965) *Processus stochastiques et mouvement Brownien*, Gauthier-Villars, Paris.

Linkenkaer-Hansen L, Nikouline V, Palva JM, Ilmoniemi RJ (2001) Long-range temporal correlations and scaling behavior in human brain oscillations. *The Journal of Neuroscience*, **21**, 1370–1377.

Little CTS, Glynn SEJ, Mills RA (2004) Four-hundred-and-ninety-million-year record of bacteriogenic iron oxide precipitation at sea-floor hydrothermal vents. *Geomicrobiology Journal*, **21**, 415–429.

Lovley DR, Baedecker MJ, Lonergan DJ, Cozzarelli IM, Phillips EJP, Siegel DI (1989) Oxidation of aromatic contaminants coupled to microbial iron reduction. *Nature*, **339**, 297-300.

Lovley DR (1991) Dissimilatory Fe(III) and Mn(IV) reduction. *Microbiology Reviews*, **55**, 259–287.

Mampallil D, Mathwig K, Kang S, Lemay SG (2013) Redox Couples with Unequal Diffusion Coefficients: Effect on Redox Cycling. *Analytical Chemistry*, **85**, 6053-6058.

Mandelbrot B, Taleb NN (2010) In: F. Diebold, N. Doherty, R. Herring (eds.). *The Known, the Unknown and the Unknowable in Financial Institutions*, Princeton University Press, Princeton, pp. 47–58.

Mandelbrot B (1983) *The Fractal Geometry of Nature*, Freeman, New York.

Mandelbrot B (1997) *Fractals and Scaling in Finance*, Springer, New York.

McBeth JM, Little BJ, Ray RI, Farrar KM, Emerson D (2011) Neutrophillic Iron-Oxidizing "Zetaproteobacteria" and Mild Steel Corrosion in Nearshore Marine Environments. *Applied and Environmental Microbiology*, **77**, 1405-1412.

Melton ED, Swanner ED, Behrens S, Schmidt C, Kappler A (2014) The interplay of microbially mediated and abiotic reactions in the biogeochemical Fe cycle. *Nature Reviews Microbiology*, **12**, 797-808.

Metzler R, Klafter J (2000) The random walk's guide to anomalous diffusion: a fractional dynamics approach. *Physics Reports*, **339**, 1-77.

Nemati M, Webb C (1997) A Kinetic Model for Biological Oxidation of Ferrous Iron by Thiobacillus ferrooxidans. *Biotechnology and Bioengineering*, **53**, 478-486.

Neubauer SC, Emerson D, Megonigal JP (2002) Life at the Energetic Edge: Kinetics of Circumneutral Iron Oxidation by Lithotrophic Iron-Oxidizing Bacteria Isolated from the Wetland-Plant Rhizosphere. *Applied and Environmental Microbiology*, **68**, 3988-3995.

Newman DK, Banfield JF (2002) Geomicrobiology: How Molecular-Scale Interactions Underpin Biogeochemical Systems. *Science*, **296**: 1071-1077.

Ojumu TV, Petersen J, Hansford GS (2008) The effect of dissolved cations on microbial ferrous-iron oxidation by Leptospirillum ferriphilum in continuous culture. *Hydrometallurgy*, **94**, 69-76.

Oldham KB (1966) A Diffusion-Layer Treatment of Transient Electrochemical Phenomena. *Electrochimica Acta*, **11**, 1475-1490.

Patzelt F, Riegel M, Ernst U, Pawelzik K (2007) Self-organized critical noise amplification in human closed loop control. *Frontiers in Computational Neuroscience*, **1**, doi: 10.3389/neuro.10.004.2007.

Peine A, Tritschler A, Küsel K, Peiffer S (2000) Electron flow in an iron-rich acidic sediment—evidence for an acidity-driven iron cycle. *Limnology and Oceanography*, **45**, 1077–1087.

Peng C-K, Buldyrev SV, Havlin S, Simons M, Stanley HE, Goldberger AL (1993a) Long-range anticorrelations and non-Gaussian behavior of the heartbeat. *Physics Review Letters*, **70**, 1343–1346.

Peng C-K, Buldyrev SV, Goldberger AL, Havlin S, Simons M, Stanley HE (1993b) Finite size effects on long-range correlations: implications for analyzing DNA sequences. *Physical Reviews E*, **47**, 3730–3733.

Peng C-K, Buldyrev SV, Havlin S, Simons M, Stanley HE, Goldberger AL (1994) Mosaic organization of DNA nucleotides. *Physical Reviews E*, **49**, 1685-1689.

Peng C-K, Havlin S, Stanley H, Goldberger A (1995) Quantification of scaling exponents and crossover phenomena in nonstationary heartbeat time series. *Chaos*, **5**, 82-87.

Penzel T, Kantelhardt JW, Becker HF, Peter JH, Bunde A (2003) Detrended fluctuation analysis and spectral analysis of heart rate variability for sleep stage and apnea identification. *Computational Cardiology*, **30**, 307–310.

Pierson BK, Parenteau MN, Griffin BM (1999) Phototrophs in high-iron-concentration microbial mats: physiological ecology of phototrophs in an iron-depositing hot spring. *Applied and Environmental Microbiology*, **65**, 5474–5483.

Puteanus D, Glasby GP, Stoffers P, Kunzendorf H (1991) Hydrothermal iron-rich deposits from the Teahitia-Mehitia and Macdonald hot spot areas, southwest Pacific. *Marine Geology*, **98**, 389–409.

Rabaey K, Rodriguez J, Blackall LL, Keller J, Gross P, Batstone D, Verstraete W, Nealson KH (2007) Microbial ecology meets electrochemistry: electricity-driven and driving communities. *The ISME Journal*, **1**, 9-18.

Ralph DE, Stevenson JM (1995) The role of bacteria in well clogging. *Water Research*, **29**, 365-369.

Ramanujan VK, Biener G, Herman BA (2006) Scaling behavior in mitochondrial redox fluctuations. *Biophysical Journal: Biophysical Letters*, **90**, L70-L72. doi: 10.1529/biophysj.106.083501.

Rentz JA, Kraiya C, Luther GW III, Emerson D (2007) Control of Ferrous Iron Oxidation within Circumneutral Microbial Iron Mats by Cellular Activity and Autocatalysis. *Environmental Science & Technology*, **41**, 6084-6089.

Richardson LF (1926) *Proceedings of the Royal Society*, **110**, 709.

Roden EE, Sobolev D, Glazer B, Luther GW (2004) Potential for microscale bacterial Fe redox cycling at the aerobic-anaerobic interface. *Geomicrobiology Journal*, **21**, 379–391.

Roden EE, McBeth JM, Blöthe M, Percak-Dennett EM, Fleming EJ, Holyoke RR, Luther III GW, Emerson D, Schieber J (2012) The microbial ferrous wheel in a neutral pH groundwater seep. *Frontiers in Microbiology*, **3**, 172.

Rozanova EP, Dubinina GA, Lebedeva EV, Suntsova LA, Lipovskikh VM, Tsvetkov NN (2003) Microorganisms in heat supply lines and internal corrosion of steel pipes. *Microbiology*, **72**, 179-186.

Sampedro JA, Rosas N, Valdez B (1999) A reference electrode system for electrochemical measurements at high temperature. *Corrosion Reviews*, **17**, 253-262.

Schottky W (1918) Uber spontane Stromschwankungen in verschiedenen Elektrizita¨tsleitern. *Annals of Physics*, **362**, 541–567.

Schwertmann U, Cambier P, Murad E (1985) Properties of goethites of varying crystallinity. *Clays and Clay Minerals*, **33**, 369–378.

Schwertmann U, Cornell RM (1991) *Iron Oxides in the Laboratory – Preparation and Characterization*. Wiley-VCH Verlag, Weinheim.

Schwertmann U, Bigham JH, Murad E (1995) The first occurrence of schwertmannite in a natural stream environment. *European Journal of Mineralogy*, **7**, 547–552.

Singer PC, Stumm W (1970) Acidic mine drainage: The rate determining step. *Science*, **167**, 1121-1123.

Singer E, Emerson D, Webb EA, Barco RA, Kuenen JG, Nelson WC, Chan CS, Cornoli LR, Ferriera S, Johnson J, Heidelberg JF, Edwards KJ (2011) Mariprofundus ferrooxydans PV-1 the first genome of a marine Fe(ii) oxidizing Zetaproteobacterium. *PLoS ONE* **6**: 1–9.

Smith JH, Gilbert RG, Miller JB (1978) Redox potentials in a cropped potato processing waste water disposal field with a deep water table. *Journal of Environmental Quality*, **7**, 571-574.

Sobolev D, Roden EE (2001) Suboxic deposition of ferric iron by bacteria in opposing gradients of Fe(II) and oxygen at circumneutral pH. *Applied and Environmental Microbiology*, **67**, 1328–1332.

Sobolev D, Roden EE (2002) Evidence for rapid microscale bacterial redox cycling of iron in circumneutral environments. *Antonie van Leeuwenhoek*, **181**, 587–597.

Stanley HE, Amaral LA, Goldberger AL, Havlin S, Ivanov PCh, Peng C-K (1999) Statistical physics and physiology: Monofractal and multifractal approaches. *Physica A*, **270**, 309-324.

Steefel CI, Van Cappellen P (1990) A new kinetic approach to modeling water–rock interaction: the role of nucleation, precursors, and Ostwald ripening. *Geochimica et Cosmochimica Acta*, **54**, 2657–2677.

Stone AT (1997) Reactions of extracellular organic ligands with dissolved metal ions and mineral surfaces. In: Banfield J, Nealson KH (eds.) *Geomicrobiology: Interaction between microbes and minerals*. Washington, DC: Mineralogical Society of America. p 309–344.

Straub KL, Benz M, Schink B, Widdel F (1996) Anaerobic, Nitrate-Dependent Microbial Oxidation of Ferrous Iron. *Applied and Environmental Microbiology*, **62**, 1458-1460.

Straub KL, Benz M, Schink B (2001) Iron metabolism in anoxic environments at near neutral pH. *FEMS Microbology Ecology*, **34**, 181-186.

Stumm J, Morgan JJ (1996) *Aquatic chemistry: chemical equilibria and rates in natural waters*, 3rd, ed.; Wiley Interscience: U.S.A.

Sung W, Morgan JJ (1980) Kinetics and product of ferrous iron oxygenation in aqueous systems. *Environmental Science & Technology*, **14**, 561–68.

Swerhone GDW, Lawrence JR, Richards JG, Hendry MJ (1999) Construction and Testing of a Durable Platinum Wire Eh Electrode for In Situ Redox Measurements in the Subsurface. *GWMR*, 132-136.

Takayasu H (1990) *Fractals in the Physical Sciences*, Manchester University Press, Manchester.

Taqqu MS, Samorodnitsky G (1992) Linear models with long-range dependence and finite or infinite variance. In: *New directions in time series analysis, Part II*, IMA Volumes in Mathematics and its Applications 46, Springer, p 325–340.

Toner BM, Santelli CM, Marcus MA, Wirth R, Chan CS, McCollom T, Bach W, Edwards KJ (2009) Biogenic iron oxyhydroxide formation at mid-ocean ridge hydrothermal vents: Juan de Fuca Ridge. *Geochimica et Cosmochimica Acta*, **73**, 388–403.

Tuhela L, Carlson L, Tuovinen OH (1997) Biogeochemical transformations of Fe and Mn in oxic groundwater and well-water environments. *Journal of Environmental Science and Health*, **A32**, 407–26.

Uppaluri S, Nagler J, Stellamanns E, Heddergott N, Herminghaus S, Engstler M, Pfohl T (2011) Impact of microscopic motility on the overall swimming behaviour of parasites. *PLoS Computational Biology* **7**:e1002058.

van Bochove E, Beauchemin S, Theriault G (2002) Continuous Multiple Measurement of Soil Redox Potential Using Platinum Microelectrodes. *Soil Science Society of America Journal*, **66**, 1813-1820.

van der Ziel A (1950) On the noise spectra of semi-conductor noise and of flicker effect. *Physica*, **16**, 359–372.

Varotsos C, Ondov J, Efstathiou M (2005) Scaling properties of air pollution in Athens, Greece, and Baltimore, Maryland. *Atmospheric Environment*, **39**, 4041-4047.

Vershinin AV, Rozanov AGv (1983) The Platinum Electrode as an Indicator of Redox Environment in Marine Sediments. *Marine Chemistry*, **14**, 1-15.

Vollrath S, Behrends T, Van Cappellen P (2012) Oxygen Dependency of Neutrophilic Fe(II) Oxidation by Leptothrix Differs from Abiotic Reaction. *Geomicrobiology Journal*, **29**, 550-560.

Vollrath S, Behrends T, Koch CB, Van Cappellen P (2013) Effects of temperature on rates and mineral products of microbial Fe(II) oxidation by Leptothrix cholodnii at microaerobic conditions. *Geochimica et Cosmochimica Acta*, **108**, 107-124.

Voss RF, Clarke J (1975) '1/f noise' in music and speech. *Nature*, **258**, 317–318.

Warren LW, Ferris FG (1998) Continuum between sorption and precipitation of Fe(III) on microbial surfaces. *Environmental Science & Technology*, **32**, 2331-2337.

Weber KA, Achenbach LA, Coates JA (2006) Microorganisms pumping iron: anaerobic microbial iron oxidation and reduction. *Nature Reviews Microbiology*, **4**, 752–764.

Wehrli B, Sulzberger B, Stumm W (1989) Redox processes catalyzed by hydrous oxide surfaces. *Chemical Geology*, **78**, 167–179.

Weiss JV, Emerson D, Backer SM, Megonigal JP (2003) Enumeration of Fe(II)-oxidizing and Fe(III)-reducing bacteria in the root zone of wetland plants: Implications for a rhizosphere iron cycle. *Biogeochemistry*, **64**, 77–96.

Weiss JV, Rentz JA, Plasia T, Neubauer SC, Merrill-Flody M, Lilburn T, Bradburne C, Megonigal JP, Emerson D (2007) Characterization of neutrophilic Fe(ii)-oxidizing bacteria isolated from the rhizosphere of wetland plants and description of Ferritrophicum radicicola gen. nov. sp. Nov., and Sideroxydans paludicola sp. Nov. *Geomicrobiology Journal*, **24**, 559–570.

Whitfield M (1969) Eh as an Operational Parameter in Estuarine Studies. *Limnology and Oceanography*, **14**, 547-558.

Widdel F, Schnell S, Heising S, Ehrenreich A, Assmus B, Schink B (1996) Ferrous iron oxidation by anoxygenic phototrophic bacteria. *Nature*, **362**, 834-836.

Wiener NJ (1923) Differential Space. *Journal of Mathematical Physics*, **2**, 131-174.

Willinger W, Taqqu MS, Sherman R, Wilson DV (1997) Self-similarity through high-variability: statistical analysis of ethernet LAN traffic at the source level. *IEEE ACM Transactions Network*, **5**, 71–86.

Witt A, Malamud BD (2013) Quantification of long-range persistence in geophysical time series: conventional and benchmark-based improvement techniques. *Surveys in Geophysics*, **34**, 541-651.

Wiuf C, Feliu E (2013) Power-Law Kinetics and Determinant Criteria for the Preclusion of Multistationarity in Networks of Interacting Species. *SIAM Journal of Applied Dynamical Systems*, **12**, 1685-1721.

Zuo R, Wood TK (2004) Inhibiting mild steel corrosion from sulfate reducing and iron-oxidizing bacteria using gramicidin-S producing biofilms. *Applied Microbiology and Biotechnology*, **65**, 747-753.

Figures

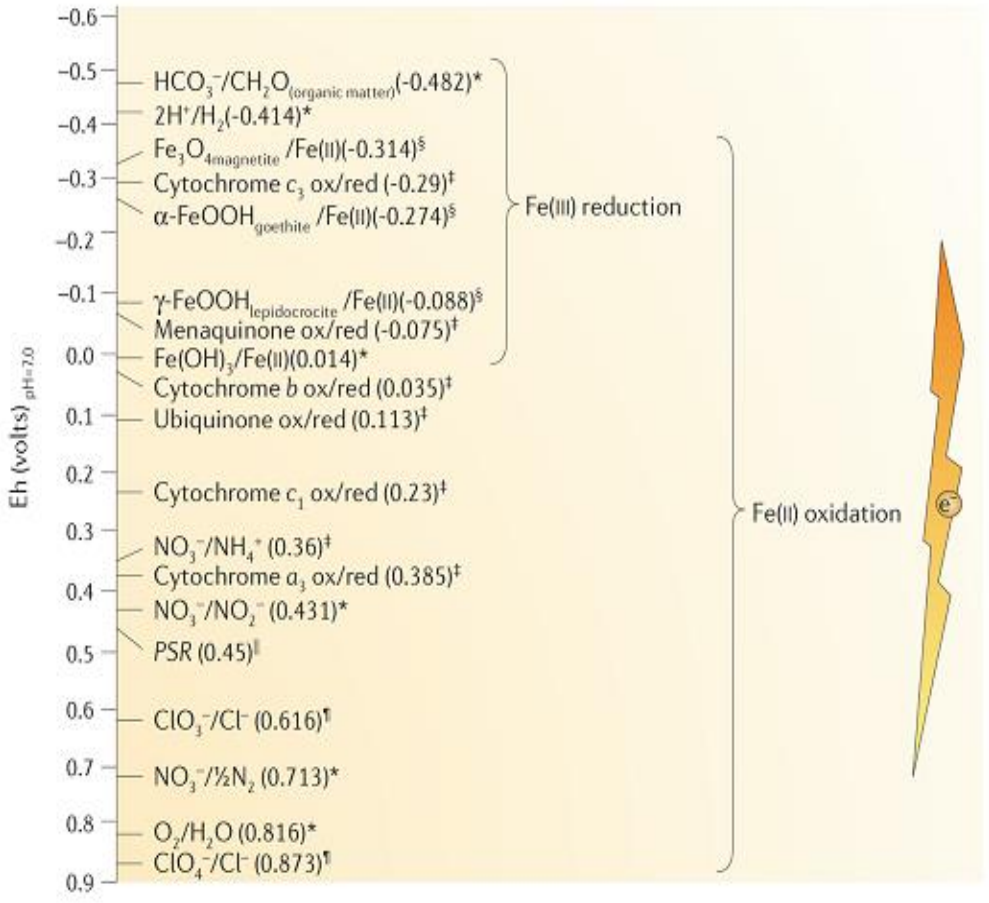

Figure 1.1: From Weber *et al.*, (2006). A redox ladder of possible electron donors and acceptors involved in iron redox cycling, calculated at circumneutral pH; electron donors have more negative potential than electron acceptors, and electrons will flow from top to bottom.

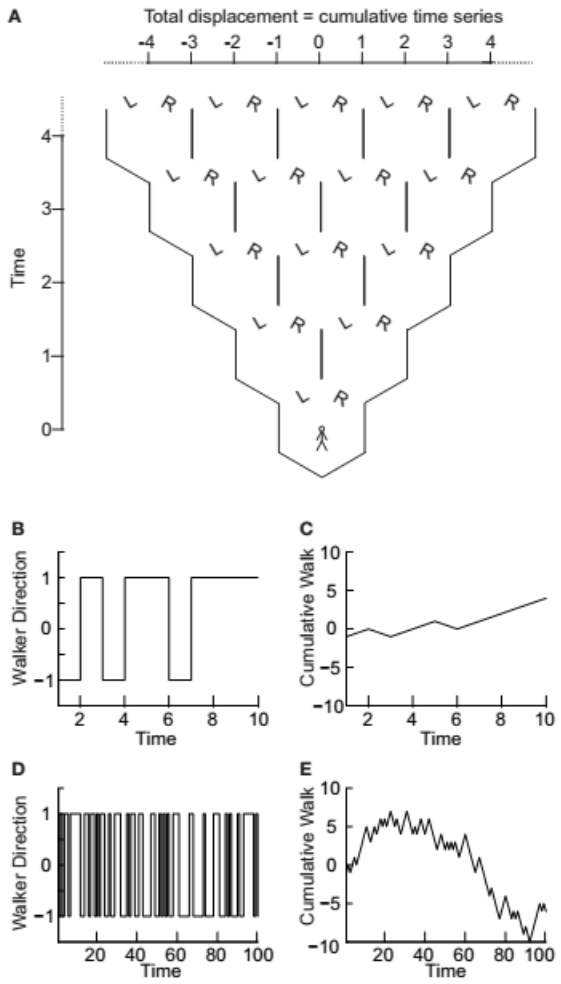

Figure 1.2: From Hardstone *et al.*, (2012). Visualizing normal Brownian motion as a random walk. **(A)** The walker takes one step for each time increment, and can take it either to the left or the right, with equal probability. **(B)** The walker's steps from a stationary time series, as its value does not depend on time; this is a visual representation of stationary increments. **(C)** The signal profile is the cumulative path of steps taken by the walker, it can take arbitrarily large values as time increases. **(D)** The standard deviation of the time series of steps is constant at large time scales because the step length never changes in size. **(E)** The cumulative sum, also called the random walk or integrated time series, shows greater variance in long time scales compared to short ones; this is the basis for scale-free behaviour.

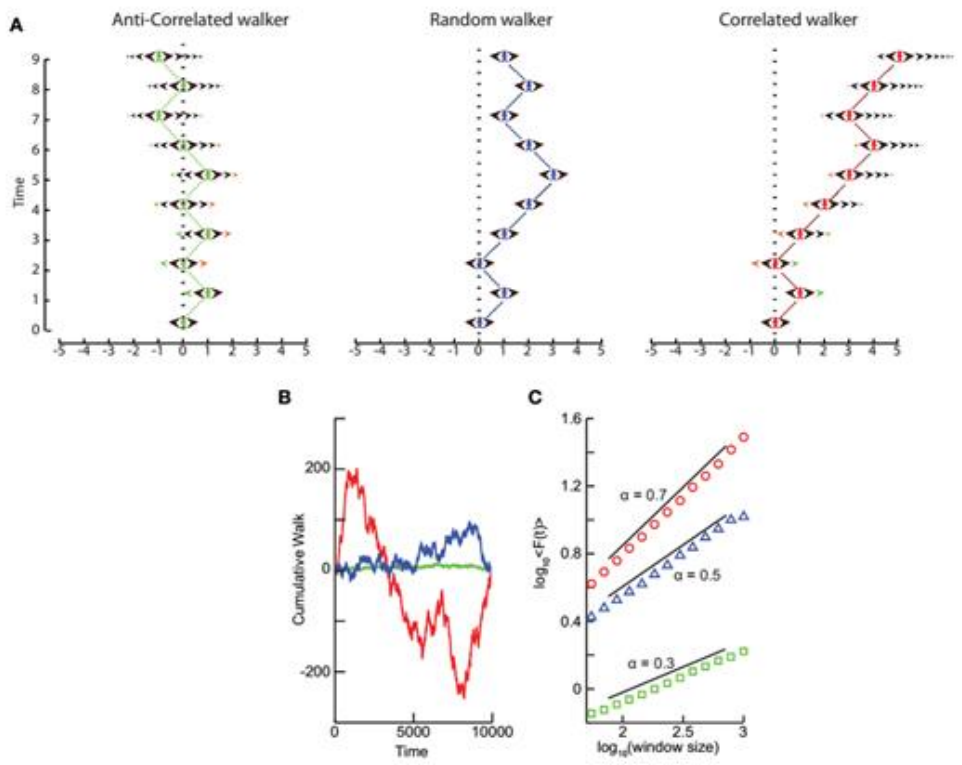

Figure 1.3: From Hardstone *et al.*, (2012). Correlation occurs when the walker's previous steps influence the probability of the direction of the next step. **(A - Left)** Anti-correlated walk: Each step the walker takes is based on cumulative weighted influence of the previous steps taken. The weight of the influence is illustrated by the size of the arrows pointing left and right. Each action the walker takes influences future actions, such that the walker is more likely to next step in the opposite direction of the step just taken. This is illustrated as a gradual accumulation of arrows that refer to past actions, but also decrease in their size over time, because the strength of influence decays over time. **(A - Center)** True random walk: The walker is not influenced by previous actions, and as such always has equal probability of going left or right. **(A - Right)** Correlated walk: Each step the walker takes influences future actions by making the walker more likely to step in the same direction. The green arrows show that by taking a right step at time 0, the walker is more likely to go right in future time steps with the cumulative influence getting smaller as time goes on. **(B)** Cumulative signal profiles (integrated walks) for a positively correlated (red), uncorrelated (blue), and anti-correlated walk (green). **(C)** Root-mean-square (RMS) fluctuation plotted as a function of time for each of the profiles in (B). We quantify the differences between these time series. The positively correlated walk has a scaling exponent of 0.7, the uncorrelated walk has a scaling exponent of 0.5, and the anti-correlated walk has a scaling exponent of 0.3.

Chapter 2
Low-level Fluctuation Analysis of Iron-Oxidizing Microbial Systems[1]

2.1 Abstract

We developed a novel method for detecting the presence of iron-oxidizing bacterial activity in liquid medium using oxidation-reduction (redox) potential time series data. The instrument and processing algorithm were tested by immersing the tip of a Pt electrode with an Ag-AgCl reference electrode in municipal tap water, uninoculated artificial groundwater (AGW) microbial growth medium, and an active iron-oxidizing biofilm in medium. We used detrended fluctuation analysis to demonstrate that live systems were characterized by different average root-mean-square fluctuation behaviour, as evidenced by electrode response. The differences in scaling exponents were significantly different at $p < 0.001$. This method can be applied in any environment where redox potential is presently measured. Due to the simplicity, portability, and small size, it may be suitable for extraterrestrial environments such as Europa, Enceladus, and Mars.

2.2 Introduction

Measurement of oxidation-reduction (redox) potential is one of the most elementary and fundamental aspects of characterizing microbial ecological niches and bacterial habitats. The redox state of any aqueous environment is the quotient of the chemical activity of dissolved oxidized and reduced chemical species, as shown in the Nernst equation:

$$E = E^0 + \frac{RT}{nF} \ln Q \qquad (2.1)$$

where E is the electrochemical potential of the cell in mV, R is the universal gas constant, T is absolute temperature, *n* is the number of electrons participating per atom, F is Faraday's constant,

[1] This chapter is currently under review by "Astrobiology"

and Q is the reaction quotient, $\frac{[oxidized\ species]}{[reduced\ species]}$. Redox potential is sensitive even to subtle changes in chemical speciation. Environmental factors including temperature, pH, and the presence of multiple redox couples can influence the redox potential of a microbial system, in addition to microbe-specific factors such as nutrient levels, solution chemistry, growth substrate factors, and oxygen availability (Newman & Banfield, 2002). Microbial bioenergetic metabolic activity is entirely based on redox reactions, and, in this way, all metabolically active microorganisms directly influence the relative abundance of redox active substances in their environment (van Bochove *et al.*, 2002; Bethke *et al.*, 2011). Microbes interact with their environment by driving redox reactions that have the potential to cause significant changes in pH and redox potential. In particular, organisms that exploit the Fe(III)/Fe(II) redox couple to fuel cellular growth underpin global biogeochemical cycling of iron (Weber *et al.*, 2006; Emerson *et al.*, 2010; Kendall *et al.*, 2012).

Characterizing *in situ* microbial activity remains a pressing issue in environmental microbiology as 99% of microorganisms cannot be cultured (Hugenholtz *et al.*, 1998). At present, describing bacterial activity in pristine and contaminated environments most often involves measurement of specific metabolite concentrations in samples recovered from study sites of interest. *In situ*, continuous measurement of redox potential has been used to infer changes in microbial community dynamics and shifts in physiological processes (van Bochove *et al.*, 2002), including shifts from aerobic to anaerobic respiration. Redox potentials are measured in many environmental systems to assess the type and role of biological activity (Bohn, 1971).

When they transfer electrons, microbes oxidize the donor species and reduce the acceptor, directly regulating the redox state and chemical properties of their environment (Bethke *et al.*, 2011). Since redox potential represents a physically-constrained measurement of a biological system, this influence creates an opportunity to directly examine microbial influence on physicochemical system parameters. If fluctuations in a system arise from random motions of particles (Gabrielli *et al.*, 1993), also known as Brownian motion, or normal diffusion (Eliazar & Shlesinger, 2013), we can now relate the system observable of fluctuations to the small-scale motion of diffusing particles. We are assuming here that the electrode selected is responsive to the diffusing species of interest; in this case, a Pt electrode sensing dissolved Fe, which is well documented in literature (Vershinin & Rozanov, 1993; Stumm & Morgan, 1996), provided concentrations of dissolved Fe(II) are above 10^{-5} M.

Brownian motion is the characteristic non-stationary process; it is stochastic with stationary, independent Gauss-distributed increments (Wiener, 1923; Metzler & Klafter, 2000; Eliazar & Shlesinger, 2013; Witt & Malamud, 2013). Nonstationary processes with correlated increments are termed fractional Brownian motions (Eliazar & Shlesinger, 2013). In a plot of the mean-squared-displacement (MSD) through time, a Brownian motion will give a linear result (Metzler & Klafter, 2000; Witt & Malamud, 2013; Jeon *et al.*, 2014; Kim, 2014). When the MSD is described by non-linear growth through time, typically taking a scale-free, power-law form, diffusion is described as "anomalous" (Metzler & Klafter, 2000; Witt & Malamud, 2013; Jeon *et al.*, 2014; Kim, 2014). Anomalous diffusion was first described in 1926 (Richardson, 1926; Metzler & Klafter, 2000). Both anomalous diffusion and fractional Brownian motion have been described in a wide variety of physical systems (Metzler & Klafter, 2000; Witt & Malamud, 2013 and references therein).

Correlation is a property of a time series or process that describes the statistical dependence of directly and distantly neighboured values (Witt & Malamud, 2013); long-range correlations are where all or almost all values are correlated with one another, that is, values are correlated with one another at very long lags in time (Taqqu & Samorodnitsky, 1992; Beran 1994; Witt & Malamud, 2013). Detrended fluctuation analysis (DFA) calculates a relationship between mean-square displacement (MSD) and time in time series fluctuation data, by quantifying the strength of long range correlation in a time series (Hardstone *et al.*, 2012; Witt & Malamud, 2013). The algorithm will be described in the methods section.

Here we present a novel method of analyzing *in situ* bacterial activity by quantifying fluctuations in the redox potential of bulk fluid medium. This technique does not rely on constraining any environmental or physiochemical conditions under which the microbes are living; instead, it depends on the diffusion of redox active species in solution (Oldham, 1966; Frateur *et al.*, 1999; Mampallil *et al.*, 2013). The method uses low-cost, straightforward instrumentation, allows broad comparisons between diverse microbiological niches, and does not necessitate either removing organisms from their niches or taking direct samples of biomass for genomic analysis, as all data is collected passively *in situ*. Any microbial niche which can be reached by an electrode is suitable for this type of analysis.

In taking a systems approach by measuring fluctuations of a single observable, we adopt a model first proposed by Bak *et al.*, (1987): complex chemical and biological systems exist in a quasi-stable state that arises from the interactions of multiple chemical constituents – a time-invariant

condition. Under such a model, all chemical species, even those which are not redox active, indirectly influence potential through interactions with other chemical species.

We hypothesize that statistically significant differences in fluctuation patterns of redox potential, as evidenced by differences in scaling exponents, are the result of biological influences on redox transformations, or, in the case of chemical systems, the lack of biological activity. We suggest that measuring the redox potential time series could be a good complement to the analyses of metabolites and genetic sequences, i.e., multiple measurements of several different system parameters. Fluctuation analysis is used to assess time-domain, self-similarity and correlation behaviour in biological and chemical systems. Iron-oxidizing systems are well suited for this type of analysis because of the obvious link between iron redox state to both cellular metabolism and the redox potential of a solution, with a concomitant voltage change. In addition to varied terrestrial systems, this method may specifically be relevant to future missions to Europa, Enceladus, or other environments where liquids are present. Redox instability has been documented on the surface of Mars (McSween Jr. *et al.*, 1999), implying that given suitable geochemical conditions, Fe-based biological activity might be possible.

2.3 Methods

2.3.1 Field Site

The study site has been described in detail by James & Ferris (2004). Briefly, it is an anoxic anaerobic iron-rich groundwater seep colonized by a thriving microbial mat produced by *Leptothrix ochrachea* with a minor component of *Gallionella ferruginea* (James & Ferris, 2004). The seep intersects a fully aerated stream about 3 m from the seep source, the reduced, anoxic groundwater is spatially confined to the narrow, shallow (3-15 cm) creek.

2.3.2 Test Solutions

In addition to *in situ* measurement of the biofilm, potentials were recorded from a chemically-defined artificial groundwater growth medium (Ferris *et al.*, 2004), and autoclaved City of Toronto tap water, which were both sterile, dilute but chemically complex solutions. This ensured that it was possible to attribute differences in redox potential fluctuations to biological activity, and not just to chemical interactions in the solutions. As a means of testing a solution close to

thermodynamic equilibrium, a potential was recorded for an electrode which had been immersed in 3 M KCl reference solution for several weeks.

2.3.3 Hardware

A schematic of the instrument is shown in Fig. 2.1. The instrument is intended for measuring voltage time-series in aqueous environments with a design that: (1) allows portability for use in the field, (2) is straightforward for interfacing and programming, and (3) provides a cost-effective tool for accurate and reproducible measurements.

Measurements are performed by immersing the tip of a double-junction, gel-filled redox electrode in the aqueous medium for sampling. Once immersed, redox-active ions in solution become mobile across a ceramic plug in the tip of the electrode due to the difference in electrochemical potential between the Pt tip and a reference Ag wire immersed in a KCl gel (see Fig. 2.1). Voltage fluctuations between the Pt working electrode and Ag/AgCl reference electrode, typically 150-250 mV in our samples, were measured at intervals of 0.1 s (i.e., 10 Hz measurement frequency) using a National Instruments USB-6009 multifunction data-acquisition device (DAQ) interfaced to a Windows 7 laptop PC running LabVIEW using the standard National Instruments DAQmx VIs. Measurements lasted about an hour, for a total time series length of at least n=36000. Collecting longer time series allowed for a larger pool of estimates for statistical testing.

The DAQ was configured to measure voltage from the electrode in analog mode using differential inputs, where the Pt wire was ground-referenced to a heavy iron rod driven at least 18 cm into soil, located a minimum of 2 m from the point of sampling in a hydrologically separated area. This reference location is typically in an unsaturated zone above and away from the measured environment. The DAQ was placed inside a metal box which was fitted with a BNC feedthrough to connect the differential inputs of the DAQ to the BNC signal cable from the electrode and a USB outlet for connecting the DAQ to the PC. The shielding of the electrode BNC signal cable, the DAQ ground, and the ground of the PC were all connected to the heavy iron grounding rod. This strategy was found to eliminate pickup noise.

By measuring the potential across the electrode in differential mode, any further variations in common mode noise were eliminated. Additional testing to assess the impact of aliasing was achieved using a Tektronix TDS 3054B oscilloscope, and testing indicated no visible contributions from common noise sources. It must be noted that no anti-aliasing filters were applied, because

specifying a low-pass band assumes *a priori* knowledge of the chemical reactions contributing to fluctuations.

A Pt electrode was selected due to the extensive use of Pt electrodes in environmental electrochemical studies (Flühler *et al.*, 1976; Faulkner *et al.*, 1989; Vershinin & Rozanov, 1993; Swerhone *et al.*, 1999; van Bochove *et al.*, 2002; Sampedro *et al.*, 1999; Kasem & Jones, 2008; Ojumu *et al.*, 2008), often for measuring redox potential and dissolved O_2 (Whitfield, 1969; Swerhone *et al.*, 1999). These electrodes have been used continuously for measurements recorded over years, with either no or minimal changes in performance over the time scale of the study (Smith *et al.*, 1978; Austin & Huddleston, 1999; Swerhone *et al.*, 1999; van Bochove, 2002), and are known to be reliable under a variety of environmental conditions (Kasem & Jones, 2008). One particular benefit of a Pt electrode in the context of studying an iron-oxidizing microbial community is that Pt electrodes are predominantly responsive to iron species when concentrations exceed 10^{-5} M (Vershinin & Rozanov, 1993; Stumm & Morgan, 1996).

When describing electrode response in diffusion-limited systems, both theoretical and laboratory studies have indicated that current is influenced by the redox state of the species in bulk solution, and not by the electrode making the measurements (Mampallil *et al.*, 2013); this is important as it confirms that redox potential and fluctuations being measured arise from the dynamics of the system as a whole, and not from the microenvironment immediately surrounding the electrode tip.

2.3.4 Processing Method

Collected time series were analyzed in MatLAB using a custom detrended fluctuation analysis (DFA) routine (Peng *et al.*, 1994). Shuffled data sets were created by shuffling the time series index using the "rand" function approximately 50-100 times before processing.

The first step in DFA data processing is to remove the mean and integrate the time series. The time series is divided into windows of length n. A least squares fit is calculated for each window, and the integrated signal is detrended by subtracting the local trend. The average fluctuation per window is calculated using a root mean square (RMS) algorithm, and the value for the average fluctuation, F(n), is plotted against the window-size, n, in log space. If a straight line is observed over a range of time windows, the time-series is persistent within that range. The slope of this line is the α value, or scaling exponent. Finally, the magnitude of α provides information about the strength of the long-range correlation behaviour of the time series. Brownian motion gives rise

to a scaling exponent $\alpha = 1$ (Metzler & Klafter, 2000; Ramanujan *et al.*, 2006); with $1 < \alpha < 2$ relating to processes exhibiting fractional Brownian motion (Metzler & Klafter, 2000; Eliazar & Shlesinger, 2013). In random uncorrelated time series, such as Gaussian white noise $\alpha = 0.5$ (Metzler & Klafter, 2000; Witt & Malamud, 2013), while $\alpha < 0.5$ indicates negative persistence and $\alpha > 0.5$ indicates positive persistence (Peng *et al.*, 1994; Peng *et al.*, 1995; Metzler & Klafter, 2000; Hardstone *et al.*, 2012; Witt & Malamud, 2013).

The relatively high sampling rate came with the benefit of shorter sampling intervals to obtain DFA-optimized lengths of realizations of $n = \sim 10^3$ measurements (Metzler & Klafter, 2000; Shao *et al.*, 2012). The inherent variability of field conditions over hours and days created a preference for shorter windows where stable conditions over the measurement window could be reasonably expected. Thus, the decision was made to sample at 10 Hz, and downsample to 1 Hz and 2 Hz, providing several realisations of the same process and permitting statistical evaluation of the calculated fluctuation exponents.

DFA provides two significant advantages over the more common Fourier analysis: no assumption of linearity, stationarity or independence of measurements is made, and the amount of time required for a complete data set is achieved at $n = \sim 10^3$, regardless of the sampling frequency (Shao *et al.*, 2012). It is, however, important to note that the minimum time series length as it relates to scaling range, may need to be longer than this specified minimum. Collection of very long (several hours) low-frequency time series is complicated in field settings due to changes in conditions, such as temperature and light, over the course of a day. Environmental time series analyses are also complicated by the complexity of the chemical interactions being studied, the slower time scales of kinetic processes that give rise to fluctuations, and inherent variability of dilute aqueous systems. While several other time domain techniques are available, such as fluctuation analysis, adaptive fractal analysis, (Riley *et al.*, 2012), and detrended moving average analysis, DFA consistently performs well while requiring time series of only n=1000 measurements (Shao *et al.*, 2012).

2.4 Results

Times series for each of the three test solutions collected by the DAQ at a frequency of 10 Hz are presented in Figure 2.2; both raw and integrated profiles. The 10 second windows better highlight the dynamic nature of each time series in Figure 2.3. The electrode measured different

conditions in each of the three systems, as evidenced by the different potentials at which the electrode stabilized within each of the different liquids (Fig. 2.3).

Fluctuations and the resulting α values are plotted in Figure 2.4 for the time window 0-2500 seconds, for a 1 Hz (measurement frequency) downsample of the original data. The values reported in Table 2.1 show the average α value (scaling exponent) and standard error of 24 realizations for each of the three test systems: the live system (BIOS – bacteriogenic iron oxides; $\alpha = 1.574 \pm 0.011$); tap water from the City of Toronto (Tap; $\alpha = 1.500 \pm 0.016$); and uninoculated artificial groundwater chemical growth medium (Ferris *et al.*, 2004) (AGW; $\alpha = 1.157 \pm 0.009$). By comparison, when the same processing steps were applied to one realization from the electrode in its KCl storage solution, the scaling exponent was $\alpha = 0.61$; slightly higher than for the same realization, shuffled, $\alpha = 0.501$. Both are either uncorrelated or very weak correlation, and represent the intrinsic instrument noise of this design; confirming that the observed scaling exponents result from correlation behaviour within the measured systems. This is reasonable in the context of diffusion literature; a solution at true thermodynamic equilibrium, such as the KCl solution should exhibit no correlation and in essence, no diffusion, while the three test systems give rise to scaling exponents indicating strong correlation, diffusion, and reaction (Metzler & Klafter, 2000; Jeon *et al.*, 2014).

2.5 Discussion

2.5.2 Scaling Range and Sampling Frequency

In figure 2.4, the smallest window size (n=10) and the largest window size (n=1250), deviate from the strong linear trend defined from window sizes s=20 (20 seconds in length) to s=1000 (1000 seconds in length). These two window sizes limit the range of self-similar scaling or long-range correlation to 20-1000 s. The shortest time series which will exhibit long-range correlation would be 20 seconds in length, regardless of frequency, and the longest time interval which will exhibit long-range correlation is 1000 s; if window sizes were so large as to be larger than 1000s, long-range correlation may not be observed. Additionally, this indicates that the minimum time series length required to fully constrain the scaling behaviour in these systems in 1000 s; regardless of sampling frequency. This scaling range confirms that measurement frequency as low as 1 Hz is sufficient to fully characterize these systems. The protocol of measuring at a rate of 10 Hz to create

a temporally-link pool of realizations appears to provide consistent and reliable characterizations of scaling behaviour and correlation.

2.5.1 Scaling Exponents

DFA revealed that all three systems exhibit fractional Brownian motion, but within that fairly broad classification, each solution can be distinguished by its respective scaling exponent. Perhaps most unexpected scaling exponent was the case of tap water; however, a number of redox-active species are present in tap water, albeit at fairly low concentrations. These are reported to include: NO_2^- = 6 x 10^{-3} μmol/L, NO_3^- = 6 μmol/L, SO_4^{2-} = 0.275 mmol/L, Mn^{2-} = 7 x 10^{-3} μmol/L, Fe(II) = 0.229 μmol/L, Co = 5 x 10^{-5} μmol/L, and Cu = 3.5 x 10^{-2} μmol/L (City of Toronto, n.d.). The biologically-active system consistently exhibits the strongest correlation.

2.6 Conclusion

We have developed a novel method for measuring RMS fluctuations of redox potential in chemical and biological systems, and confirmed that such fluctuation behaviour is distinct between chemical and biological systems; with the key benefit of this approach being utility in field settings. Biological systems consistently exhibit statistically significant stronger correlation behaviour than the chemical solutions measured here. This technique has the potential to be applied to a wide variety of environments as it requires only the possibility of placing an electrode in contact with the system to be measured. Measuring rates of microbial metabolic activity by using diffusion dynamics has the potential to dramatically increase the capability of *in situ* monitoring to describe microbial ecology, as well as provide a physically constrained method of distinguishing biological from chemical oxidation of iron.

2.7 Acknowledgements

This work was generously supported by a Natural Sciences and Engineering Research Council of Canada (NSERC) Discovery Grant to FGF. The Ogilvies are thanked for access to the field site.

2.8 References

Austin WE, Huddleston JH (1999) Visibility of permanently installed platinum redox electrodes. *Soil Science Society of America Journal*, **63***,* 1757-1762.

Bak P, Tang C, Wiesenfeld K (1987) Self-Organized Criticality: An Explanation of 1/f Noise. *Physical Review Letters*, **59**, 381-384.

Beran J (1994) *Statistics for long-memory processes*. Chapman & Hall/CRC, New York.

Bethke CM, Sanford RA, Kirk MF, Jin Q, Flynn TM (2011) The Thermodynamic Ladder in Geomicrobiology. *American Journal of Science*, **311**, 183-210.

Bohn HI (1971) Redox Potentials. *Soil Science*, **112**, 39-45.

DeLaune RD, Reddy KR (2004) Redox Potential. In *Encyclopedia of Soils in the Environment*, Hillel D (ed.) Academic Press. p 366-371.

Eke A, Herman P, Kocsis L, Kozak LR (2002) Fractal characterization of complexity in temporal physiological signals. *Physiologic Measurement* **23**, R1-R38.

Eliazar II, Shlesinger MF (2013) Fractional motions. *Physics Reports*, **527**, 101-129.

Emerson D, Fleming EJ, McBeth JM (2010) Iron-oxidizing bacteria: an environmental and genomic perspective. *Annual Reviews of Microbiology*, **64**, 561–583.

Faulkner SP, Patrick WH, Gambrell RP (1989) Field techniques for measuring wetland soil parameters. *Soil Science Society of America Journal*, **59**, 1044-1051.

Ferris FG, Phoenix V, Fujita Y, Smith RW (2004) Kinetics of Calcite Precipitation Induced by Ureolytic Bacteria at 10 to 20°C in Artificial Groundwater. *Geochimica et Cosmochimica Acta*, **68**, 1701-1722.

Flühler H, Ardakani MS, Stolzy LH (1976) Field measured nitrous oxide concentrations, redox potentials, oxygen diffusion rates, and oxygen partial pressures in relation to denitrification. *Soil Science*, **122**, 107-114.

Frateur I, Bayet E, Keddam M, Tribollet B (1999) Local redox potential measurement. *Electrochemistry Communications*, **1**, 336-340.

Gabrielli C, Huet F, Keddam H (1993) Fluctuations in electrochemical systems. I. General theory on diffusion limited electrochemical reactions. *Journal of Chemical Physics*, **99**, 7232-7239.

Hardstone R, Poil S-S, Schiavone G, Jansen R, Nikulin VV, Mansvelder HD, Linkenkaer-Hansen K (2012) Detrended fluctuation analysis: a scale-free view on neuronal fluctuations. *Frontiers in Physiology*, **3**, 450.

Hugenholtz P, Goebel BM, Pace NR (1998) Impact of culture-independent studies on the emerging phylogenetic view of bacterial diversity. *Journal of Bacteriology*, **180**, 4765-4774.

James RE, Ferris FG (2004) Evidence for microbial-mediated iron oxidation at a neutrophilic groundwater spring. *Chemical Geology*, **212**, 301-311.

Jeon J-H, Chechkin AV, Metzler R (2014) Scaled Brownian motion: a paradoxical process with a time dependent diffusivity for the description of anomalous diffusion. *Physical Chemistry Chemical Physics*, **16**, 15811.

Kasem KK, Jones S (2008) Platinum as a Reference Electrode in Electrochemical Measurements. *Platinum Metals Review*, **52**, 100-106.

Kim H-J (2014) Anomalous diffusion induced by enhancement of memory. *Physical Reviews E*, **90**, 012103.

Mampallil D, Mathwig K, Kang S, Lemay SG (2013) Redox Couples with Unequal Diffusion Coefficients: Effect on Redox Cycling. *Analytical Chemistry*, **85**, 6053-6058.

Metzler R, Klafter J (2000) The random walk's guide to anomalous diffusion: a fractional dynamics approach. *Physics Reports*, **339**, 1-77.

Newman DK, Banfield JF (2002) Geomicrobiology: How Molecular-Scale Interactions Underpin Biogeochemical Systems. *Science*, **296**: 1071-1077.

Ojumu TV, Petersen J, Hansford GS (2008) The effect of dissolved cations on microbial ferrous-iron oxidation by Leptospirillum ferriphilum in continuous culture. *Hydrometallurgy*, **94**, 69-76.

Oldham KB (1966) A Diffusion-Layer Treatment of Transient Electrochemical Phenomena. *Electrochimica Acta*, **11**, 1475-1490.

Peng C-K, Buldyrev SV, Havlin S, Simons M, Stanley HE, Goldberger AL (1994) Mosaic organization of DNA nucleotides. *Physical Reviews E*, **49**, 1685-1689.

Peng C-K, Havlin S, Stanley H, Goldberger A (1995) Quantification of scaling exponents and crossover phenomena in nonstationary heartbeat time series. *Chaos*, **5**, 82-87.

Ramanujan VK, Biener G, Herman BA (2006) Scaling behavior in mitochondrial redox fluctuations. *Biophysical Journal: Biophysical Letters*, **90**, L70-L72. doi: 10.1529/biophysj.106.083501.

Richardson LF (1926) *Proceedings of the Royal Society*, **110**, 709.

Riley MA, Bonnette S, Kuznetsov N, Wallot S, Gao J (2012) A tutorial introduction to adaptive fractal analysis. *Frontiers in Physiology*, **3**, 371.

Sampedro JA, Rosas N, Valdez B (1999) A reference electrode system for electrochemical measurements at high temperature. *Corrosion Reviews*, **17**, 253-262.

Shao YH, Gu GF, Jiang SZQ, Zhou WX, Sornette D (2012) Comparing the performance of FA, DFA and DMA using different synthetic long-range correlated time series. *Scientific Reports*, **2**, 835, doi: 10.1038/srep00835.

Smith JH, Gilbert RG, Miller JB (1978) Redox potentials in a cropped potato processing waste water disposal field with a deep water table. *Journal of Environmental Quality*, **7**, 571-574.

Stanley HE, Amaral LA, Goldberger AL, Havlin S, Ivanov PCh, Peng C-K (1999) Statistical physics and physiology: Monofractal and multifractal approaches. *Physica A*, **270**, 309-324.

Stumm J, Morgan JJ (1996) *Aquatic chemistry: chemical equilibria and rates in natural waters*, 3rd, ed.; Wiley Interscience: U.S.A.

Swerhone GDW, Lawrence JR, Richards JG, Hendry MJ (1999) Construction and Testing of a Durable Platinum Wire Eh Electrode for In Situ Redox Measurements in the Subsurface. *GWMR*, 132-136.

Taqqu MS, Samorodnitsky G (1992) Linear models with long-range dependence and finite or infinite variance. In: *New directions in time series analysis, Part II*, IMA Volumes in Mathematics and its Applications 46, Springer, p 325–340.

van Bochove E, Beauchemin S, Theriault G (2002) Continuous Multiple Measurement of Soil Redox Potential Using Platinum Microelectrodes. *Soil Science Society of America Journal*, **66**, 1813-1820.

Vershinin AV, Rozanov AG (1983) The Platinum Electrode as an Indicator of Redox Environment in Marine Sediments. *Marine Chemistry*, **14**, 1-15.

Weber KA, Achenbach LA, Coates JA (2006) Microorganisms pumping iron: anaerobic microbial iron oxidation and reduction. *Nature Reviews Microbiology*, **4**, 752–764.

Whitfield M (1969) Eh as an Operational Parameter in Estuarine Studies. *Limnology and Oceanography*, **14**, 547-558.

Wiener NJ (1923) Differential Space. *Journal of Mathematical Physics*, **2**, 131-174.

Witt A, Malamud BD (2013) Quantification of long-range persistence in geophysical time series: conventional and benchmark-based improvement techniques. *Surveys in Geophysics*, **34**, 541-651.

Tables

Table 2.1: The average α values (scaling exponents) and standard error (SE) on slope determined for 24 realizations of time series in each of three different systems: the live system (BIOS), and two chemical systems: artificial groundwater (AGW), and tap water (tap).

	BIOS	AGW	Tap
α	1.567	1.157	1.500
SE	0.011	0.009	0.016

Figures

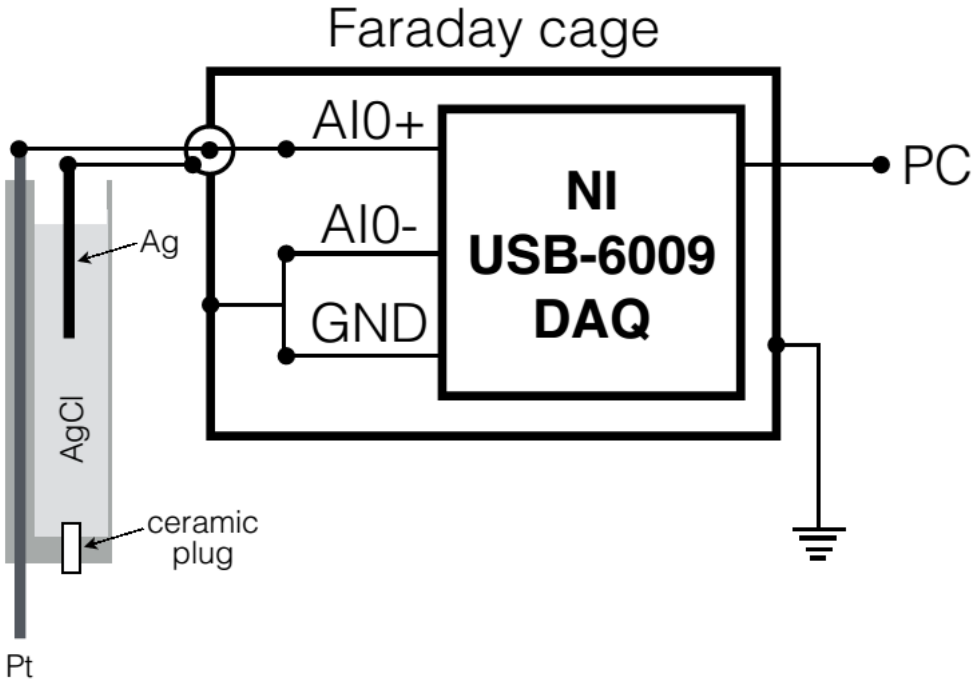

Figure 2.1: Schematic diagram of the instrument designed to measure redox potential using a Pt working electrode and Ag/AgCl reference electrode. AI0+, AI0-, and GND describe specific pins on the NI-6009 USB Data Acquisition Device (DAQ).

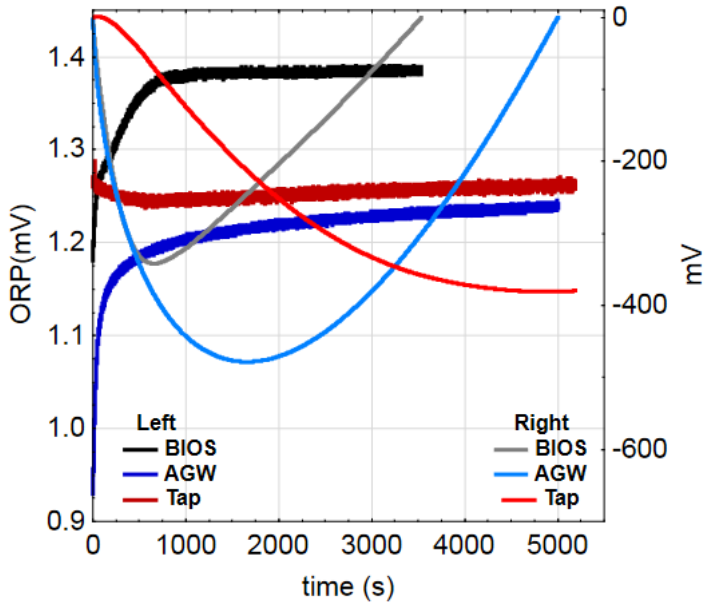

Figure 2.2: Redox potential (ORP) raw time series and integrated profiles from each of the three processes; raw data, in mV, plotted against left axis, while integrated signal profiles are plotted against the right. Live system (BIOS) is in black, artificial groundwater medium (AGW) is in blue, and tap water (Tap) is in red.

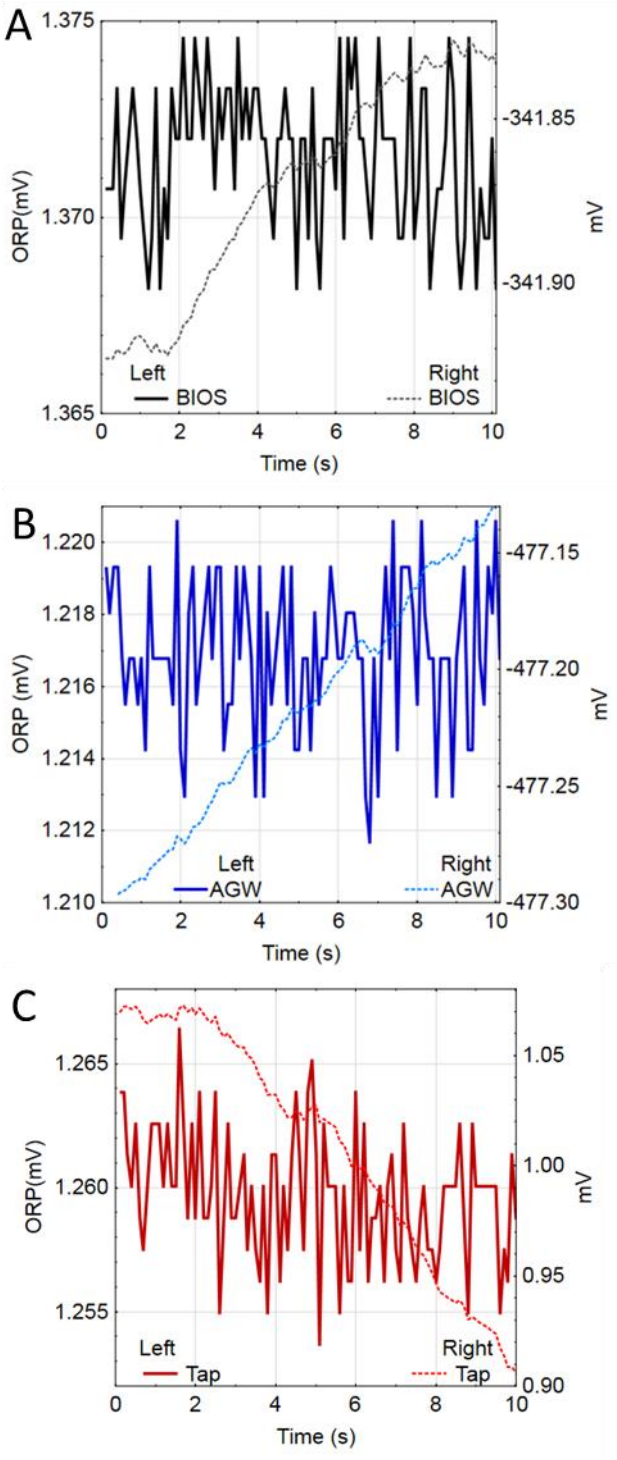

Figure 2.3: Redox potential and random walk profiles recorded over a 10 s interval from each of the three time series. Raw data is plotted on the left as solid lines, and integrated profiles are plotted on the right as dashed lines. **(A)** Live system (BIOS) is in black. **(B)** Artificial groundwater medium (AGW) is in blue. **(C)** Tap water (Tap) is in red.

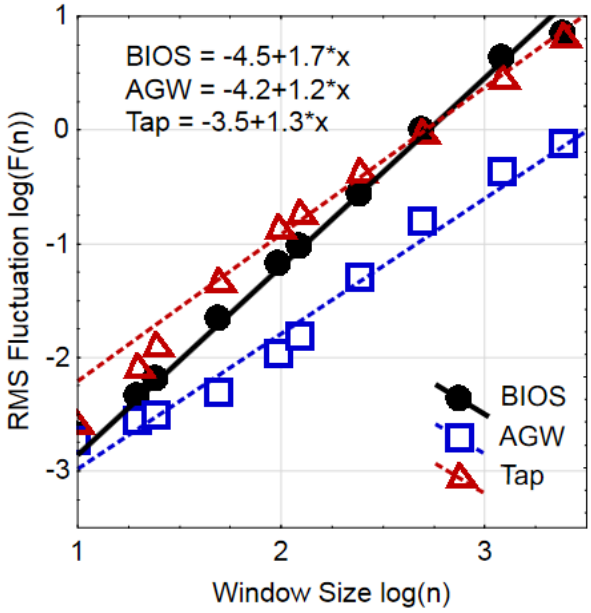

Figure 2.4: Detrended fluctuation analysis results for three experimental systems. These results represent α calculated for a single realization of each process with n = 2500, downsampled from the raw data to 1 Hz. RMS is root-mean-square fluctuation as calculated using detrended fluctuation analysis (DFA). The live system (BIOS) is identified by filled black circles. The first chemical system, artificial groundwater medium (AGW) is shown with blue squares and a blue dashed line, and the second chemical system, tap water (Tap) is shown with red triangles and a red dashed line.

Chapter 3
Bacterial Fe(II)-oxidation Distinguished by Long-Range Correlation in Redox Potential

3.1 Abstract

Redox potential is determined by the diffusivity of oxidized and reduced chemical species in solution; giving rise to small amplitude fluctuations which can be measured as electrode response. The key statistical quantity characterizing such diffusion-driven fluctuations is root-mean-square (RMS) deviation of the diffusing species. RMS deviations of redox potential time series were used to calculate power law scaling exponents in a flow through cell colonized by the circumneutral iron-oxidizing bacterium *Gallionella ferruginea*, and the flow cell's bacteriogenic iron oxide (BIOS)-free inflow pipe. Measurements of physiochemical parameters and of total and ferrous iron before, during, and after time series collection indicate a steady-state condition. Modelling using observed chemical species concentrations indicates non-equilibrium conditions persist in the bioreactor. The calculated pseudo-first order rate constant for the biological system is 0.00386 s^{-1}, significantly higher than the calculated pseudo-first-order abiotic rate constant, 0.00156 s^{-1}. The scaling exponent for redox potential fluctuations in the flow cell is 1.89, while the scaling exponent for the inlet is 1.67. Both scaling exponents indicative of anomalous diffusion behavior, however, the two exponents are significantly different at $p < 0.01$. Anomalous diffusion present in both systems, but the differences between the two is attributed to the differences in oxidation of Fe(II) and subsequent precipitation of hydrous ferric oxides caused by the presence of the iron-oxidizing microbial mat.

3.2 Introduction

Microbial manipulations of the Fe(III)/Fe(II) redox couple have profound geological significance, controlling the global biogeochemical cycling of iron (Weber *et al.*, 2006). In the environment, Fe exists in one of two valence states: oxidized Fe(III) or reduced Fe(II). At circumneutral pH, Fe(III) is poorly soluble, while Fe(II) is soluble, making it more bioavailable

(Melton *et al.*, 2014). However, in the presence of oxygen, Fe(II) will rapidly oxidize to Fe(III), hydrolyze, and precipitate as some form of hydrous ferric oxide (HFO); typically poorly crystalline 2-line ferrihydrite (Fortin & Langley, 2005; Melton *et al.*, 2014; Ferris *et al.*, in press).

The strict kinetic controls on the availability of Fe(II) mean that environments where Fe(II) is sufficiently abundant to be used as an energy source are spatially limited; despite this, a number of different niches where microaerophilic circumneutral iron-oxidizing bacteria (FeOB) can survive by coupling the oxidation of Fe(II) to the reduction of O_2. These niches arise where anaerobic, Fe(II) bearing fluids come into contact with aerated bodies of water, forming redoxclines (Emerson, 2012). The main limits on such environments are O_2 levels and pH (Stumm & Morgan, 1996; Emerson & Weiss, 2004).

The kinetics of Fe(II)-oxidation are critically dependent upon pH and O_2 concentrations (Stumm & Morgan, 1996; Emerson & Weiss, 2004), and the two most important requirements for microbial circumneutral microaerophilic Fe(II)-oxidation are a constant source of Fe(II) and pO_2 below approximately 10% atmospheric levels (Emerson & Revsbech, 1994; Neubauer *et al.*, 2002; Emerson & Weiss, 2004; James & Ferris, 2004; Roden *et al.*, 2004; Ferris, 2005; Weber *et al.*, 2006; Rentz *et al.*, 2007; Druschel *et al.*, 2008; Emerson, 2012; Kendall *et al.*, 2012; Roden *et al.*, 2012; Vollrath *et al.*, 2013; Melton *et al.*, 2014; Emerson & de Vet, 2015). At pH 7, the half-life for Fe(II) in fully aerated freshwater is <15 min (Stumm & Morgan, 1996; Emerson & Weiss, 2004; Emerson, 2012; Emerson & de Vet, 2015); this half-life increases to about 2 hours at 12°C (Emerson & de Vet, 2015). Lowering pH can have a similar effect on prolonging the stability of Fe(II) (Emerson & Weiss, 2004). The lowered levels of dissolved O_2 act to limit the rate of abiotic oxidation, allowing bacteria to compete (Stumm & Morgan, 1996; James & Ferris, 2004; Roden *et al.*, 2004; Ferris, 2005; Weber *et al.*, 2006; Rentz *et al.*, 2007; Druschel *et al.*, 2008; Emerson *et al.*, 2010; McBeth *et al.*, 2011; Melton *et al.*, 2014). Within these narrowly geochemical and spatial constraints, however, FeOB thrive (Neubauer *et al.*, 2002; Emerson & Weiss, 2004; James & Ferris, 2004; Roden *et al.*, 2004; Ferris, 2005; Druschel *et al.*, 2008; Melton *et al.*, 2014; Emerson & de Vet, 2015).

Sustained microbial iron redox cycling has been observed in various redox interfacial environments, including groundwater (Anderson *et al.*, 2003; Anderson *et al.*, 2006), iron seeps (James & Ferris, 2004; Rentz *et al.*, 2007; Druschel *et al.*, 2008; Langley *et al.*, 2009b; Gault *et al.*, 2011; Ferris *et al.*, in press), plant roots and the rhizosphere (Emerson *et al.*, 1999; Weiss *et al.*, 2003; Emerson & Weiss, 2004), wetlands (Sobolev & Roden, 2001; Emerson & Weiss, 2004; Druschel *et al.*, 2008), caves (Kasama & Murakami 2001), and volcanic seamounts, hydrothermal vents, and

ridge flanks (Edwards *et al.*, 2003; Kennedy *et al.*, 2003; Edwards *et al.*, 2004; Langley *et al.*, 2009), to name but a few. FeOB are also capable of growth on steel (McBeth *et al.*, 2011), and regularly colonize human-made environments such as water distribution systems and drainage ditches (Emerson & Revsbech, 1994; Emerson & de Vet, 2015) where they regularly wreak havoc on infrastructure, contributing to biocorrosion through their manipulation of pH and redox potential (Rentz *et al.*, 2007; McBeth *et al.*, 2011; Emerson & de Vet, 2015). This manipulation can also have the consequence of enhancing the mobility of some contaminants in the environment (Chuan *et al.,* 2000).

Despite these detrimental effects, FeOB can be especially helpful microorganisms which are capable of sequestering contaminants in water systems (Anderson & Pedersen, 2003; James & Ferris, 2004; Roden *et al.*, 2004; Ferris, 2005; Anderson *et al.*, 2006; Rentz *et al.*, 2007; Blöthe & Roden, 2009; Gault *et al.*, 2011; Emerson & de Vet, 2015; Ferris *et al.*, in press), and the storage of nuclear waste (Warren & Ferris, 1998; Anderson & Pedersen, 2003; James & Ferris, 2004; Anderson *et al.*, 2006; Roden *et al.*, 2012).

3.2.1 Oxidation of Fe(II)

Both bacterial and abiotic oxidation of Fe(II) in the presence of O_2 depend on the Fe(III)/Fe(II) and O_2/H_2O redox couples, which have half-cell reactions:

$$Fe^{3+} + e^- \leftrightarrow Fe^{2+} \qquad (3.1)$$

$$0.25\ O_2 + H^+ + e^- \leftrightarrow 0.5H_2O \qquad (3.2)$$

with the corresponding overall reaction

$$Fe^{2+} + 0.25O_2 + H^+ \leftrightarrow Fe^{3+} + 0.5H_2O \qquad (3.3).$$

Oxidation of Fe(II)at circumneutral pH always comes with the concomitant precipitation and hydrolysis of Fe(III) (King *et al.*, 1995; Schwertmann *et al.*, 1995; Ferris, 2005; Emerson *et al.*, 2010), according to

$$Fe^{2+} + 3H_2O \leftrightarrow Fe(OH)_3 + 3H^+ \qquad (3.4).$$

The rate law for the oxidation of Fe(II) by O_2 can be written as

$$\frac{-d[Fe^{2+}]}{dt} = \frac{k[O_2][Fe^{2+}]}{[H^+]^2} \qquad (3.5)$$

with the overall fourth-order rate constant $k = 3 \times 10^{-12}$ mol L^{-1} min^{-1} at 25 °C (Stumm & Morgan, 1996). If pH and dissolved O_2 remain constant; the rate expression becomes pseudo-first order with respect to Fe(II)

$$-\frac{d[Fe^{2+}]}{dt} = k'[Fe^{2+}] \qquad (3.6)$$

with rate constant, k'

$$k' = \frac{k[O_2]}{[H^+]^2} \qquad (3.7).$$

This rate law describes the rate for homogenous, abiotic Fe(II) oxidation, where both Fe(II) and oxygen are dissolved (Melton *et al.*, 2014). In systems with Fe(II) oxidizing microbial activity, the total oxidation rate also includes two other processes: the microbial enzymatic oxidation, and abiotic autocatalytic oxidation (Sung & Morgan, 1980; Rentz *et al.*, 2007; Emerson, 2012; Vollrath *et al.*, 2012; Melton *et al.*, 2014). The rate constants for these processes are often much greater than the homogenous abiotic oxidation rate constants, however it is difficult to evaluate their respective contributions separately (Neubauer *et al.*, 2002; James & Ferris, 2004; Rentz *et al.*, 2007; Druschel *et al.*, 2008; Melton *et al.*, 2014).

Autocatalytic Fe(II) oxidation occurs when precipitated Fe(III) oxyhydroxides act as an adsorbent for dissolved Fe(II), which is then heterogeneously oxidized by O_2; with the reductant and oxidant are in two different physical phases (Melton *et al.*, 2014). Autocatalytic oxidation presents yet another challenge for FeOB to overcome; not only does the biogenic reaction product become a substrate competitor for the FeOB (Warren & Ferris, 1998; Neubauer *et al.*, 2002; James & Ferris, 2004; Rentz *et al.*, 2007; Melton *et al.*, 2014), but Fe(III) precipitates will entomb the cell if

they are not prevented from accumulating, cutting of their energy source (Emerson *et al.*, 2010; Vollrath *et al.*, 2012). The solubility of Fe(III) oxyhydroxides is documented to be suppressed in the presence of FeOB (Vollrath *et al.*, 2013; Ferris *et al.*, in press).

Until recently, the importance of microbial contributions to circumneutral Fe(II)-oxidation have been discounted due to the rapid chemical oxidation of Fe(II) in the presence of O_2 at circumneutral pH, however the environmental significance of this process is now being recognized (Weber *et al.*, 2006; Melton *et al.*, 2014). Distinguishing contributions from each of the three contributing oxidation processes remains difficult (Rentz *et al.*, 2007; Druschel *et al.*, 2008). Here we will distinguish iron oxidation in a mature, circumneutral Fe(II) oxidizing microbial mat from its microbial mat-free inflow to assess how cell count and substrate availability affect fluctuation fluctuations in oxidation-reduction (redox) potential.

3.2.2 Redox Potential

FeOB can manipulate the geochemistry of their environment through bioenergetic metabolic reactions where they transfer electrons from reduced species (Fe(II)) to oxidized ones (O_2) (Bohn, 1971; Bethke *et al.*, 2011), exerting direct control on the relative proportion of reduced and oxidized species in their environment (van Bochove *et al.*, 2002). Microbes interact with their environment by driving redox reactions that can cause significant changes in pH and redox potential (Druschel *et al.*, 2008). Additionally, microaerophilic circumneutral FeOB contribute to iron cycling in oxic environments where they couple metabolism to growth (Ghiorse, 1984; Emerson & Moyer, 1997; Sobolev & Roden, 2001; Edwards *et al.*, 2003; Weber *et al.*, 2006). As such, FeOB may significantly impact the geochemistry of their environment as they control the movement of chemical species within their niche (Druschel *et al.*, 2008).

The redox state of an environment is inherently linked to redox potential, which is described by the Nernst equation:

$$E = E^0 + \frac{RT}{nF} \ln \frac{[\text{oxidized species}]}{[\text{reduced species}]} \qquad (3.8)$$

where E is the redox potential of the cell (mV), E° is the electrochemical potential of the cell at standard conditions, R is the universal gas constant, T is absolute temperature, n is the number of electrons participating per ion, F is Faraday's constant, and Q is the reaction quotient,

$\frac{[\text{oxidized species}]}{[\text{reduced species}]}$. Environmental factors including temperature, pH, and the presence of multiple redox couples can influence the redox potential of a microbial system, in addition to microbe-specific factors including nutrient levels, solution chemistry, growth substrate factors, and oxygen availability (Newman & Banfield, 2002). Considering its sensitivity to so many aspects of an environment, it is no surprise that redox potential is intricately linked to biological activity (Swerhone *et al.*, 1999; Ferris, 2005). This makes it an excellent candidate as a physicochemical observable parameter of biological activity.

If concentrations of all other redox active species remain constant, as in the case in a steady-state system, the Nernst equation can be rewritten to attribute all changes in redox potential to redox transformations of iron species (Nemati & Webb, 1997):

$$E = E^0 + \frac{RT}{nF} \ln \frac{[Fe^{3+}]}{[Fe^{2+}]} \qquad (3.9).$$

In this special case of steady-state conditions, with no other relevant redox couples, changes in the redox state of the system are directly attributed to changes in the oxidation states of iron.

3.2.3 Fluctuation Analysis and Brownian Motion

Fluctuations in potential are thought to arise from the random collisions of particles in solution, and are typically sub-mV in (Gabrielli *et al.*, 1993). This basis in particle collisions creates a link between the diffusion of chemical species in solution, and redox potential as an observable. This also allows us to model fluctuations using random walks, or Brownian motion. Brownian motions are non-stationary stochastic processes with stationary, uncorrelated, Gauss-distributed increments (Wiener, 1925; Eliazar & Shlesinger, 2013). Processes with correlated increments are called fractional Brownian motions (fBm) (Eliazar & Shlesinger, 2013).

Correlation is a property of a time series or process that describes the statistical dependence of directly and distantly neighboured values (Witt & Malamud, 2013). Long-range correlations are where all or almost all values are correlated with one another, that is, values are correlated with one another at very long lags in time (Taqqu & Samorodnitsky, 1992; Beran 1994; Witt & Malamud, 2013). Persistence is where large values tend to follow large ones, and small values tend to follow small ones, on average, more of the time than if the time series were uncorrelated (Witt &

Malamud, 2013). The strength of both persistence and anti-persistence can vary from weak to very strong; as defined by the magnitude of the correlation coefficient (Witt & Malamud, 2013).

Brownian motion describes the motion of a single particle diffusing according to Fick's laws (Metzler & Klafter, 2000), and the path of that particle through time creates linear scaling in a plot of mean-squared-displacement (MSD) through time (Metzler & Klafter, 2000; Witt & Malamud, 2013; Jeon *et al.*, 2014; Kim, 2014). When the MSD is described by non-linear growth through time, most often in the form of a scale-free power law, diffusion is described as "anomalous" (Metzler & Klafter, 2000; Witt & Malamud, 2013; Jeon *et al.*, 2014; Kim, 2014).

3.2.4 Detrended Fluctuation Analysis

Detrended fluctuation analysis (DFA) determines the strength of correlation in a time series of fluctuations by calculating the relationship between root-mean-square (RMS) and time window length in fluctuation time series data (Peng *et al.*, 1994). A brief description of the steps is given in the methods section.

3.2.5 Anomalous Diffusion

Self-affine processes have at least one measurement, temporal, or statistical distribution which follows a power-law function, which is the only mathematical function without a characteristic scale (Hardstone *et al.*, 2012). Self-affine phenomena are therefore called "scale-free" (Hardstone *et al.*, 2012). Instead, scale-free phenomena are better described by the exponent of a power-law function, because it captures the relationship between objects or fluctuations on different scales (Hardstone *et al.*, 2012). This exponent is the correlation coefficient calculated by DFA. Diffusion processes are known to be self-affine, with self-similar spatial trajectories (Levy, 1965; Feller, 1971; Mandelbrot, 1983; Fedder, 1988; Falconer, 1990; Takayasu, 1990; Gouyet, 1992; Hughes, 1995; Metzler & Klafter, 2000).

In this context, and conforming with random walk theory, Brownian motion, or normal diffusion, should give rise to a scaling exponent, $\alpha = 1$ (Metzler & Klafter, 2000; Ramanujan *et al.*, 2006), and correlation coefficients $1 < \alpha < 2$ arise from processes exhibiting fractional Brownian motion (Metzler & Klafter, 2000; Eliazar & Shlesinger, 2013). Additionally, in random uncorrelated time series $\alpha = 0.5$, whereas $\alpha < 0.5$ indicates negative persistence and $\alpha > 0.5$ indicates positive persistence (Peng e *et al.*, 1994; Peng *et al.*, 1995; Metzler & Klafter, 2000; Hardstone & 2012; Witt & Malamud, 2013). This further implies that exponents deviating from 1 represent systems

exhibiting anomalous diffusion processes. By calculating correlation coefficients for the flow-through cell and its microbial-mat-free inflow pipe it is possible to compare how diffusion behaviour differs in two different circumneutral, microaerophilic iron-oxidizing systems; one affected by autocatalytic oxidation as well as a high amount of microbial activity, and one with a low cell count, and no reactive substrate.

3.3 Methods

3.3.1 Site Description

The study was conducted 297 m underground at experimental site 2200A in the Äspö Hard Rock Laboratory (HRL) near Oskarshamm on the Baltic coast of Sweden (599685 m E 6366835 m N UTM zone 33V). At the site, groundwater from a hydraulically conductive fracture is delivered at a flow rate of 0.65 L min^{-1} from a packed-off section of borehole KA2198A through round 0.6 cm stainless steel tubing to a 200 x 30 x 25 cm (length x width x height) flow cell. The flow cell is approximately half-filled with granite cobble (Anderson & Pedersen, 2003), giving a nominal volume of 72L, and a specific discharge of 19.8 $cm^3\ cm^{-2}\ min^{-1}$. The flow cell has 200 mm-long in-flow chamber at each end, such that uniform linear flow can be assumed within the flow cell's main chamber.

To ensure steady state biogeochemical conditions before any experimentation, the flow through cell was allowed to operate undisturbed in the dark for a period of 12 months, allowing a natural community of *Gallionella ferruginea* and other Fe(II)-oxidizing bacteria to establish itself, and form extensive accumulations of orange-colored BIOS in the flow through cell. Details concerning the hydrogeology of the borehole and development of BIOS have been described previously (Anderson & Pedersen, 2003), as has the microbiology of these fluids (Anderson *et al.*, 2006). While not sterile, the groundwater represents a substrate-free, low cell count control for Fe(II) oxidation as no BIOS is observed within the in-flow chamber (Anderson *et al.*, 2006). The flow cell is open to air, such that pO_2 is constant.

3.3.2 Data Acquisition

Continuous monitoring of pH, temperature, dissolved O_2 and redox potential was accomplished using a YSI Environmental QS 600 multiple electrode sonde and YSI EcoWatch® data logging software. After mounting on a retort stand, the sonde was submerged to position all

electrodes and sensors at a depth of approximately 12.5 cm at the groundwater inlet and midway along the length flow cell in the BIOS. Measurements were recorded at one second intervals (i.e., at a data acquisition frequency of 1 Hz) for approximately 40 minutes.

3.3.3 Geochemical Analysis

Water samples were collected three times over 24 hours from the inlet and outlet of the flow cell; 2 hours before the start of continuous pH, temperature, dissolved O_2 and redox potential monitoring, then 2 hours and 20 hours afterwards. The samples were collected in sterile 500 mL acid-washed polypropylene bottles and 250 mL aliquots were vacuum filtered using 0.22 μm-pore-size membrane filters. Concentrations of total Fe and Fe(II) were measured on site using a HACH DR/2500 spectrophotometer with FerroVer® and 1,10 phenanthroline reagents (HACH), respectively.

3.3.4 Correlation Analysis

DFA (Peng *et al.*, 1994) was used to determine scaling exponents (i.e., α values) of RMS fluctuation amplitude of redox potential. The utility of DFA to calculate correlation coefficients in other time series has been described elsewhere (Peng *et al.,* 1994; Peng *et al.,* 1995; Varotsos *et al.,* 2005; Dingwell & Cusumano, 2010; Hardstone *et al.,* 2012). To reiterate briefly, the first step in DFA is to subtract the mean and integrate the time series to generate a random walk profile of the data. The profile is then divided into *j* windows of length *s* and local linear least squares fits are determined for each window. RMS deviations of are calculated afterwards by subtracting the local linear trend in each window from the integrated random walk profile. The RMS fluctuation amplitudes are subsequently averaged across the corresponding number of windows *j* and plotted against window size s in log-log space. A linear relationship between window size and average RMS deviation indicates scale-invariant power law behavior

$$RMS \cong Cs^{\alpha} \qquad (3.9)$$

where C represents a constant fluctuation coefficient and the scaling exponent α is a quantitative measure of long-range persistence, or time-domain self-similarity, in the time series (Peng *et al.*, 1994; Bryce & Sprague, 2012). The scaling exponent is estimated by fitting experimental data to the relationship

$$\log RMS = \alpha \log s + \log C \qquad (3.10).$$

In random uncorrelated time series $\alpha = 0.5$, whereas $\alpha < 0.5$ indicates negative persistence and $\alpha > 0.5$ indicates positive persistent with $\alpha \in (1,2)$ relating to processes exhibiting fractional Brownian motion (Metzler & Klafter, 2000; Eliazar & Shlesinger, 2013). At $\alpha = 1$, normal diffusion, or, true Brownian motion, is observed (Metzler & Klafter, 2000; Ramanujan *et al.*, 2006). For this investigation, DFA was implemented in MatLAB. Input data included the observed ~40 minute 1.0 Hz inlet and BIOS redox potential time series measurements (n=2500, at a measurement frequency of 1 sample/second), as well as corresponding randomly shuffled data sets.

Both time series were shuffled using the MatLAB "rand" function to create an index matrix which re-orders the measurements in a series. This function was used repeatedly (~100 times) in order to ensure a truly random order of the data. This step ensured no spurious correlation had been introduced by the algorithm and allowed comparison of individual windows in order to ensure there were no transient electrochemical affects or perturbations affecting the calculation of scaling exponents. To create a pool of realizations from the original 1 Hz sampling frequency time series, the full time series (n=2500), as well as 4 n=1000 realizations (n_{start} = 0, 501, 1001, 1501) time series, and 2 n=1250 realizations were created. The shortest realizations, n=1000 are consistent with the minimum reliable length for the optimal performance of DFA as described by Shao *et al*, (2012).

3.4 Results and Discussion

3.4.1 Physicochemical Conditions

Measurements for inlet temperature, pH, redox potential and dissolved O_2 indicated stable conditions throughout the period of continuous measurement in the flow cell (Fig. 3.1); vertical variations are assumed to be minimal. Specifically, temperature and pH remained steady near 12.4 ^oC and 7.4, respectively, with dissolved O_2 around 0.11 ± 0.01 mg/L. Observed temperature, pH, and dissolved O_2 were the same at the mid-point of the flow cell in the BIOS; however, mean redox potential was lower at the inlet (i.e., mean value of -135.4 ± 1.16 mV) than in the BIOS (i.e., mean value of -112.6 ± 1.91 mV).

The inlet and outlet concentrations of dissolved Fe(II) remained constant within standard errors of measurement over the 24 hour period before and after the interval of continuous monitoring of pH, temperature, dissolved O_2 and redox potential (Table 3.1). Total Fe and Fe(II) concentrations were greater at the inlet than the outlet concentrations, whereas Fe(III) concentrations (calculated as the difference between total Fe and Fe(II) concentrations) were the same at both the inlet and the outlet. These quantities are an expression of a dynamic steady state where the overall system chemistry is balanced by a combination of material fluxes and chemical reactions. Specifically, the oxidation of Fe(II) accounts for the observed decrease in concentration from 21.0 ± 0.5 μM at the inlet to 8.5 ± 0.7 μM at the outlet. Similarly, mass balance constraints associated with the hydrolysis and precipitation of Fe(III) as HFO accounts for the lower total Fe concentration at the outlet. Moreover, similar concentrations of dissolved Fe(III) at the inlet and outlet suggest that rates of Fe(II)-oxidation and HFO precipitation balance each other.

The mean inlet and BIOS redox potentials in the flow cell were lower than would be expected when compared to equilibrium values calculated using PHREEQC for the measured concentrations of Fe(II) and Fe(III) (Fig. 3.2); and measured pH is about 0.5 units lower than would be expected for this system at chemical equilibrium. These differences relate to the existence of dynamic steady state conditions in the flow cell. Specifically, protons released from the hydrolysis and precipitation of Fe(III) exert a downward push on pH while ongoing chemical and bacterial Fe(II)-oxidation drive the process (Warren & Ferris, 1998); these processes balance each other so as to maintain constant (within error) physicochemical conditions despite the fact that these processes are not at equilibrium.

3.4.2 Fe(II)- oxidation Rates

Assuming steady-state conditions within the flow cell, with a uniform flow field with an average linear velocity, ν, and negligible hydrodynamic dispersion along the principal axis, x, of the flow cell, the rate of change in Fe(II) concentration associated with reactive mass transport is (Fetter, 1999)

$$\frac{-d[\mathrm{Fe}^{2+}]}{dt} = v\frac{d[Fe^{2+}]}{dx} + k'[\mathrm{Fe}^{2+}] \qquad (3.10).$$

By definition in a steady state

$$\frac{-d[\mathrm{Fe}^{2+}]}{dt} = 0 \qquad (3.11)$$

equation 3.10 becomes

$$\frac{-d[Fe^{2+}]}{dx} = \frac{k'}{v}[\mathrm{Fe}^{2+}] \qquad (3.12).$$

Integration and rearrangement yields

$$k' = \frac{v}{x}\ln\frac{[Fe^{2+}]_x}{[Fe^{2+}]_{x=0}} \qquad (3.13).$$

From equation 3.7 with the inlet concentration $[\mathrm{Fe(II)}]_{x=0}$ = 21.0 ± 0.5 μM, outlet concentration $[\mathrm{Fe(II)}]_x$ = 8.5 ± 0.7 μM, flow cell length of 200 cm, and average linear water velocity, v, of 0.853 cm min^{-1}, the Fe(II)-oxidation rate constant k'_{BIOS} = 0.00386 ± 0.001 min^{-1}. In contrast, the measured pH and dissolved O_2 concentration in the flow cell result in the calculated value from equation 3.7 for chemical Fe(II)-oxidation k'_{Inlet} = 0.00157 min^{-1}. These values k'_{BIOS} and k'_{Inlet} are within the ranges reported for bacterial and chemical oxidation of Fe(II), and broadly similar with the reported result that biological activity can result in as much as a six-fold increase in oxidation rates (James & Ferris, 2004; Rentz *et al.*, 2007).

3.4.3 Long-Range Correlation

Inlet and BIOS redox potential measurements for a window length of s = 120 s are shown in Fig. 3.3, as are shuffled redox potential time series and corresponding random walk profiles. At the 1 sample/second (1 Hz) measurement frequency, incremental steps in inlet and BIOS redox potential show a more uniform pattern than the shuffled data. Similarly, the inlet and BIOS mV random walk profiles are smoother and traverse persistently over broader lengths of time compared to the random walk profiles of the shuffled data.

A log-log plot of RMS fluctuations in observed and shuffled random walk redox potential profiles as a function of window size is shown in Fig. 3.4. These plots demonstrate power law

scaling behavior and show how RMS deviations in redox potential fluctuations increase nonlinearly over longer windows of time. Shuffled time series data from the inlet and BIOS yielded corresponding α scaling exponents of 0.50 and 0.51 that describe random uncorrelated time series (Table 3.2). At the same time, the scaling exponent for redox potential fluctuations in the BIOS was 1.89 ± 0.03 compared to 1.67 ± 0.06 for the inlet. These α values signal the existence of strong long-range correlation in redox potential in both the presence and absence of BIOS. Furthermore, in one-sided *t*-tests, the inlet and BIOS α values were significantly different at a level of $p < 0.01$. This indicates that one or both of the factors of the presence of substrate or the number of cells appears to affect scaling behaviour. There are broad similarities in the differences in scaling exponents and oxidation rate constants, that is, higher oxidation rates can be associated with higher scaling rate values, but this relationship is rather tenuous and requires further exploration. It does, however, hint at a relationship between oxidation rate constant and scaling exponent.

3.4.4 Biogeochemical Significance

Determination of nonlinear redox potential scaling exponents for Fe(II)-oxidation conform well to the anomalous diffusion paradigm, particularly the increased level of persistence (i.e., higher α value) and greater reaction rate constant evident for FeOB. In terms of underlying reaction mechanisms, chemical Fe(II)-oxidation depends on diffusive collisions with dissolved oxidizing species in solution (Stumm & Morgan, 1996; Anderson, 2005), whereas FeOB rely on diffusion to intercept and retain Fe(II) before metabolic electron transport-mediated oxidation can occur (Bird *et al.*, 2011). FeOB diminish the activation energy barrier for HFO nucleation (Warren & Ferris, 1998; Kasama & Marakami, 2001; James & Ferris, 2004), increasing their energetic gain from iron oxidation by 10% (James & Ferris, 2004). However, recent results (Vollrath *et al.*, 2013; Ferris *et al.*, in press) indicate that the solubility of HFO is enhanced in the presence of bacteria.

Viable cell counts in the inlet have been reported as 2.76×10^4 cells/mL, compared to 1.37×10^8 cells/mL within the flow cell (Anderson *et al.*, 2006), however, with no BIOS visible in the inlet, this raises an interesting question about the influence of phase changes on fluctuation behaviour which bears further examination. It also raises the question of whether or not the number of bacteria present will impact the fluctuation behaviour.

Within this flow cell, the process most likely giving rise to the anomalous diffusion behavior as indicated by redox potential fluctuations is the oxidation of Fe(II) and formation of HFO. By maintaining proximity to soluble or nanoparticulate HFO (Vollrath *et al.*, 2013; Ferris *et al.*, in

press), bacteria appear to lower the concentration of Fe(II) in their immediate surroundings relative to the bulk solution, driving greater diffusion of Fe(II) than is observed in the chemical-oxidation dominated system at the inlet. In this way, the difference in scaling exponents observed in the chemical-oxidation and biological-oxidation systems may be directly attributed to enhanced oxidation of Fe(II) and sequestration of Fe(III), albeit not necessarily precipitation of HFO by FeOB.

The significance of this result could be profound, since power law scaling exponents associated with redox potential fluctuations are determined without any measurements of metabolites or genomics. They depend only on the physicochemical behaviour of the system, allowing direct comparison between different niches and communities. While biological activity has not been isolated here, the dramatic shift in the observed scaling exponent that can be attributed specifically to the presence of an FeOB microbial community is a promising method for distinguishing the presence of FeOB *in situ*. With significant additional data, it is possible that scaling exponents could be used as a physically-constrained biosignature to assess the presence of specific microbial metabolic pathways present in a system. It may also be fruitful to consider the use of ion-specific electrodes to assess difference in behaviour among chemical species of interest, instead of relying exclusively on the bulk parameter of redox potential. These results are promising and highlight the fact that the sensitivity of redox potential to chemical changes, and the field of fluctuation analysis at large, and have significant insight to offer environmental microbiology.

3.5 References

Anderson CR, Pedersen K (2003) In situ growth of Gallionella biofilms and partitioning of lanthanides and actinides between biological material and ferric oxyhydrides. *Geobiology*, **1**, 169-178.

Anderson CR, James RE, Fru EC, Kennedy EB, Pedersen, K (2006) In situ ecological development of a bacteriogenic iron oxide-producing microbial community from a subsurface granitic rock environment. *Geobiology*, **4**, 29-42.

Anderson G (2005) *Thermodynamics of natural systems*, 2nd, ed.; Cambridge University Press: Cambridge, U.K.

Beran J (1994) *Statistics for long-memory processes*. Chapman & Hall/CRC, New York.

Bethke CM, Sanford RA, Kirk MF, Jin Q, Flynn TM (2011) The Thermodynamic Ladder in Geomicrobiology. *American Journal of Science,* **311**, 183-210.

Bird LJ, Bonnefoy V, Newman DK (2011) Biogenergetic challenges of microbial iron metabolisms. *Trends in Microbiology*, **19**, 330-340.

Blöthe M, Roden EE (2009) Microbial Iron Redox Cycling in a Circumneutral-pH Groundwater Seep. *Applied and Environmental Microbiology*, **75**, 468-473.

Bohn HI (1971) Redox Potentials. *Soil Science*, **112**, 39-45.

Bryce RM, Sprague KB (2012) Revisiting detrended fluctuation analysis. *Scientific Reports*, **2**, 1-6.

Chuan MC, Shu GY, Liu JC (1996) Solubility of Heavy Metals in a Contaminated Soil: Effects of Redox Potential and pH. *Water, Air, and Soil Pollution*, **90**, 543-556.

Druschel GK, Emerson D, Sutka R, Suchecki P, Luther GW (2008) Low-oxygen and chemical kinetic constraints on the geochemical niche of neutrophilic iron(II) oxidizing organisms. *Geochimica et Cosmochimica Acta*, **72**, 3358-3370.

Edwards KJ, Bach W, Rogers DR (2003) Geomicrobiology of the ocean crust: a role for chemoautotrophic Fe-bacteria. *Biology Bulletin*, **204**, 180–185.

Edwards KJ, Bach W, McCollom TM, Rogers DR (2004) Neutrophilic iron-oxidizing bacteria in the ocean: their habitats, diversity, and roles in mineral deposition, rock alteration, and biomass production in the deep-sea. *Geomicrobiology Journal*, **21**, 393–404.

Eliazar II, Shlesinger MF (2013) Fractional motions. *Physics Reports*, **527**, 101-129.

Emerson D, Revsbech NP (1994) Investigation of an Iron-Oxidizing Microbial Mat Community Located near Aarhus, Denmark: Field Studies. *Applied and Environmental Microbiology*, **60**, 4022-4031.

Emerson D, Moyer CL (1997) Isolation and characterization of novel iron-oxidizing bacteria that grow at circumneutral pH. *Applied and Environmental Microbiology*, **63**, 4784–92.

Emerson D, Weiss JV, Megonigal JP (1999) Iron-oxidizing bacteria are associated with ferric hydroxide precipitates (Fe-plaque) on the roots of wetland plants. *Applied and Environmental Microbiology*, **65**, 2758–2761.

Emerson D, Weiss JV (2004) Bacterial iron oxidation in circumneutral freshwater habitats: findings from the field and the laboratory. *Geomicrobiology Journal*, **21**, 405–414.

Emerson D, Fleming EJ, McBeth JM (2010) Iron-oxidizing bacteria: an environmental and genomic perspective. *Annual Reviews of Microbiology*, **64**, 561–583.

Emerson D (2012) Biogeochemistry and microbiology of microaerobic Fe(II) oxidation. *Transactions of the Biochemical Society*, **40**, 1211-1216. doi: 10.1042/BST20120154.

Emerson D, de Vet W (2015) The Role of FeOB in Engineered Water Ecosystems: A Review. *Journal AWWA* , **107**, E47-E57.

Falconer K (1990) *Fractal Geometry: Mathematical Foundations and Applications*, Wiley, Chichester, UK.

Fedder J (1988) *Fractal*s, Plenum, New York.

Feller W (1971) *An Introduction to Probability Theory and its Applications*, Vol. 2, Wiley, New York.

Ferris FG (2005) Biogeochemical properties of bacteriogenic iron oxides. *Geomicrobiology Journal*, **22**, 79–85.

Ferris FG, Enright AML, Fortin D, Clark ID. In press. Rates of Fe(II)-oxidation and Solubility of Bacteriogenic Iron Oxides. *Geomicrobiology Journal.*

Fetter CW (1999) *Contaminant hydrogeology*, 2nd, ed.; Waveland Press: U.S.A.

Fortin D, Langley S (2005) Formation and occurrence of biogenic iron-rich minerals. *Earth Sciences Reviews*, **72**, 1-19.

Gabrielli C, Huet F, Keddam H (1993) Fluctuations in electrochemical systems. I. General theory on diffusion limited electrochemical reactions. *Journal of Chemical Physics*, **99**, 7232-7239.

Gault AG, Ibrahim A, Langley S, Renaud R., Takahashi Y, Boothman C, Lloyd JR, Clark ID, Ferris FG, Fortin D (2011) Microbial and geochemical features suggest iron redox cycling within bacteriogenic iron oxide-rich sediments. *Chemical Geology*, **281**, 41-51.

Ghiorse WC (1984) Biology of iron-and manganese-depositing bacteria. *Annual Reviews of Microbiology*, **38**, 515–50.

Gouyet J-F (1992) *Physique et Structures Fractales*, Masson, Paris.

Hardstone R, Poil S-S, Schiavone G, Jansen R, Nikulin VV, Mansvelder HD, Linkenkaer-Hansen K (2012) Detrended fluctuation analysis: a scale-free view on neuronal fluctuations. *Frontiers in Physiology*, **3**, 450.

Hughes BD (1995) *Random Walks and Random Environments*, Vol. 1: Random Walks, Oxford University Press, Oxford.

James RE, Ferris FG (2004) Evidence for microbial-mediated iron oxidation at a neutrophilic groundwater spring. *Chemical Geology*, **212**, 301-311.

Jeon J-H, Chechkin AV, Metzler R (2014) Scaled Brownian motion: a paradoxical process with a time dependent diffusivity for the description of anomalous diffusion. *Physical Chemistry Chemical Physics*, **16**, 15811.

Kasama T, Marakami T (2001) The effect of microorganisms on Fe precipitation rates at neutral pH. *Chemical Geology*, **180**, 117 - 128.

Kendall B, Anbar AD, Kappler A, Konhauser, KO (2012) The Global Iron Cycle. In *Fundamentals of Geobiology*. Knoll, A.H., Canfield, D.E., and Konhauser, K.O. (eds.) Blackwell.

Kennedy CB, Scott SD, Ferris FG (2003) Characterization of bacteriogenic iron oxide deposits from axial volcano, Juan de Fuca Ridge, Northeast Pacific Ocean. *Geomicrobiology Journal*, **20**, 199-214.

Kim H-J (2014) Anomalous diffusion induced by enhancement of memory. *Physical Reviews E*, **90**, 012103.

King DW, Lounsbury HA, Millero FJ (1995) Rates and mechanism of Fe(II) oxidation at nanomolar total iron concentrations. *Environmental Science & Technology*, **29**, 818–24.

Langley S, Gault AG, Ibrahim A, Takahashi Y, Renaud R, Fortin D, Clark ID, Ferris FG (2009a) Sorption of strontium onto bacteriogenic iron oxides. *Environmental Science & Technology*, **43**, 1008-1014.

Langley S, Gault AG, Ibrahim A, Takahashi Y, Renaud R, Fortin D, Clark ID, Ferris FG (2009b) A comparison of the rates of Fe(III) reduction in synthetic and bacteriogenic iron oxides by Shewanella putrefaciens CN32. *Geomicrobiology Journal*, **26**, 57-70.

Levy P (1965) *Processus stochastiques et mouvement Brownien*, Gauthier-Villars, Paris.

Mandelbrot B (1983) *The Fractal Geometry of Nature*, Freeman, New York.

McBeth JM, Little BJ, Ray RI, Farrar KM, Emerson D (2011) Neutrophillic Iron-Oxidizing "Zetaproteobacteria" and Mild Steel Corrosion in Nearshore Marine Environments. *Applied Environmental Microbiology* **77,** 1405-1412.

Melton ED, Swanner ED, Behrens S, Schmidt C, Kappler A (2014) The interplay of microbially mediated and abiotic reactions in the biogeochemical Fe cycle. *Nature Reviews Microbiology,* **12,** 797-808.

McBeth JM, Little BJ, Ray RI, Farrar KM, Emerson D (2011) Neutrophillic Iron-Oxidizing "Zetaproteobacteria" and Mild Steel Corrosion in Nearshore Marine Environments. *Applied and Environmental Microbiology*, **77**, 1405-1412.

Nemati M, Webb C (1997) A Kinetic Model for Biological Oxidation of Ferrous Iron by Thiobacillus ferrooxidans. *Biotechnology and Bioengineering*, **53**, 478-486.

Neubauer SC, Emerson D, Megonigal JP (2002) Life at the Energetic Edge: Kinetics of Circumneutral Iron Oxidation by Lithotrophic Iron-Oxidizing Bacteria Isolated from the Wetland-Plant Rhizosphere. *Applied and Environmental Microbiology*, **68**, 3988-3995.

Newman DK, Banfield JF (2002) Geomicrobiology: How Molecular-Scale Interactions Underpin Biogeochemical Systems. *Science*, **296**, 1071-1077.

Peng C-K, Buldyrev SV, Havlin S, Simons M, Stanley HE, Goldberger AL (1994) Mosaic organization of DNA nucleotides. *Physical Reviews E*, **49**, 1685-1689.

Peng C-K, Havlin S, Stanley H, Goldberger A (1995) Quantification of scaling exponents and crossover phenomena in nonstationary heartbeat time series. *Chaos*, **5**, 82-87.

Ramanujan VK, Biener G, Herman BA (2006) Scaling behavior in mitochondrial redox fluctuations. *Biophysical Journal: Biophysical Letters*, **90**, L70-L72. doi: 10.1529/biophysj.106.083501.

Rentz JA, Kraiya C, Luther GW III, Emerson D (2007) Control of Ferrous Iron Oxidation within Circumneutral Microbial Iron Mats by Cellular Activity and Autocatalysis. *Environmental Science & Technology*, **41**, 6084-6089.

Roden EE, Sobolev D, Glazer B, Luther GW (2004) Potential for microscale bacterial Fe redox cycling at the aerobic-anaerobic interface. *Geomicrobiology Journal*, **21**, 379–391.

Roden EE, McBeth JM, Blöthe M, Percak-Dennett EM, Fleming EJ, Holyoke RR, Luther III GW, Emerson D, Schieber J (2012) The microbial ferrous wheel in a neutral pH groundwater seep. *Frontiers in Microbiology*, **3**, 172.

Schwertmann U, Bigham JH, Murad E (1995) The first occurrence of schwertmannite in a natural stream environment. *European Journal of Mineralogy*, **7**, 547–552.

Shao YH, Gu GF, Jiang SZQ, Zhou WX, Sornette D (2012) Comparing the performance of FA, DFA and DMA using different synthetic long-range correlated time series. *Scientific Reports* **2**, 835. doi:10.1038/srep00835.

Shao YH, Gu GF, Jiang SZQ, Zhou WX, Sornette D (2012) Comparing the performance of FA, DFA and DMA using different synthetic long-range correlated time series. *Scientific Reports*, **2**, 835, doi:10.1038/srep00835.

Stumm J, Morgan JJ (1996) *Aquatic chemistry: chemical equilibria and rates in natural waters*, 3rd, ed.; Wiley Interscience: U.S.A.

Sung W, Morgan JJ (1980) Kinetics and product of ferrous iron oxygenation in aqueous systems. *Environmental Science & Technology*, **14**, 561–68.

Swerhone GDW, Lawrence JR, Richards JG, Hendry MJ (1999) Construction and Testing of a Durable Platinum Wire Eh Electrode for In Situ Redox Measurements in the Subsurface. *GWMR*, 132-136.

Takayasu H (1990) *Fractals in the Physical Sciences*, Manchester University Press, Manchester.

Taqqu MS, Samorodnitsky G (1992) Linear models with long-range dependence and finite or infinite variance. In: *New directions in time series analysis, Part II*, IMA Volumes in Mathematics and its Applications 46, Springer, pp 325–340.

van Bochove E, Beauchemin S, Theriault G (2002) Continuous Multiple Measurement of Soil Redox Potential Using Platinum Microelectrodes. *Soil Science Society of America Journal*, **66**, 1813-1820.

Varotsos C, Ondov J, Efstathiou M (2005) Scaling properties of air pollution in Athens, Greece, and Baltimore, Maryland. *Atmospheric Environment*, **39**, 4041-4047.

Vollrath S, Behrends T, Van Cappellen P (2012) Oxygen Dependency of Neutrophilic Fe(II) Oxidation by Leptothrix Differs from Abiotic Reaction. *Geomicrobiology Journal*, **29**, 550-560.

Vollrath S, Behrends T, Koch CB, Van Cappellen P (2013) Effects of temperature on rates and mineral products of microbial Fe(II) oxidation by Leptothrix cholodnii at microaerobic conditions. *Geochimica et Cosmochimica Acta*, **108**, 107-124.

Warren LW, Ferris FG (1998) Continuum between sorption and precipitation of Fe(III) on microbial surfaces. *Environmental Science & Technology*, **32**, 2331-2337.

Weber KA, Achenbach LA, Coates JA (2006) Microorganisms pumping iron: anaerobic microbial iron oxidation and reduction. *Nature Reviews Microbiology*, **4**, 752–764.

Weiss JV, Emerson D, Backer SM, Megonigal JP (2003) Enumeration of Fe(II)-oxidizing and Fe(III)-reducing bacteria in the root zone of wetland plants: Implications for a rhizosphere iron cycle. *Biogeochemistry*, **64**, 77–96.

Wiener NJ (1923) Differential Space. *Journal of Mathematical Physics*, **2**, 131-174.

Witt A, Malamud BD (2013) Quantification of long-range persistence in geophysical time series: conventional and benchmark-based improvement techniques. *Surveys in Geophysics*, **34**, 541-651.

Tables

Table 3.1: Mean concentrations and standard errors for measurements of total Fe, Fe(II), and Fe(III) over a 24 hour monitoring period in the Äspö flow through cell, 297 m underground at experimental site 2200A.

Source	Concentration μM		
	Total Fe	Fe(II)	Fe(III)
Inlet	22.1 ± 0.3	21.0 ± 0.5	1.2 ± 0.8
Outlet	9.8 ± 1.6	8.5 ± 0.7	1.3 ± 0.9
Change	-12. 3 ± 1.9	-12.5 ± 1.3	0.1 ± 1.7

Table 3.2: The time invariant scaling exponents (values) and standard errors determined from detrended fluctuation analysis of observed and randomly shuffled redox potential time series measurements at the inlet and in the BIOS mat of the Äspö flow through cell, 297 m underground at experimental site 2200A. The observed inlet and BIOS α values are significantly different at $p < 0.01$ in one-sided t-tests.

Time Series	Time Invariant Scaling Exponent (α value)	
	Measured	Shuffled
Inlet	1.67 + 0.06	0.50 + 0.01
BIOS	1.89 + 0.03	0.51 + 0.01

Figures

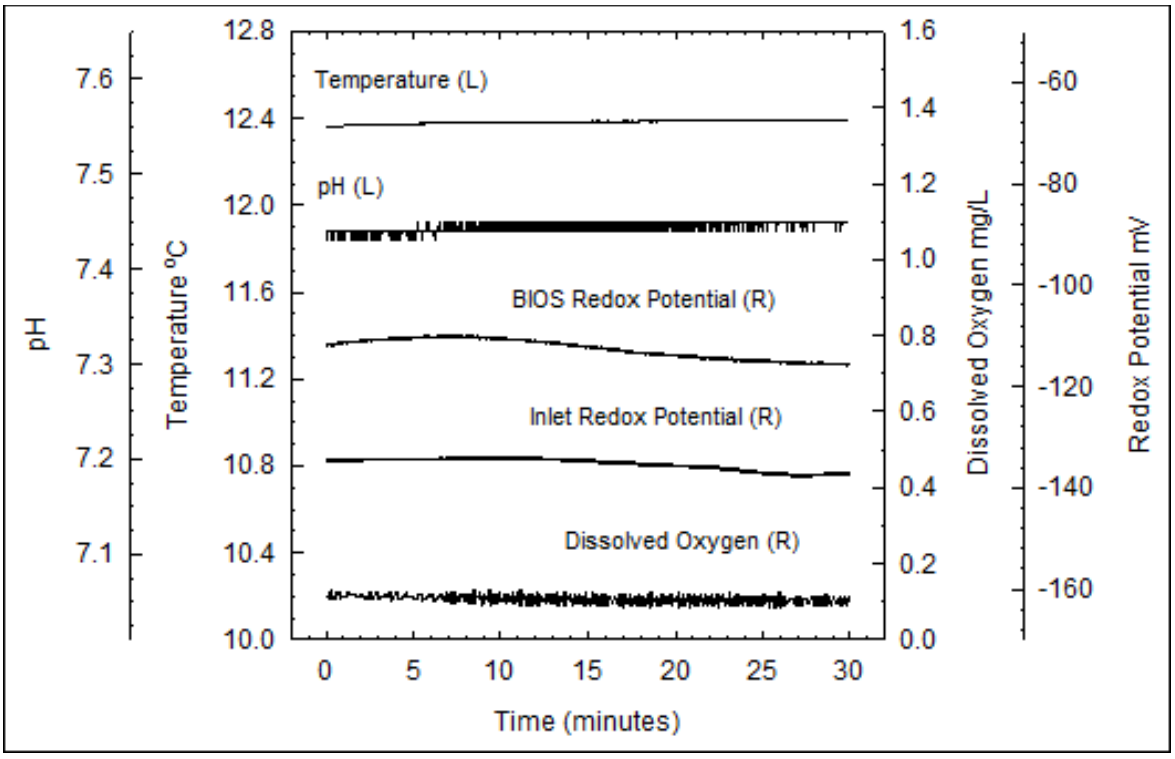

Figure 3.1: Temperature, pH, BIOS redox potential, inlet redox potential, and dissolved O_2 profiles over 30 minutes of data logging at one second intervals in the Äspö flow through cell, 297 m underground at experimental site 2200A.

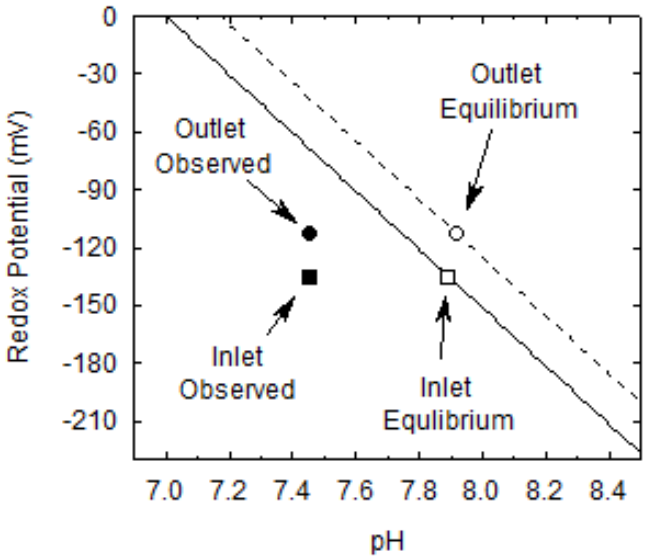

Figure 3.2: The equilibrium redox potential calculated using PHREEQC for the Äspö flow cell inlet (solid line) and outlet (dashed line) as a function of pH. The observed pH and redox potentials are shown as solid symbols; open symbols represent measured redox potential values positioned at equilibrium pH.

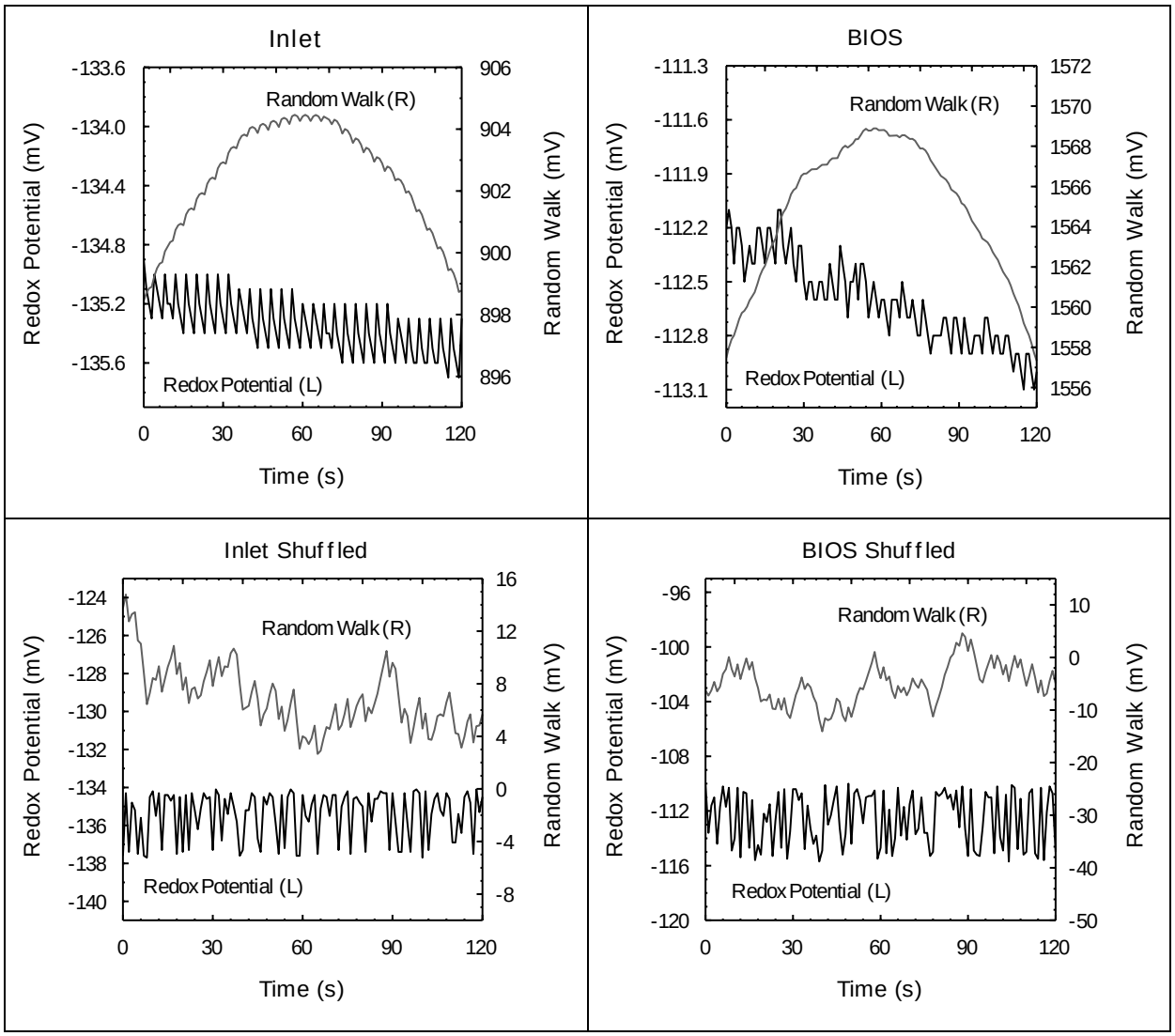

Figure 3.3: The observed (bottom, left axis) and random walk (top, right axis) redox potential across an interval of 120 seconds for the inlet, BIOS, and randomly shuffled time series measurements in the Äspö flow through cell, 297 m underground at experimental site 2200A.

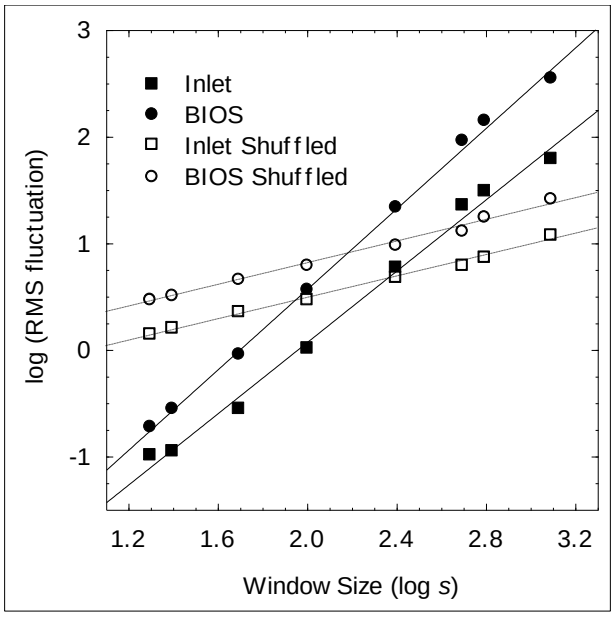

Figure 3.4: Log-log plot of root mean square fluctuations (mV) for inlet, BIOS, and randomly shuffled redox potential time series as a function of time interval window size *s* (seconds) in detrended fluctuation analysis.

Chapter 4
Comparing Oxidation Rate Constants and Diffusion of Fe(II) in Circumneutral Fe(II)-Oxidizing Microbial Communities

4.1 Abstract

Oxidation rate constants were determined for a series of four microcosms collected from an anoxic, reduced, Fe(II)-rich groundwater seep and its associated Fe(II)-oxidizing microbial mat. The four microcosms consisted of two live systems, a biological control, and a chemical control. One live system represented a system approximating the *in situ* conditions of the study site, while the other represented a system of maximal biomass. Physicochemical parameters and concentrations of dissolved ferrous and total iron concentrations were measured at 30 minute intervals. Diffusion behaviour was characterized using fluctuation analysis of time series of oxidation-reduction (redox) potential. The power-law scaling exponents of root-mean-square (RMS) fluctuations in oxidation-reduction (redox) potential were compared to instantaneous oxidation rates, revealing a relationship between rate constant and persistence in redox potential fluctuations. Calculated Damköhler numbers and scaled waiting time coefficients echo the magnitudes of the four calculated pseudo-first order oxidation rate constants, but fluctuation behaviour distinguishes the biological and abiotic systems, independent of substrate availability or cell numbers.

4.2 Introduction

Until now, detrended fluctuation analysis has revealed that biological systems exhibit stronger correlation behaviour than abiotic systems (Chapter 2), and there appears to be some influence from the presence of hydrous ferric oxides (HFO) and cell count on the strength of correlations (Chapter 3). Understanding how microbial mats outpace abiotic oxidation processes on the scale of a microbial community, and being able to measure biological activity *in situ* would provide significant new information about the chemical dynamics of microbial mats. Here, four microcosms will allow a direct comparison between correlation behaviour in a completely abiotic system with only homogenous abiotic Fe(II)-oxidation, a killed system with a combination of

autocatalytic and homogenous abiotic Fe(II)-oxidation, a live system approximating natural conditions at the field site, and a maximal biomass live system, to assess the influence of cell number on both oxidation rate and fluctuation behaviour.

4.2.1 Environmental Significance of Fe(II)-oxidizing Bacteria

In modern biogeochemistry, global cycling of iron is relies on microorganisms exploiting the Fe(III)/Fe(II) redox couple in both oxidative and reductive metabolic pathways (Weber *et al.*, 2006; Melton *et al.*, 2014). Iron is an abundant microbial energy source (Emerson *et al.*, 2012); however the oxygenation of Earth's atmosphere imposed limits on its spatial extent due mostly to the rapid chemical oxidation of Fe(II) at circumneutral pH in the presence of O_2. Until very recently, this meant the global geological and evolutionary significance of aerobic Fe(II) oxidation at circumneutral pH was discounted (Davison & Seed, 1983; Weber *et al.*, 2006). Microaerophilic, circumneutral Fe(II)-oxidizing bacteria (FeOB) oxidize Fe(II) by coupling this oxidation to the reduction of dissolved O_2. These bacteria are major players in a wide range of ancient and modern environmental systems, performing key roles in sequestering contaminants (Edwards *et al.*, 2004; Emerson & Weiss, 2004; Kappler & Newman, 2004; Roden *et al.*, 2004; Ferris, 2005; Anderson *et al.*, 2006; Rentz *et al.*, 2007; Druschel *et al.*, 2008; Langley *et al.*, 2009; Emerson *et al.*, 2010; Gault *et al.*, 2011; Kennedy *et al.*, 2011; Ferris *et al.*, in press), and the storage of nuclear waste (Warren & Ferris, 1998; Anderson & Pedersen, 2003; James & Ferris, 2004; Anderson *et al.*, 2006; Roden *et al.*, 2012). FeOB are also thought to contribute significantly to weathering processes (Edwards *et al.*, 2004; Weber *et al.*, 2006).

The oxygenation of Earth's atmosphere dramatically limited the availability of dissolved, Fe(II), however, in a number of niches of environmental interest and significance, Fe(II) is abundant enough to act as an energy source to robust communities of FeOB (Emerson *et al.*, 2012). Harsh chemical realities confine these niches; in order to compete with abiotic oxidation, FeOB require a pH range of 5.5 to 7.2 (Emerson *et al.*, 2010), partial pressure of O_2 of approximately 10% atmospheric levels (Roden *et al.*, 2004; Roden *et al.*, 2012), and a steady source of Fe(II) (Stumm & Morgan, 1996; Emerson & Moyer, 1997; Sobolev & Roden, 2001; James & Ferris, 2004; Roden *et al.*, 2004; Ferris, 2005; Weber *et al.*, 2006; Rentz *et al.*, 2007; Druschel *et al.*, 2008; Emerson *et al.*, 2010; McBeth *et al.*, 2011; Vollrath *et al.*, 2012; Vollrath *et al.*, 2013; Melton *et al.*, 2014).

Environments where FeOB tend to thrive most often involve anoxic, Fe(II)-rich water intersecting an oxygenated body of water (James & Ferris 2004; Emerson *et al.*, 2010; Gault *et al.*,

2011; McBeth *et al.*, 2011; Melton *et al.*, 2014); microbial iron redox cycling has been investigated include iron-rich groundwater seeps (James & Ferris, 2004; Rentz *et al.*, 2007; Duckworth *et al.*, 2009), the rhizosphere (Emerson & Weiss, 2004); oceanic ridges and hydrothermal vents (Kennedy *et al.*, 2003; Edwards *et al.*, 2004; Langley *et al.*, 2009), wetlands, (Sobolev & Roden, 2001; Druschel *et al.*, 2008; Vollrath *et al.*, 2012), and caves (Kasama & Murakami, 2001). FeOB also colonize a significant number of human-made environments, where they frequently contribute to biocorrosion through the alteration of pH and redox potential (Emerson & Revsbech, 1994; Rozanova *et al.*, 2003; Zuo & Wood, 2004; Rentz *et al.*, 2007; McBeth *et al.*, 2011; Emerson & de Vet, 2015).

4.2.2 Iron Oxidation

Chemical and biological oxidation of Fe(II) in the presence of oxygen depend on the Fe(III)/Fe(II) and O_2/H_2O redox couples, which have half-cell reactions:

$$Fe^{3+} + e^- \leftrightarrow Fe^{2+} \qquad (4.1)$$

and

$$0.25\ O_2 + H^+ + e^- \leftrightarrow 0.5H_2O \qquad (4.2)$$

with corresponding overall reaction

$$Fe^{2+} + 0.25O_2 + H^+ \leftrightarrow Fe^{3+} + 0.5H_2O \qquad (4.3).$$

Oxidation of Fe(II)at circumneutral pH always comes with the concomitant precipitation and hydrolysis of Fe(III) (King *et al.*, 1995; Schwertmann *et al.*, 1995; Ferris, 2005; Emerson *et al.*, 2010), according to

$$Fe^{2+} + 3H_2O \leftrightarrow Fe(OH)_3 + 3H^+ \qquad (4.4).$$

The rate law for the oxidation of iron by oxygen can be written as

$$\frac{-d[Fe^{2+}]}{dt} = \frac{k[O_2][Fe^{2+}]}{[H^+]^2} \qquad (4.5)$$

with the overall fourth-order rate constant $k = 3 \times 10^{-12}$ mol L^{-1} min^{-1} at 25 °C (Stumm & Morgan, 1996). When pH and dissolved O_2 are constant, rate constant becomes pseudo-first order with respect to Fe(II), and the rate expression can be simplified:

$$-\frac{d[Fe^{2+}]}{dt} = k'[Fe^{2+}] \qquad (4.6)$$

with rate constant, k'

$$k' = \frac{k[O_2]}{[H^+]^2} \qquad (4.7).$$

This rate law describes the rate for homogenous, abiotic Fe(II) oxidation, where both Fe(II) and O_2 are dissolved (Melton *et al.,* 2014); the abiotic oxidation rate is proportional to O_2 concentration and pH (Singer & Stumm, 1970; Rentz *et al.*, 2007).

Two additional processes contribute to the total oxidation rate of Fe(II) at circumneutral pH: microbially-mediated Fe(II) oxidation, and autocatalytic, or heterogeneous Fe(II) oxidation (Sung & Morgan, 1980; Wehrli *et al.*, 1989; Rentz *et al.*, 2007; Emerson, 2012; Vollrath *et al.*, 2012; Melton *et al.*, 2014). Autocatalytic Fe(II) oxidation occurs when precipitated Fe(III) oxyhydroxides act as an adsorbent for dissolved Fe(II), which is then heterogeneously oxidized by oxygen; the reductant and oxidant are in two different physical phases (Melton *et al.*, 2014).

The reaction rates of heterogeneous and microbial Fe(II) oxidation can be as much as six times larger than homogeneous Fe(II) oxidation rates (James & Ferris, 2004; Neubauer *et al.*, 2002; Rentz *et al.*, 2007; Druschel *et al.*, 2008; Melton *et al.*, 2014). As a consequence, the biogenic mineral product is a substrate competitor for microbial Fe(II) oxidation (Warren & Ferris, 1998; Neubauer *et al.*, 2002; James & Ferris, 2004; Rentz *et al.*, 2007; Melton *et al.*, 2014). This presents another hurdle for FeOB to overcome; unless Fe(III) precipitates are prevented from accumulating cells may become entombed in them, cutting off their energy source (Emerson *et al.*, 2010; Vollrath *et al.*, 2012).

Hydrous ferric oxides (HFO) are produced by microaerophilic Fe(II) oxidation when Fe(III) rapidly hydrolyzes and precipitates as nanoparticulate, poorly crystalline Fe(III) minerals (Bird *et al.*, 2001; Kasama & Murakami, 2001; Emerson & Weiss, 2004; Druschel *et al.*, 2008; Blöthe & Roden, 2009; Duckworth *et al.*, 2009; Emerson, 2012; Kato *et al.*, 2012; Melton *et al.*, 2014; Ferris *et al.*, in press) most commonly two-line ferrihydrite (Kasama & Murakami, 2001; Kennedy *et al.*, 2003; Ferris, 2005; Emerson *et al.*, 2010). Bacteriogenic iron oxides, or BIOS, refer to HFO that precipitate in close association with bacterial cells, ether as a result of direct microbial enzymatic oxidation or through autocatalysis (Warren & Ferris, 1998; Banfield *et al.*, 2000; Châtelier *et al.*, 2001; Rentz *et al.*, 2007; Emerson *et al.*, 2010; Emerson, 2012; Vollrath *et al.*, 2013; Ferris *et al.*, in press); typically intermixed with cellular debris and associated organic matter (Gault *et al.*, 2011).

4.2.3 Redox Potential

Metabolically active microorganisms directly influence the relative abundance of redox active substances in their environment through the transfer of electrons in bioenergetic metabolic reactions, directly regulating the redox state and chemical character (including pH) of their environment (van Bochove *et al.*, 2002; Druschel *et al.*, 2008; Bethke *et al.*, 2011). FeOB use energy from Fe(II)-oxidation to carry out cellular functions, such as maintenance and CO_2 fixation to create biomass (Emerson & Moyer, 1997; Weber *et al.*, 2006; Bethke *et al.*, 2011; Bird *et al.*, 2011).

The redox state of an environment is inherently linked to redox potential, which is described by the Nernst equation:

$$E = E^0 + \frac{RT}{nF} \ln \frac{[\text{oxidized species}]}{[\text{reduced species}]} \qquad (4.8)$$

where E is the redox potential of the cell (mV), E° is the electrochemical potential of the cell at standard conditions, R is the universal gas constant, T is absolute temperature, n is the number of electrons participating per ion, F is Faraday's constant, and Q is the reaction quotient, $\frac{[\text{oxidized species}]}{[\text{reduced species}]}$. Environmental factors including temperature, pH, and the presence of multiple redox couples can influence the redox potential of a microbial system, in addition to microbe-specific factors including nutrient levels, solution chemistry, growth substrate factors, and oxygen availability (Newman & Banfield, 2002). Considering its sensitivity to so many elements, it is no

surprise that redox potential is intricately linked to biological activity (Swerhone *et al.*, 1999; Ferris, 2005).

If the concentrations of all other redox active species remain constant, we can simplify the Nernst equation to attribute all changes in redox potential to transformations of dissolved iron species (Nemati & Webb, 1997):

$$E = E^0 + \frac{RT}{nF} \ln \frac{[Fe^{3+}]}{[Fe^{2+}]} \qquad (4.9).$$

This directly links metabolite consumption (iron oxidation) to changes in redox potential.

4.2.4 Fluctuations, Random Walks and Anomalous Diffusion

Generally, fluctuations in potential are thought to arise from random particle collisions in solution (Gabrielli *et al.*, 1993). This physical link allows fluctuations to be modelled as random walks. Relationships between diffusion coefficients and electrochemical potential have been described elsewhere (Oldham, 1966; Frateur *et al.*, 1999; Mampallil *et al.*, 2013) we can extend these models to link fluctuation characteristics to diffusion behaviour *in situ* (Metzler & Klafter, 2000).

Stationary processes have statistical moments which are invariant, irrespective of time and length of the process being examined (Witt & Malamud, 2013); these processes can be fully described by measures of central tendency and have a characteristic scale (Hardstone *et al.*, 2012). The values of a stationary process are uncorrelated; a classic example would be Gaussian white noise (Witt & Malamud, 2013). By contrast, nonstationary processes, such as Brownian motion, have stationary, uncorrelated Gauss-distributed increments (Wiener, 1923; Metzler & Klafter, 2000; Eliazar & Shlesinger, 2013; Witt & Malamud, 2013). Nonstationary processes with correlated increments are called fractional Brownian motions (Eliazar & Shlesinger, 2013). Correlation is a property of a time series or process that describes the statistical dependence of directly and distantly neighboured values (Witt & Malamud, 2013). The strength of correlation can vary from weak to very strong (Witt & Malamud, 2013). Each different class of processes has different correlation properties, which gives the fluctuations different characteristics when measured as time series (Metzler & Klafter, 2000). The characteristics which allow them to be distinguished are the result of interactions between disturbances from internal and external control mechanisms (Eke *et al.*, 2000).

Brownian motion models diffusion, according to Fick's law (Metzler & Klafter, 2000). In a plot of the mean-squared-displacement (MSD) through time, a Brownian motion will exhibit linearity (Metzler & Klafter, 2000; Witt & Malamud, 2013; Jeon *et al.*, 2014; Kim, 2014). When the MSD is described by non-linear growth through time, often taking a power-law form, diffusion is described as "anomalous" (Metzler & Klafter, 2000; Witt & Malamud, 2013; Jeon *et al.*, 2014; Kim, 2014). The existence of anomalous diffusion inside cells has been linked with cytoplasm dynamics and with transport across cellular membranes (Haugh, 2009 and references therein), and was examined at the microbial community scale in Chapter 3.

4.3 Methods

4.3.1 Site Description

The study site, Ogilvie Creek, is located at Meilleurs Bay, approximately 10 km west of Deep River, Ontario, Canada. The creek is the outflow path of a small lake located on the southeast side of the Ottawa River, but is also fed by a reduced, anoxic groundwater seep which hosts a thriving-year round microbial mat composed primarily of *Leptothrix ochracea*, with a smaller component of *Gallionella ferruginea* (James & Ferris, 2004). The bedrock at the site is dominated by monzonitic gneiss from the Grenville Province (Carr *et al.*, 2000), but most areas are overlain by thick deposits of glacial material left behind when the Ottawa Valley was deglaciated (Singer & Cheng, 2002). Geochemical data for the creek as well as microcosm experiments to establish oxidation rates and bacterial community types have been described in detail elsewhere (James & Ferris, 2004; Shirokova & Ferris, 2013).

4.3.2 Microcosm Design

BIOS samples were collected in sterile syringes; a total of 720 mL of material, collected in 60 mL aliquots, was collected for each microcosm. Syringes of BIOS were taken from the thickest part of the BIOS mat by submerging the tip of the syringe to a depth of 1-2 cm, and drawing upwards aiming to get as much of the flocculent BIOS material as possible while avoiding contact with the sediment underlying the microbial mat. Syringes of creek water were collected by placing the tip of the syringe 1-2 cm below the surface of the water, in thinner areas of the mat, where small pools of clear water were visible. Collection points for both creek water and BIOS were next to each other, at the same distance from the creek source.

For the ALL system, 720 mL of BIOS were collected. For the LIVE system, 180 mL of BIOS, and 540 mL of unfiltered creek water were used. For the AUTO system, 180 mL of BIOS that was sterilized by autoclaving, and 540 mL of 0.22 μm filtered water were used. For the CREEK system, 720 mL of 0.22 μm filtered creek water was used. Each microcosm was prepared in a large, ethanol-sterilized 1.5 L plastic container. Autoclaving precipitates as a method of killing cells has been used elsewhere (Emerson & Revsbech, 1994).

4.3.3 Physicochemical Measurements

Temperature, pH, dissolved O_2, and oxidation-reduction potential were measured using a YSI 600 QS Sonde which was calibrated for pH, redox potential, and DO before each microcosm. Voltage across a Pt combination electrode was measured continuously for the entire length of each microcosm, at a sampling rate of 10 measurements / second (10 Hz). This data was logged using LabVIEW and a laptop for fluctuation analysis, which will be described below. After completion, the contents of each microcosm was dried at 70 °C for 2 hours and weighed.

Dissolved Fe and physical chemical water measurements were taken every 30 minutes until Fe(II) values were at least one order of magnitude lower than they were at the beginning, or, all the Fe(II) was consumed. Dissolved Fe_{total} and Fe(II) measurements were made in triplicate using a HACH DR 9800 Colorimeter, and HACH methods 8146 (Ferrous iron), and 8008 (Total iron) by carefully drawing an aliquot from the microcosm, filtering with a 0.22 μm syringe filter, and mixing with reagents. Samples were allowed to react for 3 minutes before taking measurements, conforming with the manufacturer's directions. In total, less than 5 minutes passed from time to drawing to time of analysis.

4.3.4 Precipitate Analysis

Scanning electron microscopy was performed on a Zeiss EVO 50 series Scanning Electron Microscope with Extended Pressure capability. Images were collected in backscatter electron mode and chemical analysis was accomplished using the Oxford EDS system including X-MAX 150 Silicon Drift Detector, INCA Energy 450 software and the AZtec Energy 2.2 microanalysis software.

X-ray diffraction analyses were performed using oriented settled mounts on a Bruker D8 Advance equipped with a graphite monochromator, Co Kα radiation set at 40 kV and 40 mA.

Analysis was performed using Jade (v.6.0) software (Materials Data, Inc.). Analyses were performed at the Geological Survey of Canada Mineralogy Lab in Ottawa, Canada.

4.3.5 Determination of Oxidation Rate Constants

Pseudo-first order rate constants were calculated for each of the four systems according to:

$$[Fe^{2+}]_t = [Fe^{2+}]_0 \exp(-k't) \qquad (4.10).$$

which is the integrated form of equation 4.6. Data was plotted and fit in Statistica v.12.

4.3.6 Determination of Scaling Coefficients

Detrended fluctuation analysis (DFA) (Peng *et al.*, 1994) was used to calculate correlation coefficients. The first step in DFA is to generate a random walk profile of the realization by subtracting the mean and integrating the time series. The profile (length n) is divided into j windows of length s and local linear least squares fits are calculated for each window. Root-mean-square (RMS) deviations of are measured by subtracting the linear trend calculated for each window from the integrated random walk profile and summing the fluctuations from this local trend. The RMS deviations are subsequently averaged across the corresponding number of windows j and plotted against window size s in log-log space. A linear relationship between window size and average RMS deviation indicates scale-invariant power law behavior

$$\mathrm{RMS} \cong Cs^{\alpha} \qquad (4.11)$$

where C represents a constant fluctuation coefficient and the scaling exponent α is a quantitative measure of long-range persistence, or time-domain self-similarity, in the time series (Witt & Malamud, 2013). The scaling exponent is estimated by fitting experimental data to the relationship

$$\log \mathrm{RMS} = \alpha \log s + \log C \qquad (4.12).$$

Conforming with random walk theory, Brownian motion will give rise to $\alpha = 1$ (Metzler & Klafter, 2000; Ramanujan *et al.*, 2006; Haugh, 2009), and $\alpha \in (1, 2)$ relating to processes exhibiting fractional Brownian motion (Metzler & Klafter, 2000; Eliazar & Shlesinger, 2013). Additionally, in random

uncorrelated time series $\alpha = 0.5$, whereas $\alpha < 0.5$ indicates negative persistence and $\alpha > 0.5$ indicates positive persistence (Peng *et al.*, 1994; Peng *et al.*, 1995; Metzler & Klafter, 2000; Hardstone *et al.*, 2012; Witt & Malamud, 2013).

DFA was implemented in MatLAB. The original 10 Hz (measurement frequency) time series were downsampled to ten 1 Hz realizations, and α values were calculated as the average value of all realizations for the same start and end points (a total of nine realizations). Two sets of analyses were performed; first, scaling exponents (i.e., α values) of the first 30 minutes of each microcosm (n=1800) were determined. Next, in order to compare changes in correlation structure with changes in oxidation rate through time, scaling exponents were calculated for 1000 second-long time series with start times staggered by 1 minute (i.e., t_{start} = 0 minutes, 1 minute, 2 minutes, 3 minutes, etc…) for the first 27 minutes of the microcosm.

4.3.7 Relating Oxidation Rate Constants and Diffusion

The relationship between scaling exponent, α, and reaction-based waiting time, τ_r, takes the general form (Haugh, 2009):

$$\tau_r = \frac{1}{D_a}\theta^{\frac{1}{\alpha}} \qquad (4.13)$$

where τ_r is time-dependent and related to oxidation rate constant (Hänngi *et al.*, 1990):

$$\frac{1}{\tau_r} = k'_{ox}\exp(-k'_{ox}t) \qquad (4.14)$$

and D_a is the Damköhler number:

$$D_a = \frac{[rate\ of\ reaction]}{[rate\ of\ diffusion]} \qquad (4.15)$$

θ is the scaled fractional time coefficient, and α is the power-law scaling coefficient determined here by DFA. The parameters D_a and θ were estimated on the basis of equation 4.13 by non-linear regression in Statistica v.12. By relating rate and scaling mathematically, differences in both the time

coefficient and Damköhler number may provide quantification of differences in contributions from the three mechanisms of Fe(II) oxidation identified (homogenous abiotic, microbial, and autocatalytic).

4.4 Results

4.4.1 Physicochemical Parameters

Results of physicochemical measurements made in the first 90 minutes and standard deviations are presented in Table 4.1. In general, measurements within each system were fairly consistent over the length of the microcosm. High values of dissolved O_2 in the AUTO system most likely result from oxygenation occurring when the precipitates were autoclaved; there does not appear to be any significant enhancement to oxidation rate constant, despite this discrepancy.

4.4.2 Precipitate Analysis

Neither intact nor autoclaved precipitates contained any identifiable mineral phases, consistent with results reported by James & Ferris (2004) and Emerson & Revsbech, (1994). This indicates that no phase transformations of the BIOS flocs were introduced by autoclaving. For the purposes of evaluating adsorptive properties, the intact and autoclaved substrates can be considered the same.

4.4.3 Oxidation Rate Constants

Figure 4.1 shows the normalized ferrous iron concentrations as a function of time; the ALL system is completely depleted of Fe(II) within the first 30 minutes, meaning that the FeOB were essentially starved. Over the course of the microcosms, pH and dissolved O_2 levels were observed to remain reasonably constant, allowing pseudo-first order oxidation rate constants to be calculated for each system over the entire length of each microcosm. The rate constants determined for the ALL, AUTO, and CREEK systems are consistent with rate constants reported by James & Ferris (2004) for similar experiments at the same field site.

Figure 4.2 shows the relationship between dry biomass and pseudo-first order oxidation rate constant. The rate constant for the ALL system is three times the rate of the LIVE system, and has three times the dry biomass; indicating a strong dependency between rate and cell number. The rate constant for the ALL system is slightly higher than 6 times greater than the AUTO rate constant.

The rate constant for the LIVE system is 2.5 times greater than the AUTO rate constant, which is in turn more than 6 times larger than the CREEK rate constant. These results indicate that homogenous abiotic oxidation is a fairly insignificant process to overall oxidation rate, while autocatalytic oxidation may account for as much as half of the oxidation observed in the LIVE and ALL systems.

4.4.4 Scaling Behaviour: First 30 minutes

Averaged scaling exponents for the first 30 minutes (n=1800, measurement frequency of 1Hz, ten realizations) are presented in Table 4.2. The values for the ALL and LIVE systems are very similar while the AUTO and CREEK systems are much closer to the value expected for normal diffusion. The values for ALL and LIVE are higher but broadly similar to the results for the same site in Chapter 2 (BIOS), and to both biologically active systems in Chapter 3.

4.4.5 Relationship between Scaling and Oxidation Rate Constant

Figure 4.3 shows the instantaneous rates and scaling exponents as calculated for the first 27 minutes of the microcosms as a function of realization start time. The averaged α values, and standard errors are given in Table 4.3, and all of the estimates of α are available in Appendix 4. DFA reveals strong long-range correlation at the beginning of the two biologically active microcosms, while the two chemical systems start close to values of 1, which is the value for regular diffusion. This is in contrast to calculated rate constants, where the AUTO system had a much higher rate constant than the CREEK system. It would appear normal diffusion governs these systems.

By the end of the first 30 minutes, all four systems indicate scaling exponents of 0.5, consistent with uncorrelated, stationary processes. The ALL system reaches the value of 0.5 far faster than the LIVE system; it was also the first to be completely depleted of Fe(II) (below detection limit).

4.5 Discussion

4.5.1 Oxidation rate constants

The k' value for the ALL system is not well constrained as it is based on only two data points (t=0 min, t = 30 min). However, the ALL, AUTO, and CREEK oxidation rate constants are

very similar with results reported for the same field site (James & Ferris, 2004), as well as with those reported for similar microbial communities and geochemical conditions at other sites (Rentz *et al.*, 2007; Druschel *et al.*, 2008). These similarities indicates that it is likely quite accurate.

The ALL and LIVE systems represent two different types of biological activity both encompassing all three oxidation pathways for Fe(II) (homogenous abiotic, autocatalytic, and microbial), the AUTO system represents the case of autocatalytic and abiotic oxidation, while the CREEK system represents homogeneous abiotic Fe(II) oxidation.

4.5.2 Scaling exponents

In scaling exponents calculated for the first 30 minutes DFA reveals strong long range correlation in both biologically active systems, while correlations are much weaker in both abiotic systems, with exponents approximating regular diffusion. The similarity of the n=1800 scaling exponents for the ALL and LIVE point to similar chemical and biological inputs driving them. Their similarity would also indicate that cell count or biomass concentration does not affect fluctuation character. However, the ALL and LIVE systems evolve very differently. It is important to keep in mind that the n=1000 time series each represent an approximately 17 minute window. The ALL system scaling coefficients begin to drop off within a few minutes, with very few intermediate values, quickly reaching a position where no correlation dominates the time series. This behaviour is most likely representative of the system being quickly and completely depleted of Fe(II); once this species is no longer present, there are no relevant redox couples in solution to undergo electron transfer reactions which would drive a correlated fluctuation response. The LIVE system maintains its correlation behaviour for a much longer time; having one third the biomass but the same amount of initial Fe(II); this system also transitions much more gradually to uncorrelated fluctuations, suggesting a gradual decrease in biological activity. For the first 30 minutes the AUTO and CREEK systems appear to be governed by regular diffusion. Their behaviour is markedly similar in both the n=1800 and n=1000 analyses. This suggests essentially no contribution from autocatalytic oxidation to fluctuation behaviour with the implication that the differences in scaling exponents observed in biologically active and abiotic microcosms can be fully attributed to the presence of a live microbial community.

The Damköhler numbers and scaled time coefficients both appear to be related to oxidation rate constant; they follow similar patterns of magnitude.

4.6 Conclusions

Using a system of microcosms to compare biological and abiotic oxidation rates of ferrous iron, we have determined an empirical relationship between scaling behaviour and oxidation rate in a circumneutral iron-oxidizing system. Such a relationship has been described for chemical systems elsewhere (Oldham, 1966; Frateur *et al.,* 1999; Mampallil *et al.,* 2013), but never for microbial communities. The coefficients appear to be highly dependent on oxidation rate constant, while the scaling exponent parameter, α, is dependent on the presence or absence of biological activity. The presence of HFO does not appear to have any influence on scaling exponent, despite it inducing a major change in oxidation rate constant due to the onset of autocatalytic oxidation. Nor does the concentration of biomass appear to influence the correlation structure, although it does influence the evolution of the fluctuations through time; mostly due to depletion of the primary metabolite.

Scaling exponents in and of themselves do not appear to predict oxidation rate constants, however, they seem to be able to conclusively distinguish between microbial and abiotic Fe(II) oxidation.

4.7 Acknowledgements

This work was supported by an NSERC Discovery grant to FGF. The Ogilvies are thanked for continued access to the field site. Jeanne Percival, Pat Hunt, and Igor Bilot at the Geological Survey of Canada are thanked for XRD and SEM analyses.

4.8 References

Anderson CR, Pedersen K (2003) In situ growth of Gallionella biofilms and partitioning of lanthanides and actinides between biological material and ferric oxyhydrides. *Geobiology*, **1**, 169-178.

Anderson CR, James RE, Fru EC, Kennedy EB, Pedersen, K (2006) In situ ecological development of a bacteriogenic iron oxide-producing microbial community from a subsurface granitic rock environment. *Geobiology*, **4**, 29-42.

Banfield JF, Welch SA, Zhang H, Ebert TT, Penn RL (2000) Aggregation-based growth and microstructure development in natural iron oxyhydroxide biomineralization products. *Science*, **289,** 751-754.

Bethke CM, Sanford RA, Kirk MF, Jin Q, Flynn TM (2011) The Thermodynamic Ladder in Geomicrobiology. *American Journal of Science*, **311**, 183-210.

Bird LJ, Bonnefoy V, Newman DK (2011) Biogenergetic challenges of microbial iron metabolisms. *Trends in Microbiology*, **19**, 330-340.

Blöthe M, Roden EE (2009) Microbial Iron Redox Cycling in a Circumneutral-pH Groundwater Seep. *Applied and Environmental Microbiology*, **75**, 468-473.

Carr SD, Easton RM, Jamieson RA, Culshaw NG (2000) Geologic transect across the Grenville orogeny of Ontario and New York. *Canadian Journal of Earth Sciences*, **37**, 193–216.

Châtellier X, Fortin D, West M, Leppard GG, Ferris FG (2001) Effect of the presence of bacterial surfaces during the synthesis of Fe-oxides by oxidation of ferrous ions. *European Journal of Mineralogy*, **13**, 705-714.

Davison W, Seed G (1983) The kinetics of the oxidation of ferrous iron in synthetic and natural waters. *Geochimica et Cosmochimica Acta* **47**, 67–79.

Druschel GK, Emerson D, Sutka R, Suchecki P, Luther GW (2008) Low-oxygen and chemical kinetic constraints on the geochemical niche of neutrophilic iron(II) oxidizing organisms. *Geochimica et Cosmochimica Acta*, **72**, 3358-3370.

Duckworth OW, Holmström, SJM, Peña J, Sposito G (2009) Biogeochemistry of iron oxidation in a circumneutral freshwater habitat. *Chemical Geology*, **260**, 149-158.

Edwards KJ, Bach W, McCollom TM, Rogers DR (2004) Neutrophilic iron-oxidizing bacteria in the ocean: their habitats, diversity, and roles in mineral deposition, rock alteration, and biomass production in the deep-sea. *Geomicrobiology Journal*, **21**, 393–404.

Eke A, Herman P, Bassingthwaite JB, Raymond GM, Percival DB, Cannon M, Balla I, Ikrenyi C (2000) Physiological time series: distinguishing fractal noises from motions. *European Journal of Physiology*, **439**, 403-415.

Eliazar II, Shlesinger MF (2013) Fractional motions. *Physics Reports*, **527**, 101-129.

Emerson D, Revsbech NP (1994) Investigation of an Iron-Oxidizing Microbial Mat Community Located near Aarhus, Denmark: Field Studies. *Applied and Environmental Microbiology*, **60**, 4022-4031.

Emerson D, Moyer CL (1997) Isolation and characterization of novel iron-oxidizing bacteria that grow at circumneutral pH. *Applied and Environmental Microbiology*, **63**, 4784–92.

Emerson D, Weiss JV, Megonigal JP (1999) Iron-oxidizing bacteria are associated with ferric hydroxide precipitates (Fe-plaque) on the roots of wetland plants. *Applied and Environmental Microbiology*, **65**, 2758–2761.

Emerson D, Weiss JV (2004) Bacterial iron oxidation in circumneutral freshwater habitats: findings from the field and the laboratory. *Geomicrobiology Journal*, **21**, 405–414.

Emerson D, Fleming EJ, McBeth JM (2010) Iron-oxidizing bacteria: an environmental and genomic perspective. *Annual Reviews of Microbiology*, **64**, 561–583.

Emerson D (2012) Biogeochemistry and microbiology of microaerobic Fe(II) oxidation. *Transactions of the Biochemical Society*, **40**, 1211-1216. doi:10.1042/BST20120154.

Emerson D, Roden E, Twining BS (2012) The microbial ferrous wheel: iron cycling in terrestrial, freshwater, and marine environments. *Frontiers in Microbiology*, **3**, 383.

Emerson D, de Vet W (2015) The Role of FeOB in Engineered Water Ecosystems: A Review. *Journal AWWA* , **107**, E47-E57.

Ferris FG (2005) Biogeochemical properties of bacteriogenic iron oxides. *Geomicrobiology Journal*, **22**, 79–85.

Ferris FG, Enright AML, Fortin D, Clark ID. In press. Rates of Fe(II)-oxidation and Solubility of Bacteriogenic Iron Oxides. *Geomicrobiology Journal*.

Frateur I, Bayet E, Keddam M, Tribollet B (1999) Local redox potential measurement. *Electrochemistry Communications*, **1**, 336-340.

Gabrielli C, Huet F, Keddam H (1993) Fluctuations in electrochemical systems. I. General theory on diffusion limited electrochemical reactions. *Journal of Chemical Physics*, **99**, 7232-7239.

Gault AG, Ibrahim A, Langley S, Renaud R., Takahashi Y, Boothman C, Lloyd JR, Clark ID, Ferris FG, Fortin D (2011) Microbial and geochemical features suggest iron redox cycling within bacteriogenic iron oxide-rich sediments. *Chemical Geology*, **281**, 41-51.

Hänngi P, Talkner P, Borkovec M (1990) Reaction-rate theory: fifty years after Kramers. *Reviews of Modern Physics*, **62**, 251-342.

Hardstone R, Poil S-S, Schiavone G, Jansen R, Nikulin VV, Mansvelder HD, Linkenkaer-Hansen K (2012) Detrended fluctuation analysis: a scale-free view on neuronal fluctuations. *Frontiers in Physiology*, **3**, 450.

Haugh JM (2009) Analysis of Reaction-Diffusion Systems with Anomalous Subdiffusion. *Biophysical Journal*, **97**, 435-442.

James RE, Ferris FG (2004) Evidence for microbial-mediated iron oxidation at a neutrophilic groundwater spring. *Chemical Geology*, **212**, 301-311.

Jeon J-H, Chechkin AV, Metzler R (2014) Scaled Brownian motion: a paradoxical process with a time dependent diffusivity for the description of anomalous diffusion. *Physical Chemistry Chemical Physics*, **16**, 15811.

Kappler A, Newman DK (2004) Formation of Fe(III)- minerals by Fe(II)-oxidizing photoautotrophic bacteria. *Geochimica et Cosmochimica Acta*, **68**, 1217–1226.

Kasama T, Marakami T (2001) The effect of microorganisms on Fe precipitation rates at neutral pH. *Chemical Geology*, **180**, 117 - 128.

Kato S, Kikuchi S, Kashiwarbara T, Takahashi Y, Suzuki K, Itoh T, Ohkuma M, Yamagishi A (2012) Prokaryotic abundance and community composition in a freshwater iron-rich microbial mat at circumneutral pH. *Geomicrobiology Journal*, **29**, 896-905.

Kennedy CB, Scott SD, Ferris FG (2003) Characterization of bacteriogenic iron oxide deposits from axial volcano, Juan de Fuca Ridge, Northeast Pacific Ocean. *Geomicrobiology Journal*, **20**, 199-214.

Kennedy CB, Gault AG, Fortin D, Clark ID, Ferris FG (2011) Retention of iodide by bacteriogenic iron oxides. *Geomicrobiology Journal*, **28**, 387-395.

Kim H-J (2014) Anomalous diffusion induced by enhancement of memory. *Physical Reviews E*, **90**, 012103.

King DW, Lounsbury HA, Millero FJ (1995) Rates and mechanism of Fe(II) oxidation at nanomolar total iron concentrations. *Environmental Science & Technology*, **29**, 818–24.

Langley S, Gault AG, Ibrahim A, Takahashi Y, Renaud R, Fortin D, Clark ID, Ferris FG (2009a) Sorption of strontium onto bacteriogenic iron oxides. *Environmental Science & Technology*, **43**, 1008-1014.

Mampallil D, Mathwig K, Kang S, Lemay SG (2013) Redox Couples with Unequal Diffusion Coefficients: Effect on Redox Cycling. *Analytical Chemistry*, **85**, 6053-6058.

McBeth JM, Little BJ, Ray RI, Farrar KM, Emerson D (2011) Neutrophillic Iron-Oxidizing "Zetaproteobacteria" and Mild Steel Corrosion in Nearshore Marine Environments. *Applied and Environmental Microbiology*, **77**, 1405-1412.

Melton ED, Swanner ED, Behrens S, Schmidt C, Kappler A (2014) The interplay of microbially mediated and abiotic reactions in the biogeochemical Fe cycle. *Nature Reviews Microbiology*, **12**, 797-808.

Metzler R, Klafter J (2000) The random walk's guide to anomalous diffusion: a fractional dynamics approach. *Physics Reports*, **339**, 1-77.

Nemati M, Webb C (1997) A Kinetic Model for Biological Oxidation of Ferrous Iron by Thiobacillus ferrooxidans. *Biotechnology and Bioengineering*, **53**, 478-486.

Neubauer SC, Emerson D, Megonigal JP (2002) Life at the Energetic Edge: Kinetics of Circumneutral Iron Oxidation by Lithotrophic Iron-Oxidizing Bacteria Isolated from the Wetland-Plant Rhizosphere. *Applied and Environmental Microbiology*, **68**, 3988-3995.

Newman DK, Banfield JF (2002) Geomicrobiology: How Molecular-Scale Interactions Underpin Biogeochemical Systems. *Science*, **296**, 1071-1077.

Oldham KB (1966) A Diffusion-Layer Treatment of Transient Electrochemical Phenomena. *Electrochimica Acta*, **11**, 1475-1490.

Peng C-K, Buldyrev SV, Havlin S, Simons M, Stanley HE, Goldberger AL (1994) Mosaic organization of DNA nucleotides. *Physical Reviews E*, **49**, 1685-1689.

Peng C-K, Havlin S, Stanley H, Goldberger A (1995) Quantification of scaling exponents and crossover phenomena in nonstationary heartbeat time series. *Chaos*, **5**, 82-87.

Ramanujan VK, Biener G, Herman BA (2006) Scaling behavior in mitochondrial redox fluctuations. *Biophysical Journal: Biophysical Letters* **90**, L70-L72. doi: 10.1529/biophysj.106.083501.

Rentz JA, Kraiya C, Luther GW III, Emerson D (2007) Control of Ferrous Iron Oxidation within Circumneutral Microbial Iron Mats by Cellular Activity and Autocatalysis. *Environmental Science & Technology*, **41**, 6084-6089.

Roden EE, McBeth JM, Blöthe M, Percak-Dennett EM. Fleming EJ, Holyoke RR, Luther III GW, Emerson D, Schieber J (2012) The microbial ferrous wheel in a neutral pH groundwater seep. *Frontiers in Microbiology*, **3**, 172.

Rozanova EP, Dubinina GA, Lebedeva EV, Suntsova LA, Lipovskikh VM, Tsvetkov NN (2003) Microorganisms in heat supply lines and internal corrosion of steel pipes. *Microbiology*, **72**, 179-186.

Schwertmann U, Bigham JH, Murad E (1995) The first occurrence of schwertmannite in a natural stream environment. *European Journal of Mineralogy*, **7**, 547–552.

Shirokova VL, Ferris FG (2013) Microbial Diversity and Biogeochemistry of a Shallow Pristine Canadian Shield Groundwater System. *Geomicrobiology Journal*, **30**, 140-149.

Singer SN, Cheng CK (2002) *An Assessment of Groundwater Resources of Northern Ontario.* Toronto, Ontario, Canada: Ministry of the Environment.

Singer PC, Stumm W (1970) Acidic mine drainage: The rate determining step. *Science*, **167**, 1121-1123.

Sobolev D, Roden EE (2001) Suboxic deposition of ferric iron by bacteria in opposing gradients of Fe(II) and oxygen at circumneutral pH. *Applied and Environmental Microbiology* , **67** , 1328–1332.

Stumm J, Morgan JJ (1996) *Aquatic chemistry: chemical equilibria and rates in natural waters*, 3rd, ed.; Wiley Interscience: U.S.A.

Sung W, Morgan JJ (1980) Kinetics and product of ferrous iron oxygenation in aqueous systems. *Environmental Science & Technology*, **14**, 561–68.

Swerhone GDW, Lawrence JR, Richards JG, Hendry MJ (1999) Construction and Testing of a Durable Platinum Wire Eh Electrode for In Situ Redox Measurements in the Subsurface. *GWMR*, 132-136.

van Bochove E, Beauchemin S, Theriault G (2002) Continuous Multiple Measurement of Soil Redox Potential Using Platinum Microelectrodes. *Soil Science Society of America Journal*, **66**, 1813-1820.

Vollrath S, Behrends T, Van Cappellen P (2012) Oxygen Dependency of Neutrophilic Fe(II) Oxidation by Leptothrix Differs from Abiotic Reaction. *Geomicrobiology Journal*, **29**, 550-560.

Vollrath S, Behrends T, Koch CB, Van Cappellen P (2013) Effects of temperature on rates and mineral products of microbial Fe(II) oxidation by Leptothrix cholodnii at microaerobic conditions. *Geochimica et Cosmochimica Acta*, **108**, 107-124.

Warren LW, Ferris FG (1998) Continuum between sorption and precipitation of Fe(III) on microbial surfaces. *Environmental Science & Technology*, **32**, 2331-2337.

Weber KA, Achenbach LA, Coates JA (2006) Microorganisms pumping iron: anaerobic microbial iron oxidation and reduction. *Nature Reviews Microbiology*, **4**, 752–764.

Wehrli B, Sulzberger B, Stumm W (1989) Redox processes catalyzed by hydrous oxide surfaces. *Chemical Geology*, **78**, 167–179.

Wiener NJ (1923) Differential Space. *Journal of Mathematical Physics*, **2**, 131-174.

Witt A, Malamud BD (2013) Quantification of long-range persistence in geophysical time series: conventional and benchmark-based improvement techniques. *Surveys in Geophysics*, **34**, 541-651.

Zuo R, Wood TK (2004) Inhibiting mild steel corrosion from sulfate reducing and iron-oxidizing bacteria using gramicidin-S producing biofilms. *Applied Microbiology and Biotechnology*, **65**, 747-753.

Tables

Table 4.1: Physicochemical parameters, with calculated standard deviation, and calculated pseudo-first order rate constants for each of the four microcosms.

System	k'(/min)	R^2	pH	DO (mM)	T (°C)
All	0.1425	1.00	6.15±0.04	0.095±0.039	15.3±0.4
Live	0.0575	0.98	6.38±0.14	0.100±0.10	16.4±0.5
Auto	0.0225	0.86	6.67±0.34	0.259±0.029	21.0±0.2
Creek	0.0036	0.90	6.40±0.10	0.148±0.017	15.4±0.4

Table 4.2: Alpha values for n=1800 time series, at 1 Hz sampling frequency representing the first 30 minutes of each microcosm.

System	α	SE
All	1.794	0.004
Live	1.817	0.004
Auto	0.998	0.013
Creek	1.095	0.022

Table 4.3: Estimates of α for n=1000, 1 Hz measurement frequency time series for the first 27 minutes of the microcosm, calculated as the average of 10 realizations, and the standard error (SE) of each estimate.

Start (min)	All	SE	Live	SE	Auto	SE	Creek	SE
0.00	1.80	0.01	1.83	0.01	0.98	0.01	1.18	0.01
1.00	1.34	0.01	1.80	0.01	1.12	0.02	1.24	0.01
2.00	1.43	0.01	1.83	0.01	1.18	0.13	1.17	0.01
3.00	1.35	0.03	1.85	0.01	1.17	0.01	0.94	0.02
4.00	1.31	0.01	1.88	0.01	0.72	0.02	0.61	0.02
5.00	0.97	0.02	1.84	0.02	0.58	0.02	0.59	0.02
6.00	1.00	0.03	1.43	0.01	0.59	0.02	0.59	0.02
7.00	0.94	0.02	1.31	0.02	0.61	0.02	0.59	0.02
8.00	0.82	0.02	1.33	0.01	0.56	0.01	0.55	0.03
9.00	0.81	0.04	1.13	0.01	0.52	0.02	0.54	0.02
10.00	0.79	0.02	0.86	0.02	0.54	0.01	0.53	0.03
11.00	0.72	0.02	0.62	0.02	0.54	0.02	0.53	0.02
12.00	0.68	0.03	0.72	0.01	0.52	0.02	0.51	0.02
13.00	0.70	0.02	0.62	0.02	0.51	0.01	0.50	0.02
14.00	0.69	0.02	0.57	0.02	0.59	0.01	0.49	0.03
15.00	0.62	0.02	0.56	0.02	0.51	0.01	0.52	0.03
16.00	0.60	0.03	0.64	0.02	0.52	0.02	0.50	0.03
17.00	0.58	0.01	0.60	0.02	0.50	0.02	0.48	0.02
18.00	0.57	0.02	0.63	0.01	0.55	0.02	0.51	0.02
19.00	0.56	0.03	0.57	0.02	0.54	0.02	0.52	0.01
20.00	0.55	0.02	0.59	0.02	0.51	0.02	0.53	0.01
21.00	0.52	0.03	0.60	0.02	0.49	0.02	0.52	0.02
22.00	0.54	0.02	0.60	0.02	0.49	0.01	0.47	0.03
23.00	0.53	0.03	0.55	0.02	0.51	0.02	0.51	0.02
24.00	0.55	0.03	0.58	0.03	0.50	0.01	0.45	0.02
25.00	0.63	0.03	0.57	0.02	0.52	0.02	0.46	0.03
26.00	0.50	0.02	0.56	0.01	0.52	0.02	0.46	0.02
27.00	0.58	0.03	0.60	0.01	0.53	0.02	0.48	0.02

Table 4.4: Coefficients, D_a and Θ, and R^2 values for the relationship between scaling exponent, α and instantaneous oxidation rate, r_{ox}, as a function of oxidation rate constant, k'.

	Da	SE	θ	SE
All	4.747	3.181	34.96	12.429
Live	0.083	0.023	2.415	0.407
Auto	0.036	0.007	1.567	0.183
Creek	0.004	0.00	1.064	0.010

Figures

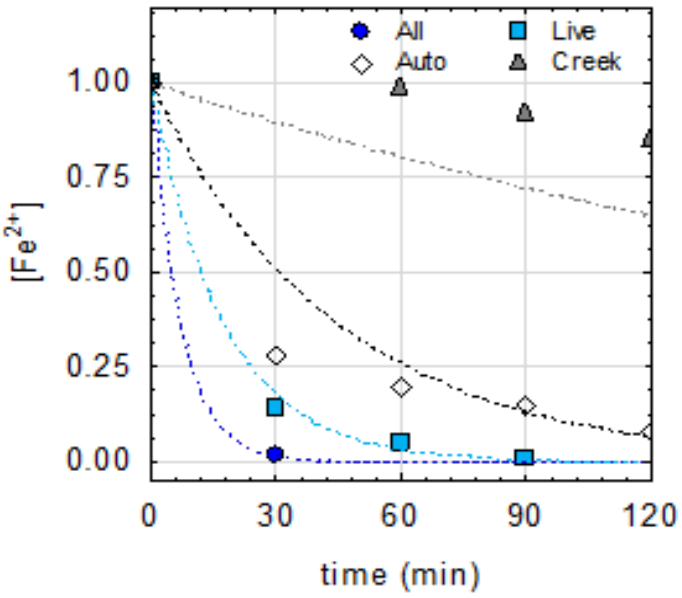

Figure 4.1: Concentration of Fe(II), normalized to the initial concentration (t=0), as a function of time, in each of the four microcosms. ALL system (dark blue circles), LIVE system (light blue squares), AUTO system (white diamonds), and CREEK system (grey triangles).

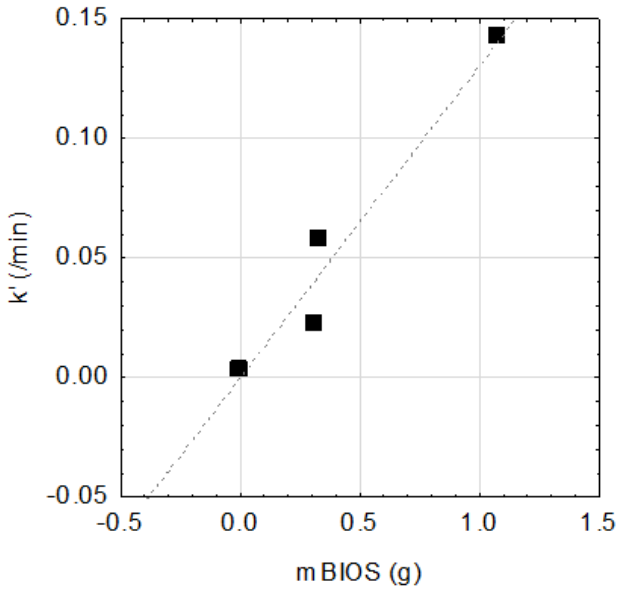

Figure 4.2: Pseudo-first order oxidation rate constants as a function of the mass of dried precipitate in each microcosm.

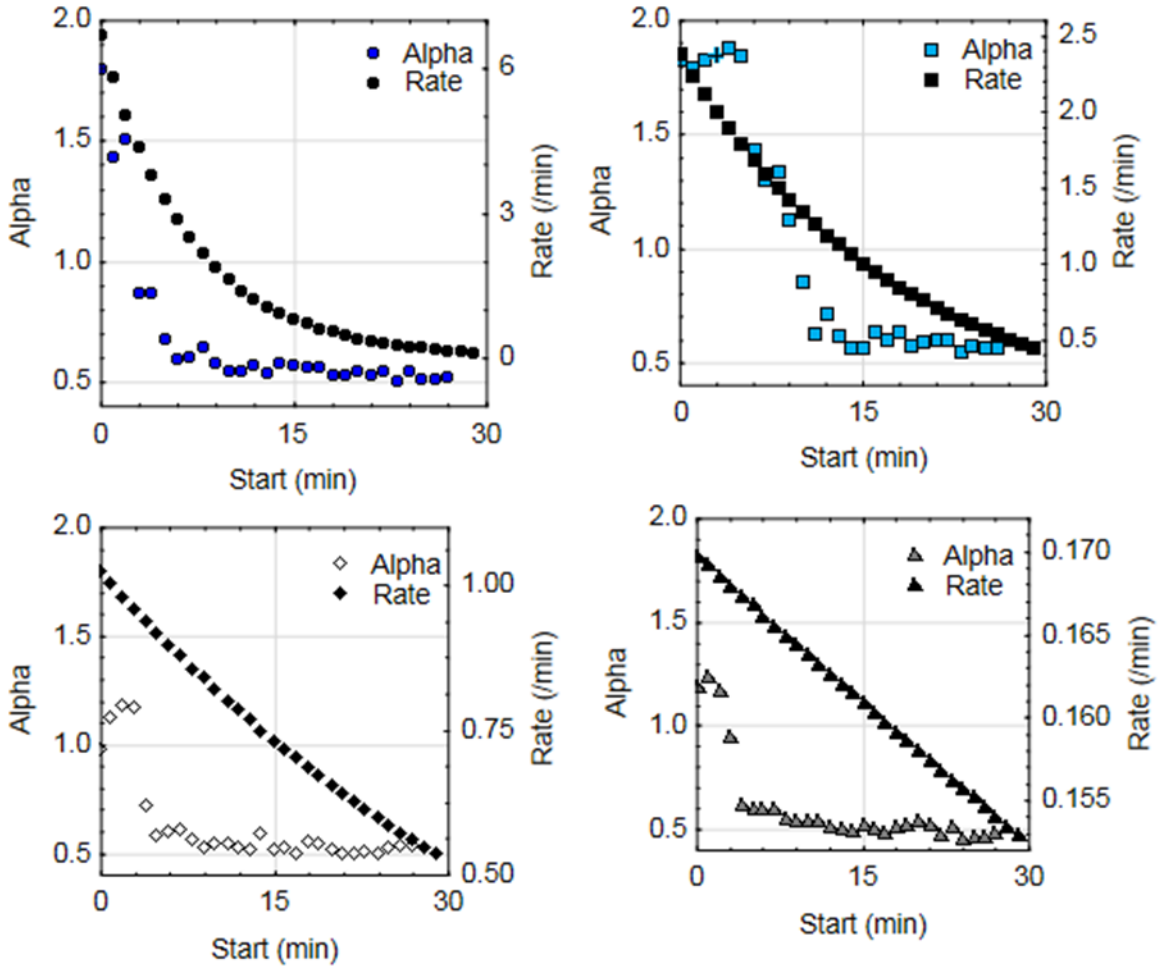

Figure 4.3: Calculated scaling exponents (α) for time series n=1000, 1 Hz sampling frequency, and instantaneous oxidation rates r_{ox} as a function of the start time corresponding with n_0..

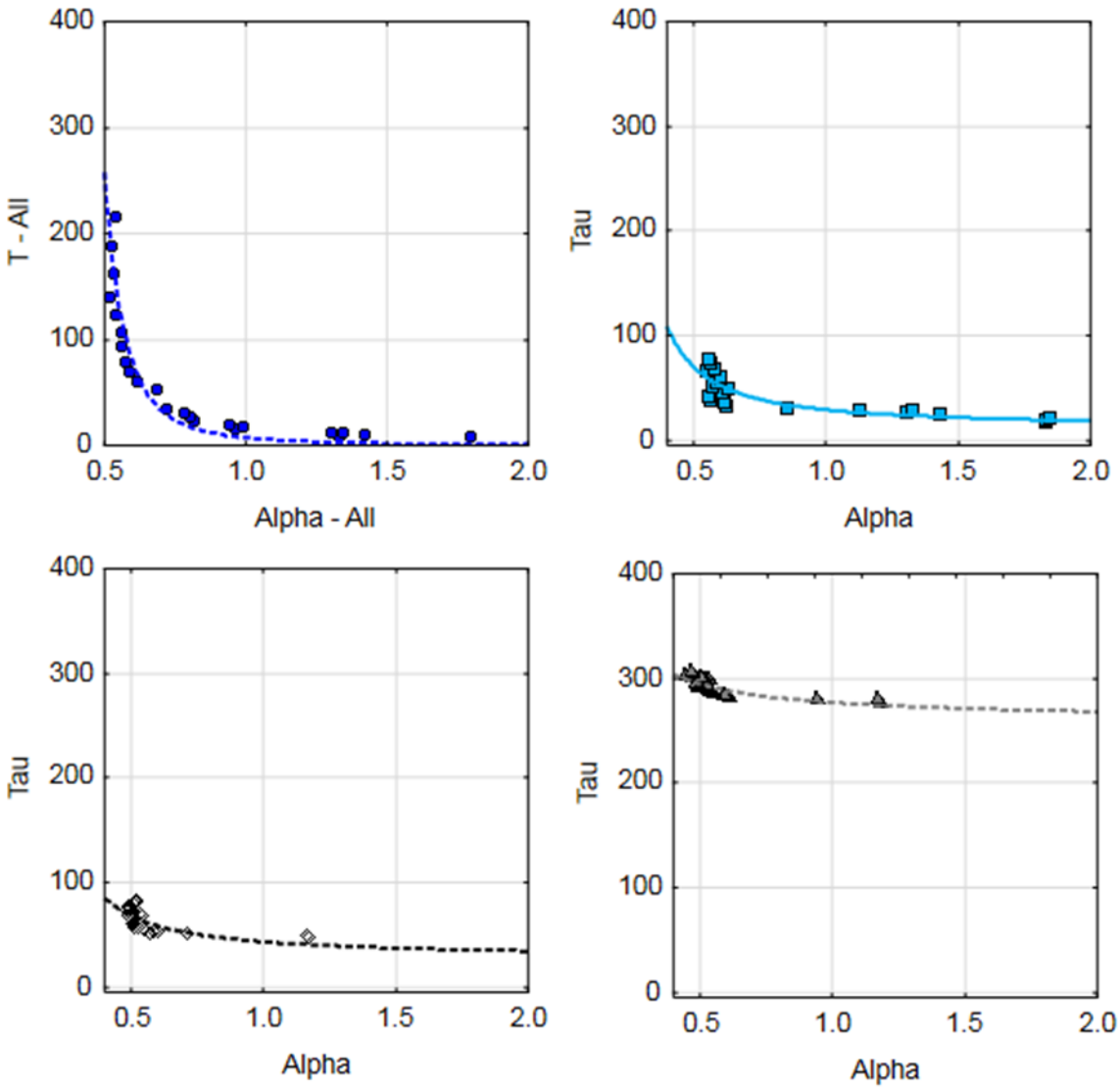

Figure 4.4: τ as a function of scaling exponent, α for each microcosm system. ALL is top left (dark blue circles), LIVE is top right (light blue circles), AUTO is bottom left (white diamonds), CREEK is bottom right (grey triangles).

Chapter 5
Looking Forward

5.1 Introduction

My primary aim with this thesis was to assess the utility of using small-scale fluctuations in oxidation-reduction (redox) potential to distinguish microbial from chemical iron oxidation *in situ,* with the idea that such analysis could eventually be expanded to include other metabolites and more complex microbial communities, as well as providing a diagnostic signature of extant Fe(II)-oxidizing microbial activity. This was accomplished using the time series technique of detrended fluctuation analysis with redox potential fluctuation time series data sets.

Fe(III)/Fe(II) metabolizing bacteria are tremendously important, both in the context of Earth evolution, and due to their significant contribution to modern biogeochemical cycling of iron (Weber *et al.*, 2006; Emerson *et al.*, 2010). Additionally, iron bacteria are strong contenders as organisms that could be discovered outside of Earth (Emerson & Weiss, 2004; Weber *et al.*, 2006; Druschel *et al.*, 2008), especially as redox equilibria are known to exist on the Martian surface, creating the possibility for geochemical conditions which might support iron metabolism (McSween Jr. *et al.*, 1999; Neubauer *et al.*, 2002). This made FeOB attractive test candidates for a methodology centred on electrochemical measurement of redox transformations as a biosignature.

5.2 Summary

5.2.1 Comparing Scaling Exponents

In initial testing, three different systems: two chemical and one live, at steady state were characterized. This study acted as proof of concept, and allowed refinement of data collection protocol and processing algorithms. This study also provided context for the interpretation of all new results.

In the first test to distinguish biological Fe(II)-oxidation by comparing a bioreactor to its bacteriogenic iron oxide (BIOS)-free inflow pipe, scaling exponents, as determined by DFA, differed significantly and elucidated that the underlying diffusion behaviour in a chemical system is

affected by biology. Moreover, dramatic differences between chemical systems and an equilibrium test case indicated that the electrode was, in fact, sensitive to diffusion behaviour in the solution of interest, confirming that fluctuations did not arise from instrument noise or external factors.

In a final study, a series of microcosms were used to determine the relationship between scaling exponent, measuring correlation strength, and oxidation rate. This relationship has a power-law form. The link between higher oxidation rate constant and biological activity was already well-established (James & Ferris, 2004), and the relationship between oxidation rate and diffusion had already been documented (Oldham, 1996; Frateur *et al.*, 1999; Mampallil *et al.*, 2013).

Table (5.1) summarizes the results of all three studies. There is consistency between results of Chapter 2 and Chapter 4 for the same study site, Ogilvie Creek (see value reported for single realization of BIOS in Fig 2.4), however it appears when removed from their environment, correlation is strengthened. The differences between the BIOS-active cases in Chapters 2 and 3 could arise from the different geochemical conditions or the result of different dominant FeOB species at each site (*Leptothrix ochracea* dominates Ogilvie Creek while *Gallionella ferruginea* dominates the Äspö site). It would appear that the dynamics underlying the two environments are discernably different.

The relatively high (abiotic) exponent observed for the Tap water system (Chapter 2) appears to indicate that Pt electrodes are sensitive to a variety of redox species, suggesting that these measurements are sensitive to a multitude of interactions in the system of study. However, this appears to complicate interpretation of the measurement where *a priori* knowledge of the contributing couples is not available. This may be addressed by considering ion-specific electrodes in future studies.

5.2.2 Distinguishing Biological Activity

In all three studies, systems known to be biologically active with Fe(II)-oxidizing bacteria were characterized by exponents with an approximate value of $\alpha = 1.6$, providing compelling evidence for a biological basis underlying the strong correlation structure present in these systems. Calculation of scaling exponents provides significant and compelling new information about the microscopic behaviour of these systems which was not previously available based on measurement of redox potential alone; moreover, distinguishing biological from autocatalytic influences on oxidation rate may be possible by supplementing oxidation rate determinations with fluctuation analysis. Especially, fluctuation analysis provides interesting insight into how bacteria may

manipulate the chemistry of their environment to promote conditions more favourable to their survival and growth.

5.3 Next Steps

5.3.1 Considering Other Metabolic Pathways

There are a number of exciting questions that emerge in the face of the new possibility of using fluctuations as a tool for the detection of biological activity. First and foremost, a number of other metabolic pathways await exploration. While Fe(II)- oxidation is a significant metabolic strategy in the context of global biogeochemical iron cycling, early Earth and life outside of Earth, it falls short of informing on the behaviour of more complex microbial communities. Ion-specific electrodes will likely be integral in studies of the diffusion dynamics of other metabolites, and priorities from an environmental microbiological perspective would include S^-, N^-, and Fe-reducers, as well as metabolically mixed communities. Using an array of ion-specific electrodes might be a method to compare and distinguish diffusion behaviour for mixed microbial communities.

5.3.2 Spatial Variations

Assessing the spatial sensitivity of these measurements will be a significant factor in determining the utility of this technique as a monitoring and remediation technology. While evidence suggests that fluctuations as measured at an electrode surface are representative of dynamics in the bulk solution (Frateur *et al.*, 1999; Mampallil *et al.*, 2013), the extent of this influence has not been constrained and could be extremely fruitful in detecting extents of microbial influence in remediation settings.

The influence of pH, O_2 concentration, and temperature - all parameters in the Nernst equation - were kept relatively constant in all of the test cases here; varying these parameters and evaluating their influence will be an important step in eventually developing models of fluctuation behaviour in particular geochemical niches. These are all significant new knowledge gaps.

5.3.3 Integrating with Other Analytical Techniques

Several geophysical techniques, including induced-polarization (Heenan *et al.*, 2013), self-potential (Davis *et al.*, 2010), magnetic susceptibility (Atekwana *et al.*, 2014) and complex conductivity (Mewafy *et al.*, 2013) have been explored in the context of biogeophysics, but none at

present have examined fluctuations or correlation, or have been at low enough rates to be consistent with the microbial communities explored here; and this may represent a method of definitively quantifying microbial influences on the physicochemical observables of the environments they inhabit.

5.4 Conclusions

There is very little novelty in the study of anomalous diffusion, Fe(II)-oxidizing bacteria, redox potential, or fluctuation analysis independently; however, in conjunction, these different disciplines contribute to the creation of a technique which holds significant promise in environmental microbiology not only in understanding questions of community structure and metabolite movement, but also in monitoring of contaminants and remediation, as well as in detection of life. This physically-constrained, remotely deployable, and straightforward measurement technique has the possibility to provide tremendous insight into the movement of chemical species, and especially metabolically relevant species, in microbial communities. Moreover, removing the need to draw samples, which perturbs the measurement system, and to sample destructively offers an opportunity to remove the influence of the examiner from the dynamics of the system, as well as broadening the niches available for study; by removing the need to return samples in a timely fashion for testing, more remote and extreme locations can be studied.

This contribution aimed to make an initial exploration of these parameters by using the observable of small-scale fluctuations as a proxy for the diffusion of chemical species at the microscale, linking observations at one scale to behaviour at a different one. In a broader environmental sense, the adoption of approaches that centre on scale-free observation parameters may eventually be able to link global-scale processes to those occurring on a niche- or eco-system scale, and permit broad comparisons between different niches and microbial communities, something that is generally difficult at present.

5.5 References

Atekwana EA, Mewafy FM, Abdel Aal G, Werkema Jr D, Revil A, Slater L (2014) High-Resolution Magnetic Susceptibility Measurements for Investigating Magnetic Mineral Formation during

Microbial Mediated Iron Reduction. *Journal of Geophysical Research Biogeosciences*, **119**, 80–94, doi:10.1002/2013JG002414.

Davis CA, Slater LD, Kulessa B, Ferguson A, Atekwana EA, Doherty R, Kalin R (2010) Self-potential signatures associated with an injection experiment at an in-situ biological permeable reactive barrier. *Near Surface Geophysics*, **8**, 541-555 doi:10.3997/1873-0604.2010034.

Druschel GK, Emerson D, Sutka R, Suchecki P, Luther GW (2008) Low-oxygen and chemical kinetic constraints on the geochemical niche of neutrophilic iron(II) oxidizing organisms. *Geochimica et Cosmochimica Acta*, **72**, 3358-3370.

Emerson D, Weiss JV (2002) Bacterial Iron Oxidation in Circumneutral Freshwater Habitats: Findings from the Field and the Laboratory. *Geomicrobiology Journal*, **21**, 405-414.

Emerson D, Fleming EJ, McBeth JM (2010) Iron-oxidizing bacteria: an environmental and genomic perspective. *Annual Reviews of Microbiology*, **64**, 561–583.

Frateur I, Bayet E, Keddam M, Tribollet B (1999) Local redox potential measurement. *Electrochemistry Communications*, **1**, 336-340.

Heenan J, Porter A, Ntarlagiannis D, Young L, Werkema D, Slater L (2013) Sensitivity of the spectral induced polarization method to microbial enhanced oil recovery processes. *Geophysics*, **78**, E261–E269 doi: 10.1190/geo2013-0085.1

James RE, Ferris FG (2004) Evidence for microbial-mediated iron oxidation at a neutrophilic groundwater spring. *Chemical Geology*, **212**, 301-311.

Mampallil D, Mathwig K, Kang S, Lemay SG (2013) Redox Couples with Unequal Diffusion Coefficients: Effect on Redox Cycling. *Analytical Chemistry*, **85**, 6053-6058.

McSween Jr. HY, Murchie SL, Crisp JA, Bridges NT, Anderson RC, Bell JF, Britt DT, Bruckner J, Dreibus G, Economou T, Ghosh A, Golombek MP, Greenwood JP, Johnson JR, Moore HJ, Morris RV, Parker TJ, Rieder R, Singer R, Wanke H (1999) Chemical, multispectral and textural constraints on the composition and origin of rocks at the Mars Pathfinder landing site. *Journal of Geophysical Research*, **104**, 8679–8715.

Mewafy FM, Werkema DD, Atekwana EA, Slater LD, Abdel Aal GZ, Revil A, Ntarlagiannis D (2013) Evidence that biometallic mineral precipitation enhances the complex conductivity response at a hydrocarbon contaminated site. *Journal of Applied Geophysics*, **98**, 113–123.

Neubauer SC, Emerson D, Megonigal JP (2002) Life at the Energetic Edge: Kinetics of Circumneutral Iron Oxidation by Lithotrophic Iron-Oxidizing Bacteria Isolated from the Wetland-Plant Rhizosphere. *Applied and Environmental Microbiology*, **68**, 3988-3995.

Oldham KB (1966) A Diffusion-Layer Treatment of Transient Electrochemical Phenomena. *Electrochimica Acta*, **11**, 1475-1490.

Stumm J, Morgan JJ (1996) *Aquatic chemistry: chemical equilibria and rates in natural waters*, 3rd, ed.; Wiley Interscience: U.S.A.

Vershinin AV, Rozanov AG (1983) The Platinum Electrode as an Indicator of Redox Environment in Marine Sediments. *Marine Chemistry*, **14**, 1-15.

Weber KA, Achenbach LA, Coates JA (2006) Microorganisms pumping iron: anaerobic microbial iron oxidation and reduction. *Nature Reviews Microbiology*, **4**, 752–764.

Tables

Table 5.1: Summary of calculated scaling exponents.

	α	SE	Series Length	n
Ogilvie Creek - in situ	1.567	0.011	1000-5000	24
AGW Medium	1.157	0.0009	1000-5000	24
Tap Water	1.5	0.016	1000-5000	24
Äspö Inlet	1.67	0.06	1000-2500	8
Äspö BIOS	1.89	0.03	1000-2500	8
Microcosm - ALL	1.794	0.0004	1800	9
Microcosm - LIVE	1.817	0.0004	1800	9
Microcosm - AUTO	0.998	0.013	1800	9
Microcosm - CREEK	0.1095	0.022	1800	9

Appendix 1: MatLAB Code Used for Chapter 2

```
%% DFA script for Methods Paper

clear all
close all
clc
cd C:\Users\Allison\Documents\MATLAB\RSI
load RSI_raw.mat

%% Input and Set Up
time =  [0:1:4999.9]';
start = 1;  %Specify start value as n in raw time series (10 Hz)
stop = 10000; %Spectify stop value as n in raw time series (10 Hz)
DS = 10; %10 Hz/DS = desired frequency
X = DS-1;

%% length = 4000
%{
Compiled = zeros(4000,16);
window_size = [5; 10; 20; 25; 50; 100; 125; 250; 500; 1000; 2000; 4000];
N = [800; 400; 200; 160; 80; 40; 32; 16; 8; 4; 2; 1];
%}
%% length = 5000
%{
Compiled = zeros(5000,16);
window_size = [5; 10; 20; 25; 50; 100; 125; 250; 500; 1000; 1250; 2500;↙
5000];
N = [1000; 500; 250; 200; 100; 50; 40; 20; 10; 5; 4; 2; 1];
%}
%% length - 2500
%{
Compiled = zeros(2500,16);
window_size = [5; 10; 20; 25; 50; 100; 125; 250; 500; 1250; 2500];
N = [500; 250; 125; 100; 50; 25; 20; 10; 5; 2; 1];
%}
%% length - 1000
%

Compiled = zeros(1000,6);
window_size = [5; 10; 20; 25; 50; 100; 125; 250; 500; 1000];
N = [200; 100; 50; 40; 20; 10; 8; 4; 2; 1];
%}
```

```
%%
W = length (N);
T = N(1);
L = length (Compiled);
alpha = zeros(6,X);

% Sequentially selects each downsample to be processed
% Raw files are in form (n,2) where n is the length of the raw time
% series

for x = 1:X
Compiled(:,1) = downsample(pond1_iron_sept5(start:stop,2),DS,x);
Compiled(:,2) = downsample(AGW_1_July31(start:stop,2),DS,x);
Compiled(:,3) = downsample(tapWater_October82014(start:stop,2),DS,x);
idx = randperm(L);
Compiled(:,4) = Compiled(idx,1);
idx = randperm(L);
Compiled(:,5) = Compiled(idx,2);
idx = randperm(L);
Compiled(:,6) = Compiled(idx,3);

%% Calculate the mean
Mean_raw = zeros(6,1);
for a = 1:6;
    Mean_raw(a,1) = mean(Compiled(:,a));
end

%% Mean removal
Mean_removed = zeros(L,6);
for a = 1:6;
    for c = 1:L;
        Mean_removed(c,a) = Compiled(c,a) - Mean_raw(a,1);
    end
end

%% Generate the time series profile/ random walk
YRW = zeros(L,6);
for a = 1:6;
    for c = 1:L;
       YRW(c,a) = sum(Mean_removed(1:c,a));
    end
```

```
end

%% Calculate the trend in each window as a least-squares fit
Trends = zeros(T,2*W,6);
for a = 1:6;
    for d = 1:W;
        for e = 0:(N(d)-1);
        c = window_size(d)*e+1;
        m=window_size(d) - 1;
                dummy_term = polyfit(time(c:c+m,1),YRW(c:c+m,a),1);
                Trends(e+1,2*d-1,a) = dummy_term(1);
                Trends(e+1,2*d,a) = dummy_term(2);
        end
    end
end
clear dummy_term
%% Calculate the predicted value based on the estimated trends

Predicted_vals = zeros(L,W,6);
for a = 1:6;
    for d = 1:W;
        for c = 1:L;
            b = floor((c+(window_size(d)-1))/window_size(d));
            Predicted_vals(c,d,a) = ((time(c)*(Trends(b,(2*d-1),a)))↙
+Trends(b,(2*d),a));
        end
    end
end
%% Calculate the differences between the predicted value and the↙
measurement

Diffs = zeros(L,W,6);
for a = 1:6;
    for d = 1:W;
        for c = 1:L;
            Diffs(c,d,a) = YRW(c,a) - Predicted_vals(c,d,a);
        end
    end
end

% Square the differences to create time series of RMS fluctuation
```

```
Diffs_sq = zeros(L,W,6);
for a = 1:6;
    for d = 1:W;
        for c = 1:L;
        Diffs_sq(c,d,a) = Diffs(c,d,a)^2;
        end
    end
end

% Average the fluctuations in each window
Averages = zeros(T,W,6);
for a = 1:6;
    for d = 1:W;
        for e = 0:N(d)-1;
            c = window_size(d)*e+1;
            m = window_size(d)-1;
            Averages(e+1,d,a) = mean(Diffs_sq((c:c+m),d,a));
        end
    end
end
%%
Averages_s = zeros(W,6);
for a = 1:6;
    for d = 1:W;
        Averages_s(d,a) = sum(Averages(:,d,a));
    end
end

Averages_N = zeros(W,6);
for a = 1:6;
    for d = 1:W;
        Averages_N(d,a) = Averages_s(d,a)/N(d);
    end
end

% Calculate RMS fluctuations
F_t = zeros(W,6);
for a = 1:6;
    for d = 1:W;
        F_t(d,a) = Averages_N(d,a).^0.5;
    end
```

```
end

% Calculate scaling exponents
temp = zeros(2,1);
for a = 1:6;
    temp = polyfit(log(window_size(:)),log(F_t(:,a)),1);
    alpha(a,x) = temp(1,1);
end

clear↙
('a','b','c','d','e','m','temp','Diffs','Diffs_sq','Averages','Averages_N↙
','Averages_s')
end
clear↙
('X','x','T','Compiled','DS','L','idx','Mean_removed','Predicted_vals','T↙
rends','W','YRW','time','AGW_1_July31','Mean_raw','tapWater_October82014'↙
,'pond1_iron_sept5')
```

Appendix 2: MatLAB Code Used for Chapter 3

```
clear all
close all
clc
cd C:\Users\Allison\Documents\MATLAB\ASPO
load ASPO_raw.mat

%% Input and Set Up
IN = InletORPmV (649:3148,1);% set up the raw data files, trim to length↙
of 2500 points
BIOS = BiosORPmV (126:2625,1);
time =  [0:1:2499]'; % create the time vector

%% Shuffle the time series (destroy correlation)
idx = randperm(length(IN));
shufIN = IN(idx);
idx = randperm(length(BIOS));
shufBIOS = BIOS(idx);
clear idx  %These are the shuffled plot
Compiled = zeros(2500,4);
Compiled(:,1) = IN(:);
Compiled(:,2) = BIOS(:);
Compiled(:,3) = shufIN(:);
Compiled(:,4) = shufBIOS(:);

clear ('shufBIOS','shufIN', 'IN','BIOS', 'InletORPmV','BiosORPmV')

%% Stats raw
Mean_raw = zeros(4,1); %allocate space for means of the time series

for a = 1:4;
    Mean_raw(a,1) = mean(Compiled(:,a)); % calculate means of the time↙
series
end

%%
Mean_removed = zeros(2500,4);
for a = 1:4;
    for c = 1:2500;
        Mean_removed(c,a) = Compiled(c,a) - Mean_raw(a,1); %
```

```
    end
end

%% DFA Step 1: Generate random walk
YRW = zeros(2500,4);
for a = 1:4;
    for c = 1:2500;
       YRW(c,a) = sum(Mean_removed(1:c,a));
    end
end

%% DFA Step 2: Create window sizes
window_size = [5; 10; 20; 50; 100; 500];  %create a matrix of the↙
coefficients for detrending. Window length and n windows
N = [500; 250; 125; 50; 25; 5];
%% DFA Step 3: Detrend the windows
Trends = zeros(500,12,4);

for a = 1:4; %
    for d = 1:6; %
        for e = 0:(N(d)-1);
        c = window_size(d)*e+1;
        m=window_size(d) - 1;
                dummy_term = polyfit(time(c:c+m,1),YRW(c:c+m,a),1);
                Trends(e+1,2*d-1,a) = dummy_term(1);
                Trends(e+1,2*d,a) = dummy_term(2);
        end
    end
end
clear dummy_term

%%
Predicted_vals = zeros(2500,6,4);
for a = 1:4;
    for d = 1:6;
        for c = 1:2500;
            b = floor((c+(window_size(d)-1))/window_size(d));
            Predicted_vals(c,d,a) = ((time(c)*(Trends(b,(2*d-1),a)))↙
+Trends(b,(2*d),a));
        end
    end
```

```
end

%% DFA Step 4: Calculate the differences between the predicted values and the observed values
Diffs = zeros(2500,6,4);
for a = 1:4;
    for d = 1:6;
        for c = 1:2500;
            Diffs(c,d,a) = YRW(c,a) - Predicted_vals(c,d,a);
        end
    end
end

Diffs_sq = zeros(2500,6,4);
for a = 1:4;
    for d = 1:6;
        for c = 1:2500;
        Diffs_sq(c,d,a) = Diffs(c,d,a)^2;
        end
    end
end

Averages = zeros(500,6,4);
for a = 1:4;
    for d = 1:6;
        for e = 0:N(d)-1;
            c = window_size(d)*e+1;
            m = window_size(d)-1;
            Averages(e+1,d,a) = mean(Diffs_sq((c:c+m),d,a));
        end
    end
end
%%
Averages_s = zeros(6,4);
for a = 1:4;
    for d = 1:6;
        Averages_s(d,a) = sum(Averages(:,d,a));
    end
end
Averages_N = zeros(6,4);
for a = 1:4;
```

```
    for d = 1:6;
        Averages_N(d,a) = Averages_s(d,a)/N(d);
    end
end

%% RMS fluctuations
F_t = zeros(6,4);
for a = 1:4;
    for d = 1:6;
        F_t(d,a) = Averages_N(d,a).^0.5;
    end
end

%% Calculate Scaling Exponents
alpha = zeros(4,1);
temp = zeros(2,1);
for a = 1:4;
    temp = polyfit(log(window_size(3:6)),log(F_t(3:6,a)),1);
    alpha(a,1) = temp(1,1);
end

%clear↙
('a','b','c','d','e','m','temp','Diffs_sq','Averages','Averages_N','Avera↙
ges_s')
```

Appendix 3: MatLAB Code Used for Chapter 4

```
%% DFA script for microcosms

clear all
close all
clc
cd C:\Users\Allison\Documents\MATLAB\DR2014\Microcosms
load micro_raw.mat
filename = 'Jul25_1Hz_1800.mat';

%% Set-Up Window Sizes

time =  [0:1:1800]';
Compiled = zeros(1800,4);
window_size = [20; 25; 30; 40; 45; 50; 60; 75; 100; 150; 200; 300; 450;↙
600; 900; 1800];
N = [90; 72; 60; 45; 40; 36; 30; 24; 18; 12; 9; 6; 4; 3; 2; 1];

%% This cell establishes how the time series will be downsampled to
% 1Hz, 2Hz, and 5 Hz to create a pool of realizations

%1Hz

start = [1]; %where in the time series to start (as n of raw series, at↙
10 Hz)
stop = [18000]; %where in the time series to end (as n of raw series, at↙
10 Hz)
alpha = zeros(9,6);
F_t = zeros(10,18,4);
DS = 10; %10 Hz/DS = desired frequency
%}

%2Hz
%{
start = [1; 601; 1201; 1801; 2401; 3001; 3601; 4201; 4801; 5401; 6001;↙
6601; 7201; 7801; 8401; 9001];
stop = [9000; 9600; 10200; 10800; 11400; 12000; 12600; 13200; 13800;↙
14400; 15000; 15600; 16200; 16800; 17400; 18000];
alpha = zeros(64,6);
F_t = zeros(65,18,4);
DS = 5;
%}
```

```
%5Hz
%{
start = [1; 601; 1201; 1801; 2401; 3001; 3601; 4201; 4801; 5401; 6001;↙
6601; 7201; 7801; 8401; 9001; 9601; 10201; 10801; 11401; 12001; 12601;↙
13201; 13801; 14401];
stop = [3600; 4200; 4800; 5400; 6000; 6600; 7200; 7800; 8400; 9000; 9600;↙
10200; 10800; 11400; 12000; 12600; 13200; 13800; 14400; 15000; 15600;↙
16200; 16800; 17400; 18000];
alpha = zeros(25,6);
F_t = zeros(26,18,4);
DS = 2;
%}

L = DS -1; %number of downsamples
reps = length(start);
dd1 = size(F_t);
dummy = dd1(1)-1;
clear dd1;

%% This block runs DFA

for z = 1:reps;
    for x = 1:L;
        % Sequentially selects each downsample to be processed
        % Raw files are in form (n,2) where n is the length of the raw↙
time
        % series
        Compiled(:,1) = downsample(July30_allBIOS_creek(start(z):stop(z),↙
2),DS,x);
        Compiled(:,2) = downsample(July23_LIVE(start(z):stop(z),2),DS,x);
        Compiled(:,3) = downsample(July23_DEADBIOS(start(z):stop(z),2),↙
DS,x);
        Compiled(:,4) = downsample(July24_creekwater(start(z):stop(z),2),↙
DS,x);

        % Calculate the mean
        Mean_raw = zeros(4,1);
            for a = 1:4;
                Mean_raw(a,1) = mean(Compiled(:,a));
            end
```

```
        Mean_removed = zeros(1800,4);
            for a = 1:4;
                for c = 1:1800;
                    Mean_removed(c,a) = Compiled(c,a) - Mean_raw(a,1);
                end
            end
        % Generate the time series profile/ random walk
        YRW = zeros(1800,4);
            for a = 1:4;
                for c = 1:1800;
                    YRW(c,a) = sum(Mean_removed(1:c,a));
                end
            end
        % Calculate the trend in each window as a least-squares fit
        Trends = zeros(90,32,4);
            for a = 1:4;
                for d = 1:16;
                    for e = 0:(N(d)-1);
                        c = window_size(d)*e+1;
                        m=window_size(d) - 1;
                        dummy_term = polyfit(time(c:c+m,1),YRW(c:c+m,a),↙
1);

                        Trends(e+1,2*d-1,a) = dummy_term(1);
                        Trends(e+1,2*d,a) = dummy_term(2);
                    end
                end
            end
        clear dummy_term

        % Calculate the predicted value based on the estimated trends
        Predicted_vals = zeros(1800,32,4);
            for a = 1:4;
                for d = 1:16;
                    for c = 1:1800;
                        b = floor((c+(window_size(d)-1))/window_size(d));
                        Predicted_vals(c,d,a) = ((time(c)*(Trends(b,(2*d-↙
1),a)))+Trends(b,(2*d),a));
                    end
                end
            end
```

```
% Calculate the differences between the predicted value and the
% measurement
Diffs = zeros(1800,16,4);
    for a = 1:4;
        for d = 1:16;
            for c = 1:1800;
                Diffs(c,d,a) = YRW(c,a) - Predicted_vals(c,d,a);
            end
        end
    end

% Square the differences to create time series of RMS fluctuation
Diffs_sq = zeros(1800,16,4);
    for a = 1:4;
        for d = 1:16;
            for c = 1:1800;
                Diffs_sq(c,d,a) = Diffs(c,d,a)^2;
            end
        end
    end

% Average the fluctuations in each window
Averages = zeros(90,16,4);
    for a = 1:4;
        for d = 1:16;
            for e = 0:N(d)-1;
                c = window_size(d)*e+1;
                m = window_size(d)-1;
                Averages(e+1,d,a) = mean(Diffs_sq((c:c+m),d,a));
            end
        end
    end
Averages_s = zeros(16,4);
    for a = 1:4;
        for d = 1:16;
            Averages_s(d,a) = sum(Averages(:,d,a));
        end
    end
Averages_N = zeros(16,4);
    for a = 1:4;
        for d = 1:16;
```

```
                    Averages_N(d,a) = Averages_s(d,a)/N(d);
                end
            end
%%
            % Calculate RMS fluctuations
            for a = 1:4;
                for d = 1:16;
                    F_t(1,d+2,a) = window_size(d);
                    F_t(L*(z-1)+x+1,1,a) = start(z);
                    F_t(L*(z-1)+x+1,2,a) = stop(z);
                    F_t(L*(z-1)+x+1,d+2,a) = Averages_N(d,a).^0.5;
                end
            end
%%
        % Calculate scaling exponents as slope using least-squares fit
        temp = zeros(2,1);
            for a = 1:4;
                for dum2 = 1:dummy;
                    temp = polyfit(log10(window_size(:)),log10(F_t↙
(dum2+1,3:18,a)'),1);
                    alpha(dum2,a+2) = temp(1,1);
                end
            end

        alpha((L*(z-1)+x),1) = start(z);
        alpha((L*(z-1)+x),2) = stop (z);
        clear↙
('a','b','c','d','e','m','temp','Diffs_sq','Averages','Averages_N','Avera↙
ges_s','YRW','Diffs','Trends','Predicted_vals','Mean_raw','Compiled')
  end
end

clear↙
('dummy','DS','L','Mean_removed','reps','start','stop','time','x','z','Ju↙
ly23_DEADBIOS','July23_LIVE','July24_creekwater','July30_allBIOS_creek','↙
dum2')
save(filename)
clear filename
```

Appendix 4: Table of Alpha Value Estimates for Microcosms

Table A1: All estimates of α for the microcosms at a measurement frequency of 1 Hz, n=1000.

Start	All		Live		Auto		Creek	
	α	R2	α	R2	α	R2	α	R2
0.00	1.82	0.99	1.84	1.00	0.95	0.97	1.20	0.99
	1.78	0.99	1.83	1.00	0.97	0.98	1.17	0.98
	1.76	0.99	1.85	1.00	1.02	0.98	1.14	0.98
	1.81	0.99	1.85	1.00	0.98	0.97	1.16	0.99
	1.80	0.99	1.82	1.00	0.92	0.98	1.20	0.99
	1.78	0.99	1.84	1.00	0.98	0.97	1.18	0.99
	1.81	0.99	1.81	1.00	1.02	0.97	1.20	0.99
	1.82	0.99	1.83	1.00	1.00	0.98	1.20	0.98
	1.80	0.99	1.79	1.00	0.95	0.97	1.19	0.99
1.00	1.36	0.99	1.78	1.00	1.09	0.99	1.28	0.96
	1.31	0.99	1.82	1.00	1.04	0.98	1.26	0.98
	1.33	0.99	1.79	1.00	1.17	0.98	1.22	0.97
	1.34	0.99	1.83	1.00	1.10	0.98	1.25	0.96
	1.37	0.99	1.80	1.00	1.04	0.98	1.20	0.99
	1.30	0.99	1.80	1.00	1.17	0.97	1.26	0.96
	1.32	0.99	1.77	1.00	1.10	0.98	1.22	0.98
	1.36	0.99	1.82	1.00	1.23	0.98	1.25	0.98
	1.33	0.99	1.76	1.00	1.12	0.98	1.20	0.98
2.00	1.44	0.98	1.83	0.99	1.32	0.99	1.24	0.93
	1.37	0.98	1.84	0.99	1.27	0.99	1.16	0.96
	1.46	0.99	1.85	0.99	1.33	0.99	1.16	0.95
	1.44	0.98	1.83	0.99	1.31	0.99	1.16	0.97
	1.44	0.99	1.80	0.99	1.30	0.98	1.11	0.95
	1.37	0.98	1.84	0.99	1.32	0.99	1.19	0.95
	1.44	0.98	1.81	0.99	1.31	0.99	1.19	0.95
	1.46	0.99	1.84	0.99	1.31	0.99	1.16	0.92
	1.44	0.98	1.80	0.99	0.13	0.99	1.14	0.96
3.00	1.36	0.97	1.84	0.99	1.22	0.98	1.07	0.93
	1.26	0.92	1.89	0.99	1.15	0.98	0.93	0.93
	1.43	0.94	1.79	0.99	1.20	0.99	0.98	0.95
	1.39	0.97	1.92	1.00	1.13	0.99	0.88	0.91
	1.27	0.97	1.88	0.99	1.12	0.99	0.90	0.95
	1.22	0.93	1.84	0.99	1.19	0.99	0.92	0.94
	1.37	0.96	1.85	0.99	1.22	0.99	0.99	0.94
	1.45	0.98	1.86	0.99	1.16	0.99	0.93	0.88
	1.40	0.97	1.78	0.99	1.14	0.98	0.88	0.97

	1.32	0.94	1.88	0.99	0.73	0.99	0.68	0.95
	1.29	0.97	1.89	0.99	0.73	0.97	0.65	0.99
	1.27	0.93	1.89	0.99	0.86	0.96	0.69	0.94
	1.31	0.90	1.92	0.99	0.66	0.97	0.61	0.98
4.00	1.29	0.92	1.88	0.99	0.72	0.98	0.60	0.99
	1.29	0.95	1.94	1.00	0.63	0.97	0.56	0.98
	1.30	0.95	1.85	0.99	0.68	0.97	0.58	0.98
	1.37	0.97	1.88	0.99	0.77	0.96	0.58	0.95
	1.33	0.93	1.83	0.99	0.70	0.99	0.55	0.98
	1.04	0.90	1.81	1.00	0.55	0.98	0.64	0.96
	0.89	0.93	1.88	1.00	0.56	0.93	0.64	0.97
	0.95	0.86	1.79	0.98	0.63	0.99	0.53	1.00
	1.00	0.91	1.96	1.00	0.63	0.99	0.56	0.98
5.00	1.01	0.95	1.86	1.00	0.48	0.98	0.63	0.98
	0.95	0.93	1.85	0.99	0.53	0.97	0.59	0.98
	0.92	0.97	1.82	1.00	0.64	0.96	0.59	0.98
	0.90	0.99	1.85	1.00	0.60	0.98	0.48	0.96
	1.04	0.92	1.79	0.99	0.59	0.99	0.66	1.00
	1.09	0.95	1.46	1.00	0.60	0.98	0.62	1.00
	0.83	0.89	1.44	1.00	0.51	0.98	0.66	0.97
	1.03	0.97	1.43	1.00	0.63	0.94	0.60	0.99
	1.13	0.90	1.46	1.00	0.60	0.97	0.47	0.98
6.00	0.94	0.93	1.38	1.00	0.55	0.98	0.64	0.97
	0.88	0.89	1.46	0.99	0.67	0.97	0.54	0.99
	0.97	0.97	1.40	1.00	0.61	0.96	0.63	0.99
	1.03	0.94	1.48	1.00	0.60	0.98	0.51	0.96
	1.06	0.89	1.39	1.00	0.59	0.99	0.67	0.98
	1.00	0.89	1.32	0.99	0.66	0.98	0.66	0.97
	0.86	0.89	1.35	0.99	0.53	0.97	0.62	0.97
	0.98	0.94	1.29	0.98	0.56	0.98	0.58	0.97
	0.90	0.96	1.42	0.99	0.57	1.00	0.51	0.97
7.00	1.00	0.99	1.29	0.98	0.66	0.95	0.61	0.97
	0.83	0.96	1.32	0.98	0.59	0.97	0.56	1.00
	0.96	0.91	1.29	0.98	0.68	0.96	0.61	0.99
	1.02	0.98	1.36	0.98	0.67	0.95	0.55	0.96
	0.95	0.93	1.16	0.97	0.57	0.99	0.65	0.99
	0.80	0.95	1.34	0.96	0.54	0.99	0.63	0.99
	0.78	1.00	1.36	0.96	0.52	0.98	0.45	0.98
	0.83	0.91	1.28	0.95	0.60	0.97	0.58	0.95
	0.77	0.94	1.38	0.97	0.60	0.99	0.53	0.98
8.00	0.94	0.85	1.30	0.97	0.57	0.98	0.61	0.97
	0.73	0.91	1.37	0.96	0.52	0.93	0.58	0.97
	0.84	0.96	1.31	0.96	0.59	0.99	0.60	0.99
	0.91	0.92	1.36	0.97	0.54	0.98	0.39	0.99

	0.82	0.95	1.28	0.96	0.53	0.98	0.54	0.99
	0.90	0.94	1.13	0.95	0.43	0.96	0.63	0.99
	0.69	0.89	1.14	0.93	0.46	0.98	0.60	0.99
	0.71	0.90	1.08	0.91	0.65	0.95	0.53	0.96
	0.82	0.95	1.21	0.96	0.56	0.99	0.45	0.97
9.00	0.90	0.97	1.05	0.96	0.43	0.98	0.55	0.99
	0.98	0.87	1.15	0.92	0.53	0.98	0.52	0.91
	0.60	0.98	1.13	0.92	0.52	0.98	0.58	0.98
	0.85	0.97	1.14	0.94	0.56	1.00	0.41	0.99
	0.81	0.83	1.13	0.95	0.51	0.99	0.58	1.00
	0.86	0.94	0.87	0.99	0.57	0.98	0.63	0.98
	0.88	0.98	0.95	0.98	0.46	0.97	0.64	0.95
	0.73	0.94	0.89	0.97	0.54	0.99	0.44	1.00
	0.75	0.91	0.93	0.92	0.58	0.99	0.50	0.99
10.00	0.79	0.90	0.84	0.93	0.58	0.98	0.52	0.96
	0.77	0.92	0.89	0.93	0.49	0.99	0.51	0.99
	0.69	0.95	0.72	0.95	0.52	1.00	0.57	0.98
	0.78	0.99	0.77	0.96	0.59	0.98	0.42	1.00
	0.85	0.93	0.84	0.95	0.53	1.00	0.58	0.98
	0.80	0.97	0.54	0.97	0.64	0.97	0.56	0.97
	0.69	0.95	0.67	0.99	0.49	0.98	0.50	0.98
	0.66	0.95	0.65	0.99	0.50	0.97	0.47	0.99
	0.67	0.96	0.72	0.97	0.52	0.99	0.55	0.99
11.00	0.72	0.96	0.65	0.91	0.52	0.99	0.59	0.98
	0.80	0.97	0.66	0.95	0.52	0.98	0.53	0.95
	0.73	0.94	0.58	0.97	0.58	0.95	0.60	1.00
	0.75	0.94	0.55	0.98	0.53	1.00	0.47	0.97
	0.71	0.90	0.60	0.96	0.55	1.00	0.50	0.97
	0.67	0.96	0.76	0.97	0.55	0.98	0.57	0.99
	0.62	0.95	0.78	0.99	0.49	0.99	0.42	0.97
	0.73	0.94	0.71	0.98	0.56	0.97	0.61	0.95
	0.64	0.95	0.75	0.93	0.50	0.99	0.48	0.95
12.00	0.75	0.93	0.67	0.98	0.47	0.97	0.47	0.98
	0.60	0.99	0.71	0.91	0.60	0.97	0.51	0.98
	0.65	0.95	0.67	0.91	0.55	0.98	0.59	0.99
	0.84	0.98	0.73	0.95	0.44	0.95	0.42	0.98
	0.59	0.96	0.68	0.97	0.50	0.99	0.51	0.98
	0.68	0.93	0.65	0.96	0.53	0.99	0.62	0.99
	0.68	0.97	0.69	0.99	0.50	0.97	0.42	0.99
	0.68	0.92	0.63	0.99	0.50	1.00	0.56	0.99
13.00	0.65	0.94	0.70	0.99	0.49	0.99	0.43	0.98
	0.79	0.94	0.53	0.95	0.50	1.00	0.45	0.98
	0.71	0.94	0.58	0.97	0.55	0.98	0.54	0.96
	0.63	0.99	0.66	0.97	0.52	0.99	0.55	0.98

	0.75	0.97	0.55	1.00	0.53	1.00	0.41	0.99
	0.68	0.88	0.60	0.97	0.48	0.98	0.49	0.99
	0.70	0.98	0.59	0.99	0.56	0.96	0.57	0.98
	0.72	0.94	0.66	0.96	0.62	0.92	0.42	0.96
	0.61	0.99	0.51	0.99	0.55	0.97	0.37	0.98
	0.69	0.93	0.43	0.98	0.62	0.96	0.52	0.99
14.00	0.65	0.99	0.63	0.98	0.53	0.98	0.53	0.98
	0.75	0.95	0.59	0.91	0.60	0.96	0.53	0.97
	0.64	0.99	0.54	0.97	0.63	0.94	0.56	0.98
	0.74	1.00	0.54	0.99	0.62	0.98	0.37	0.99
	0.72	0.94	0.62	0.97	0.54	0.98	0.51	0.98
	0.60	0.97	0.53	1.00	0.51	0.98	0.67	0.99
	0.62	0.98	0.69	0.99	0.51	0.96	0.44	0.99
	0.52	0.99	0.60	1.00	0.50	0.99	0.37	0.97
	0.63	0.94	0.59	0.98	0.56	0.99	0.59	0.99
15.00	0.56	0.98	0.58	0.98	0.47	0.99	0.53	0.97
	0.65	0.99	0.57	0.98	0.51	0.98	0.49	0.96
	0.64	0.94	0.51	0.99	0.56	0.99	0.56	1.00
	0.74	0.98	0.45	0.97	0.49	0.98	0.46	0.97
	0.58	0.97	0.52	0.99	0.51	0.99	0.53	0.97
	0.65	0.98	0.66	0.97	0.51	0.97	0.61	0.99
	0.60	0.97	0.70	0.96	0.49	1.00	0.41	0.99
	0.59	0.97	0.65	0.97	0.52	0.99	0.45	1.00
	0.60	0.98	0.55	0.93	0.52	0.99	0.58	0.97
16.00	0.53	0.95	0.68	0.97	0.60	1.00	0.43	0.99
	0.54	0.98	0.66	0.96	0.54	0.98	0.56	0.99
	0.65	0.99	0.59	0.96	0.53	0.98	0.60	0.98
	0.73	0.97	0.63	0.97	0.40	0.96	0.46	0.96
	0.47	0.98	0.64	0.98	0.53	1.00	0.44	0.99
	0.62	0.98	0.61	0.98	0.47	0.98	0.56	0.97
	0.62	0.97	0.70	0.98	0.53	0.99	0.41	0.96
	0.56	0.98	0.59	1.00	0.50	0.99	0.47	0.97
	0.56	0.97	0.58	0.97	0.48	0.98	0.50	0.98
17.00	0.56	0.97	0.52	0.95	0.56	0.99	0.38	0.99
	0.59	0.96	0.62	0.98	0.55	0.99	0.56	0.98
	0.60	0.97	0.63	0.98	0.54	0.99	0.54	0.99
	0.59	0.99	0.61	0.98	0.38	0.98	0.46	0.99
	0.52	0.93	0.60	0.97	0.51	0.99	0.45	0.99
	0.65	0.97	0.62	0.97	0.46	0.96	0.58	1.00
	0.66	0.97	0.64	0.99	0.58	0.98	0.45	0.97
18.00	0.51	0.99	0.66	0.98	0.62	0.97	0.42	0.99
	0.52	0.95	0.66	0.95	0.50	0.98	0.52	0.99
	0.51	0.96	0.61	0.97	0.57	0.99	0.44	0.90
	0.57	0.97	0.63	0.99	0.49	0.99	0.61	0.98

	0.50	0.97	0.60	0.98	0.55	0.99	0.55	0.99
	0.66	0.98	0.60	0.94	0.56	0.96	0.45	0.99
	0.53	0.95	0.67	0.96	0.58	0.92	0.52	0.99
	0.61	1.00	0.55	0.97	0.48	0.95	0.57	0.98
	0.64	0.97	0.62	0.99	0.54	0.99	0.49	0.97
	0.45	0.99	0.62	0.93	0.62	0.93	0.45	0.96
	0.57	0.96	0.63	0.99	0.48	0.99	0.54	0.99
19.00	0.50	0.98	0.65	0.98	0.57	0.99	0.49	0.90
	0.51	0.97	0.54	0.97	0.50	0.98	0.54	0.97
	0.61	0.97	0.44	0.95	0.54	0.99	0.55	0.99
	0.71	0.98	0.52	0.99	0.55	0.97	0.51	0.96
	0.48	0.98	0.57	0.99	0.58	0.98	0.51	0.98
	0.60	1.00	0.51	0.99	0.55	0.98	0.58	0.99
	0.59	0.97	0.67	0.98	0.49	1.00	0.53	0.93
	0.54	0.98	0.60	1.00	0.51	0.99	0.48	0.93
	0.53	1.00	0.53	0.96	0.51	1.00	0.57	0.98
20.00	0.49	0.97	0.60	0.99	0.59	0.99	0.48	0.94
	0.49	1.00	0.67	0.98	0.55	1.00	0.57	0.99
	0.65	0.98	0.59	0.96	0.54	0.98	0.54	0.99
	0.61	0.98	0.60	0.96	0.42	0.98	0.56	0.95
	0.42	0.97	0.52	0.99	0.48	0.99	0.51	0.98
	0.59	0.99	0.54	0.98	0.44	0.99	0.50	0.97
	0.46	0.99	0.68	0.99	0.47	1.00	0.54	0.88
	0.55	0.98	0.58	1.00	0.54	0.99	0.49	0.93
	0.58	0.96	0.63	1.00	0.47	0.97	0.56	0.99
21.00	0.37	0.98	0.49	0.99	0.52	0.98	0.42	0.89
	0.48	0.98	0.64	0.99	0.56	0.99	0.56	0.99
	0.68	0.99	0.66	0.98	0.51	0.99	0.53	0.99
	0.55	0.96	0.61	0.98	0.42	0.96	0.57	0.93
	0.44	0.96	0.58	1.00	0.49	0.98	0.50	0.89
	0.64	0.97	0.58	0.99	0.45	1.00	0.51	0.98
	0.56	0.99	0.58	0.99	0.51	1.00	0.38	0.99
	0.48	0.99	0.64	0.99	0.52	0.99	0.46	0.99
	0.58	0.96	0.65	0.98	0.47	0.98	0.57	0.99
22.00	0.43	0.98	0.51	0.98	0.50	0.95	0.31	0.97
	0.51	0.99	0.52	0.98	0.53	1.00	0.56	0.99
	0.54	0.99	0.65	0.93	0.49	0.99	0.55	0.99
	0.62	0.99	0.60	0.99	0.46	0.98	0.45	0.99
	0.49	0.97	0.66	0.97	0.50	0.99	0.41	0.99
	0.56	0.99	0.44	0.99	0.50	0.95	0.54	1.00
	0.64	0.94	0.62	0.99	0.49	0.99	0.50	0.95
23.00	0.41	0.97	0.49	1.00	0.51	0.99	0.50	0.91
	0.50	0.98	0.61	1.00	0.43	0.98	0.57	0.99
	0.44	0.99	0.55	0.99	0.54	0.99	0.37	0.97

	0.51	0.99	0.56	1.00	0.49	0.99	0.54	0.99
	0.55	0.98	0.50	0.98	0.60	0.98	0.50	0.99
	0.62	0.95	0.61	0.97	0.55	0.96	0.49	0.99
	0.50	0.93	0.57	0.98	0.43	0.97	0.54	0.90
	0.52	0.99	0.46	0.98	0.50	0.98	0.49	0.96
	0.59	0.98	0.63	0.97	0.54	0.99	0.40	0.99
	0.42	0.99	0.53	0.99	0.45	1.00	0.35	0.97
	0.62	0.98	0.58	0.98	0.46	0.98	0.58	0.98
24.00	0.47	0.99	0.61	0.97	0.56	0.99	0.35	0.99
	0.57	1.00	0.66	0.97	0.48	0.99	0.49	0.99
	0.59	0.96	0.50	0.97	0.50	0.97	0.46	0.96
	0.69	0.99	0.70	0.97	0.50	0.94	0.46	0.98
	0.44	0.96	0.54	0.99	0.50	0.99	0.42	0.99
	0.65	0.90	0.49	0.99	0.41	0.99	0.51	0.96
	0.63	0.93	0.69	0.98	0.57	0.99	0.38	0.98
	0.58	0.96	0.54	0.97	0.47	0.99	0.49	0.98
	0.76	0.92	0.57	0.98	0.53	0.99	0.61	0.99
25.00	0.55	0.92	0.53	0.99	0.55	0.99	0.33	0.99
	0.51	0.99	0.62	0.99	0.51	0.99	0.54	0.98
	0.70	0.97	0.54	0.98	0.55	0.99	0.50	0.95
	0.71	0.96	0.63	0.98	0.49	0.98	0.43	0.99
	0.58	0.80	0.51	0.98	0.57	0.96	0.38	0.98
	0.48	0.99	0.53	0.98	0.38	0.99	0.47	0.97
	0.48	0.98	0.54	0.99	0.53	0.97	0.41	0.97
	0.49	0.99	0.58	0.99	0.56	0.97	0.44	0.99
	0.47	0.97	0.58	0.99	0.52	0.97	0.61	0.97
26.00	0.40	0.98	0.53	0.95	0.54	0.98	0.39	0.99
	0.51	1.00	0.53	0.99	0.52	0.99	0.53	0.98
	0.59	0.98	0.61	0.98	0.56	0.98	0.51	0.99
	0.59	0.96	0.57	0.99	0.47	0.99	0.44	0.99
	0.45	0.98	0.57	0.98	0.63	0.95	0.37	0.99
	0.50	0.99	0.54	0.98	0.44	0.99	0.49	0.99
	0.62	0.95	0.68	0.98	0.54	0.99	0.43	0.97
	0.58	0.97	0.60	0.96	0.60	0.94	0.44	0.98
	0.65	0.94	0.60	0.99	0.48	0.97	0.61	0.98
27.00	0.44	1.00	0.60	0.98	0.55	0.99	0.44	0.98
	0.52	0.98	0.60	1.00	0.53	0.99	0.55	0.99
	0.65	0.98	0.58	0.94	0.51	0.98	0.47	0.99
	0.67	0.97	0.62	0.98	0.48	0.98	0.45	0.99
	0.58	0.91	0.58	0.96	0.62	0.94	0.41	0.99